

POLITECNICO DI MILANO
SCHOOL OF INDUSTRIAL AND INFORMATION ENGINEERING
MASTER OF SCIENCE IN BIOMEDICAL ENGINEERING



**A Wearable Device for Transcutaneous
Carbon Dioxide Measurement: Hardware,
Smartphone Application and Experimental
Validation**

Supervisor: Prof. Andrea Aliverti
Co-Supervisor: Ing. Alessandra Angelucci
Co-Supervisor: Ing. Sara Bernasconi

Master thesis of:
Luca Colombo
964746

ACADEMIC YEAR 2022-2023

Ringraziamenti

Un sentito ringraziamento al Professor A. Aliverti, all'Ing. A. Angelucci e all' Ing. S. Bernasconi per l'opportunità, la disponibilità, i consigli e anche i momenti più leggeri e di svago che hanno contraddistinto questo lavoro di tesi. Ringrazio e-Novia che ha fornito importanti spunti di riflessione e suggerimenti nel corso dello sviluppo del dispositivo.

Un pensiero va ai miei genitori e alla mia famiglia, che mi ha supportato e sopportato in questo percorso accademico.

Un grande grazie e la promessa di altri momenti indimenticabili insieme ai miei compagni di corso tra cui Andrea, Nicola, Simone e Matteo, con cui ho condiviso molto in questi cinque anni, sempre con divertimento e spensieratezza. Ai ragazzi del LaRes, in uno stanzino in fondo al secondo piano dell'edificio 32, vanno i miei più stimati ringraziamenti, perchè è stato davvero bello lavorare, collaborare e confrontarsi, seppur su progetti diversi, in vostra compagnia.

Un grazie anche ai miei amici di sempre, sparsi tra la Brianza e la Val d'Aosta, che mi hanno più volte ascoltato e con cui si può sempre trovare il modo di sorridere a ogni situazione.

E' stato bello.

Abstract

In the field of healthcare, telemedicine is growing as one of the most powerful tool to deliver care and sharing medical knowledge over a certain distance. Thanks to an improvement in technology, telemedicine has covered an important role during the COVID-19 pandemic, ensuring control over individuals health status without needing to physically go to a hospital or medical centre. Moreover, telemedicine is a means through which low-income and growing countries can deliver care.

In this context, the importance of wearable devices to monitor the health condition is crucial. The term wearable sensors embraces all the devices that can be placed on the human body, such as patches attached to the skin, or sensorized garments and more. Typically these sensors are developed to detect a specific physiological parameter, that can be for instance oxygen saturation, glucose level in blood or data related to respiration. Although transcutaneous oxygen saturation is a well-known technique used to analyze O₂ partial pressure in blood, transcutaneous carbon dioxide monitoring is still under study.

Sensors to measure CO₂ pressure or concentration are various and adopting different measuring principles. Among them, the most commonly used is the Stow-Severinghaus electrode, which is based on a hydration of dissolved CO₂ into carbonic acid. An emerging frontier is the one of the Non-Dispersive InfraRed (NDIR) sensors, which instead are based on infrared absorption of carbon dioxide.

Measuring techniques for CO₂ partial pressure in blood include the Blood Gas Analysis (BGA), which is not real-time and requires blood samples to be taken from the subjects; capnometry, that detects the amount of carbon dioxide in the exhaled air, and transcutaneous techniques. The latter is usually performed with the help of electrochemical sensors (i.e. based on the Stow-Severinghaus electrode), whereas NDIR-based devices are still under development.

Starting from a literature review, a PCB-based device using a NDIR sensor is created. The device features the following components: Arduino NANO 33 BLE (or NANO 33 IoT) used as a microcontroller, NDIR CozIR sensor, used to detect CO₂ variations, Normally Open (NO) solenoid valve to regulate airflow through the chamber where transcutaneous carbon dioxide accumulates, SSM3K2615R N-channel transistors and voltage regulator to

regulate power and drive the solenoid valve and the NiChrome wire, one thermistor with a nominal resistance of 100 kOhm at 25°C, a NiChrome wire with a resistivity of 5.755 Ohm/m, a user button, a tactile switch and an external LiPo battery of 3.7V and 5000 mAh.

During the experimental campaign, following some considerations on the collected data, a new PCB is developed (but not used) including: micro-fan driving circuit, a micro-USB recharge module, a circuit for battery level monitoring and a temperature sensor with the purpose of preventing overheating in the region of the board where there is the transistor used to drive the wire.

The case for the device is built in FUSION 360® and the firmware is written on Arduino IDE, both considering the possibility of soldering either an Arduino NANO 33 BLE or 33 IoT as a microcontroller. Since the microcontroller of the NANO 33 BLE or of the NANO 33 IoT features Bluetooth Low energy connectivity, a custom smartphone app is also developed.

The application is build on Microsoft® Visual Studio Code®, in Dart language, integrating also Google Firebase® features. In particular, the application ensures scanning and connection with BLE devices (amongst which there is the one developed), the possibility of registering the user to Firebase with email and password, consulting real time data, real time plot and to save locally or on the cloud collected data.

To test the capability of the developed device to detect CO₂ variations in blood, an experimental campaign is conducted with the cooperation of the Centro Cardiologico Monzino in Milan. A number of 20 subjects is tested following a precise test protocol. Firstly the device is positioned on the right wrist of the subject; then the gold-standard device (the Sentec Digital Monitor) is positioned either on the left lobe or on the right forearm. Indeed, each subject undergoes two acquisitions, interspersed with a 40 minutes break. What differs between the two tests is the position of the Sentec device on the subject. Together with the listed apparatus, the subject breaths in a duct where a flowmeter for the measurement of the end-tidal CO₂ partial pressure is present. Moreover, the subjects wears an independent lobe-oxymeter and a ECG to monitor the heart. The test protocol consists of 10 minutes of breathing in normal air, followed by 2 minutes of rebreathing in a rebreathing bag and lastly 12 minutes of breathing in normal air again. The rebreathing maneuver is chosen to trigger production and accumulation of carbon dioxide in blood.

Collected data are subsequently analyzed by statistical means. Firstly, data are pre-processed extracting the median representative value in time windows of either 10s or 30s, taking as input the overall data collected during the two tests. Then, on the processed data the Kruskal-Wallis test, the Wilcoxon Matched Pairs test and the Friedman

Repeated Measures Analysis of Variance test are performed, followed by an evaluation on the correlation between the output data from the PCB device and the Sentec Digital Monitor. Lastly, PCB device response is also evaluated individually on each subject by means of an exponential fitting.

This Master Thesis is divided in 5 chapters:

- **Introduction:** this chapter contextualizes the thesis' research topic, introducing the concepts of telemedicine and wearable devices.
- **State of the Art:** this chapter briefly describes sensors that can be used to monitor CO₂ variations, providing insights on the techniques used to measure carbon dioxide partial pressure in the biomedical field.
- **Materials and Methods:** this chapter describes the hardware of the device, the firmware, the smartphone application, the experimental campaign and the statistical methods used to analyze the collected data from the device.
- **Results:** this chapter contains statistical analysis results, considerations concerning the collected data and exponential fitting description.
- **Conclusion:** this chapter reinforces the objective of this Master Thesis, introduces faced problems, achieved results and possible further developments.

Abstract in lingua italiana

Nel campo della sanità, la telemedicina sta crescendo come uno degli strumenti più potenti per fornire assistenza sanitaria e condividere conoscenze mediche anche a lunghe distanze. Grazie allo sviluppo tecnologico, la telemedicina ha ricoperto un ruolo importante durante la pandemia di COVID-19, permettendo un monitoraggio dello stato di salute del paziente senza la necessità di recarsi fisicamente presso un ospedale o un centro medico. Inoltre, la telemedicina rappresenta un mezzo mediante il quale paesi in via di sviluppo possono fornire assistenza sanitaria.

In questo contesto, l'importanza di avere dispositivi indossabili per monitorare lo stato di salute è cruciale. Col termine 'sensori indossabili' ci si riferisce a tutti quei dispositivi che possono essere posizionati sul corpo umano, come patches attaccate alla pelle, indumenti sensorizzati e molti altri. Tipicamente questi sensori sono creati con l'obiettivo di rilevare uno specifico parametro fisiologico, che può essere per esempio la saturazione di ossigeno o il livello di glucosio nel sangue, o ancora dati relativi alla respirazione. Nonostante la misurazione transcutanea della saturazione di ossigeno sia una tecnica ben conosciuta per analizzare la pressione parziale di ossigeno nel sangue, il monitoraggio transcutaneo dell'anidride carbonica è ancora in fase di studio.

Vari sono i sensori che si possono usare per misurare la pressione parziale o concentrazione di CO₂, differenziati per il principio di misura adottato. Tra questi, quello comunemente più usato è l'elettrodo di Stow-Severinghaus, il quale si basa sull'idratazione della CO₂ in acido carbonico. Invece, una tecnica emergente è quella che utilizza sensori basati sull'infrarosso (NDIR).

Per quanto concerne le tecniche per misurare la pressione parziale di CO₂ nel sangue, si può distinguere l'analisi dei gas sanguigni, la quale non viene effettuata real-time e richiede l'estrazione di un campione di sangue dal paziente; la capnometria, che rileva il quantitativo di anidride carbonica nell'esalato del soggetto e infine tecniche transcutanee. Queste ultime sono normalmente utilizzate insieme a sensori elettrochimici (i.e. l'elettrodo di Stow-Severinghaus), mentre dispositivi basati su sensori a infrarosso sono ancora in fase di sviluppo.

Partendo da un'analisi della letteratura è stato creato un dispositivo basato su PCB, utiliz-

zando un sensore NDIR. Il dispositivo è caratterizzato dai seguenti componenti: Arduino NANO 33 BLE (o NANO 33 IoT) impiegato come microcontrollore, il sensore NDIR Co-ZIR utilizzato per rilevare variazioni di CO₂, una valvola solenoidale normalmente aperta per regolare il flusso di aria attraverso la camera dove è accumulata l'anidride carbonica transcutanea, due transistor SSM3K2615R e un regolatore di tensione per gestire l'alimentazione e controllare la valvola solenoidale e il filo di Nichel-Cromo, un termistore con resistenza nominale di 100 kOhm a 25°C, un filo di Nichel-Cromo con una resistività di 5.755 Ohm/m, un bottone, un interruttore a tre vie e una batteria LiPo esterna da 3.7V e 5000 mAh.

Durante a campagna sperimentale è stato anche sviluppato un nuovo modello di PCB, a seguito di considerazioni sui dati collezionati, il quale include, in aggiunta: un circuito di condizionamento per una micro-ventola, un circuito di ricarica con porta micro-USB, un sensore di temperatura posizionato sulla scheda in prossimità del transistor che regola il filo di Nichel-Cromo per prevenire surriscaldamenti della PCB e un circuito per il monitoraggio del livello della batteria.

Il case del dispositivo è creato su FUSION 360®, e il firmware scritto su Arduino IDE, consideranto la possibilità di utilizzare l'Arduino NANO 33 BLE o NANO 33 IoT come microcontrollori. Poichè sia il microcontrollore del NANO 33 BLE che quello del NANO 33 IoT sono caratterizzati dall'avere la connettività Bluetooth Low Energy, è stata sviluppata anche una applicazione ad hoc per smartphone.

L'applicazione è sviluppata usando Microsoft®Visual Studio Code®, in linguaggio Dart, integrando anche alcune funzionalità di Google Firebase®. In particolare, l'applicazione permette la ricerca e connessione con dispositivi BLE (tra cui si annovera quello sviluppato), la possibilità di registrare l'utente su Firebase con email e password, la consultazione di dati e grafici real time e il salvataggio in locale o sul cloud dei dati collezionati.

Per testare la capacità del dispositivo di rilevare variazioni di CO₂ nel sangue, con la collaborazione del Centro Cardiologico Monzino a Milano è stata realizzata una campagna sperimentale. 20 soggetti sono stati testati seguendo un preciso protocollo di test. In primo luogo, il dispositivo sviluppato è posizionato sul polso destro del soggetto; poi il dispositivo utilizzato come gold-standard (il Sentec Digital Monitor) è posizionato o sul lobo sinistro o sull'avanbraccio destro. Infatti, ciascun soggetto è chiamato a svolgere due acquisizioni, separate da una pausa di 45 minuti. Ciò che cambia da un'acquisizione all'altra è il posizionamento del dispositivo Sentec sul soggetto. In aggiunta ai dispositivi appena descritti, il soggetto respira in un condotto dove è collocato un misuratore di flusso per la rilevazione della CO₂ di fine volume tidalico. Inoltre, i soggetti indossano un saturimetro da lobo indipendente e gli elettrodi per rilevare l'ECG. Per quanto riguarda il

protocollo del test, questo consiste in 10 minuti di respirazione in aria normale seguiti da 2 minuti di ri-respirazione in una sacca e infine 12 minuti di respiro nuovamente in aria normale. La manovra di ri-respirazione è scelta per stimolare la produzione e l'accumulo di anidride carbonica nel sangue.

I dati rilevati poi sono in seguito analizzati attraverso analisi statistiche. In primo luogo, i dati sono pre-elaborati estraendo, a intervalli di 10s o 30s, il valore mediano del gruppo di campioni preso in considerazione, iterativamente e raggruppando consecutivamente tutti gli istanti temporali del test effettuato. Successivamente, su questi dati elaborati vengono applicati i test di Kruskal-Wallis, il Wilcoxon Matched Pairs test e il Friedman Repeated Measures Analysis of Variance test; successivamente si è analizzata la correlazione tra i dati collezionati con il Sentec Digital Monitor e il Dispositivo PCB. Infine, la risposta del Device PCB è analizzata anche per mezzo di un fitting esponenziale su ogni soggetto.

Questa Tesi Magistrale è suddivisa in 5 capitoli:

- **Introduzione:** questo capitolo descrive il contesto in cui la tesi si inserisce, spiegando i concetti di telemedicina e dispositivi indossabili.
- **Stato dell'Arte:** questo capitolo descrive brevemente i sensori che possono essere usati per misurare variazioni di CO₂, illustrando le tecniche impiegabili per misurare la pressione parziale di anidride carbonica nel sangue in ambito biomedico.
- **Materiali e Metodi:** questo capitolo descrive l'hardware del dispositivo, il firmware, l'applicazione smartphone, la campagna sperimentale e i metodi statistici utilizzati per analizzare i dati collezionati dal dispositivo.
- **Risultati:** questo capitolo contiene i risultati dell'analisi statistica, considerazioni sui dati collezionati e una descrizione del fitting esponenziale.
- **Conclusione:** questo capitolo riafferma l'obiettivo di questa Tesi Magistrale, introduce i problemi affrontati, i risultati ottenuti e descrive i possibili sviluppi futuri.

Contents

Abstract	iii
Abstract in lingua italiana	vii
Contents	xi
Introduction	1
1 State of the Art	5
1.1 The Respiratory System	5
1.1.1 Gas exchange and carbon dioxide production	7
1.1.2 Regulation of ventilation and respiratory failure	9
1.2 CO ₂ measurement sensors	11
1.2.1 Hydration of CO ₂ into carbonic acid	12
1.2.2 Infrared absorption of CO ₂	15
1.3 CO ₂ measurement techniques in the Biomedical field	17
1.3.1 Blood Gas Analysis	18
1.3.2 Capnometry and petCO ₂	19
1.3.3 Transcutaneous CO ₂ measurement	21
1.3.4 Currently developed devices	23
2 Materials and Methods	29
2.1 Device realization	29
2.1.1 Arduino Nano 33 BLE	31
2.1.2 NDIR CO ₂ Sensor	33
2.1.3 Solenoid valve	34
2.1.4 N-channel MOSFETs and voltage regulator	36
2.1.5 Thermistors and resistances	39
2.1.6 Nichrome wire and Lithium-Ion battery	39

2.1.7	Momentary switch and tactile switch	41
2.2	PCB Design	42
2.2.1	Software and tools	42
2.3	Further PCB Improvements	44
2.3.1	Micro-USB recharge module	44
2.3.2	MOSFET temperature sensing	44
2.3.3	Battery level monitor	45
2.3.4	Motor Fan	45
2.4	Case	47
2.5	Firmware	50
2.5.1	Timer Interrupt	52
2.5.2	Idle State	52
2.5.3	Start State	52
2.5.4	Calibration State	52
2.5.5	Heating State	53
2.5.6	Measurement State	54
2.6	Software	55
2.6.1	BLUETOOTH® AND BLUETOOTH LOW ENERGY	55
2.6.2	The Smartphone Application	59
2.6.3	Workflow	61
2.6.4	Google Firebase	63
2.6.5	Application Icon	65
2.6.6	Main, Welcome Screen and Wrapper structure	66
2.6.7	Authentication and Registration Screens	67
2.6.8	Scanning Screen	71
2.6.9	Data Visualization Screen	74
2.6.10	Widgets	76
2.7	Experimental Campaign	77
2.7.1	Test Protocol	79
2.7.2	Questionnaire	80
2.8	Statistical methods	81
2.8.1	PtCO ₂ analysis	81
3	Results and Discussion	87
3.1	PCB Device Response	87
3.2	PCB Device Evaluation	90
3.3	Aggregated Data Analysis	92

3.3.1	Kruskal Wallis test results	95
3.3.2	Wilcoxon Matched Pairs Test results	96
3.3.3	Friedman test results	97
3.3.4	Bland-Altman Plots	99
3.3.5	Correlation Analysis	101
3.4	Exponential Fitting	103
4	Conclusion	111
4.1	Faced Issues and Achieved Results	111
4.2	Future Developments	112
Bibliography		113
A Appendix A: PCB Version 1		117
B Appendix B: PCB Version 2		119
C Appendix C: Case 3D rendering and dimensioning		123
List of Figures		127
List of Tables		129
Nomenclature		131

Introduction

Telemedicine

The Merriam-Webster dictionary defines *medicine* as the science and art dealing with the maintenance of health and the prevention, alleviation, or cure of disease, whereas *Tele* is a combining word meaning "distance", or "at a distance" [28].

Telemedicine (TM) can hence be defined as the delivery of health care and sharing of medical knowledge over a distance, using communication means.

Telemedicine is believed to exist for some millennia, with the first use that can be traced back to smoke signals generated by ancient civilizations to warn other clans of a contagious illness outbreak. It is indeed an exchange of medical information over a certain distance [17].

Another example is the one of Jerri Nielsen, who found a tumor in her breast while on a research assignment in Antarctica. Because of the weather conditions, the diagnosis and treatment of her breast cancer was done over distance by satellite connection, with the video and chemotherapy equipment dropped by US Air Force pilots.

Although the need to deliver medical care to distant patients has existed for several time, the use of telemedicine to meet this need has increased rapidly only in the last few decades. This is largely due to improvements in the underlying enabling digital technology. This increase in telemedicine importance is also linked with the outbreak of the COVID-19 pandemic; TM has the potential to help by permitting mildly ill patients to get the supportive care they need while minimizing their exposure to other acutely ill patients [21].

Virtual care and traditional clinical care are likely to integrate in the future. Virtual visits would not only substitute for routine health checks, but they would also complement in-person care [8]. Moreover, lower-income nations could use different mobile devices or smartphones to deliver care. Hospitals and clinics are not diffused capillary on the territory, but but smartphones are ubiquitous and can connect large populations to care. In some situations, smartphones can also be used both as a diagnostic tool (e.g. to

assess electrocardiograms) and as a therapeutic one (e.g. to connect to a midwife or obstetrician). Besides this, these tools can also help to educate local clinicians.

More in detail, TM can be divided into *asynchronous telemedicine* and *synchronous telemedicine*. The former refers to exchange of information that occurs when the provider and patient are not connected at the same time, such as email exchanges, while the latter refers to exchanges in which the provider and patient are connected at the same time, as in the case of video conferencing. Synchronous direct to consumer visits that generally occur with the patient located at their home or other non-medical facility. Such visits are done without the aid of a healthcare worker, and hence require adequate instrumentation.

In this context, wearable sensors and devices represent a new frontier in telemedicine.

Wearable technologies

The term *wearable* refers to whatever a subject can wear, like socks, watches and patches, without encumbering daily activities or restricting mobility [2]. The number of wearable device is huge nowadays, but not all of them are capable of providing parameters about the health status. Conversely, a lot of devices and sensors that measure physiological parameters are not in a wearable form.

The idea is to create devices capable of measuring physiological parameters and at the same time to be wearable; the ultimate wearable device should be installed once or continuously, it has to have a long-lasting battery, to be wireless, to have a low power consumption and to report health-related information without impeding the user.

Moreover, wearable system should be capable of providing real-time feedbacks, not only to medical staff and patients, thanks to a continuous patient's parameters monitoring. In this regard it gains importance the concept of Body Area Network (BAN).

BANs are systems constituted by a network of devices that can be implanted in the body, placed on it or carried in pockets or by hand.

The peculiarity of BANs is that the communication is entirely within or in proximity of the human body. A representation of a BAN architecture is in Figure 1.

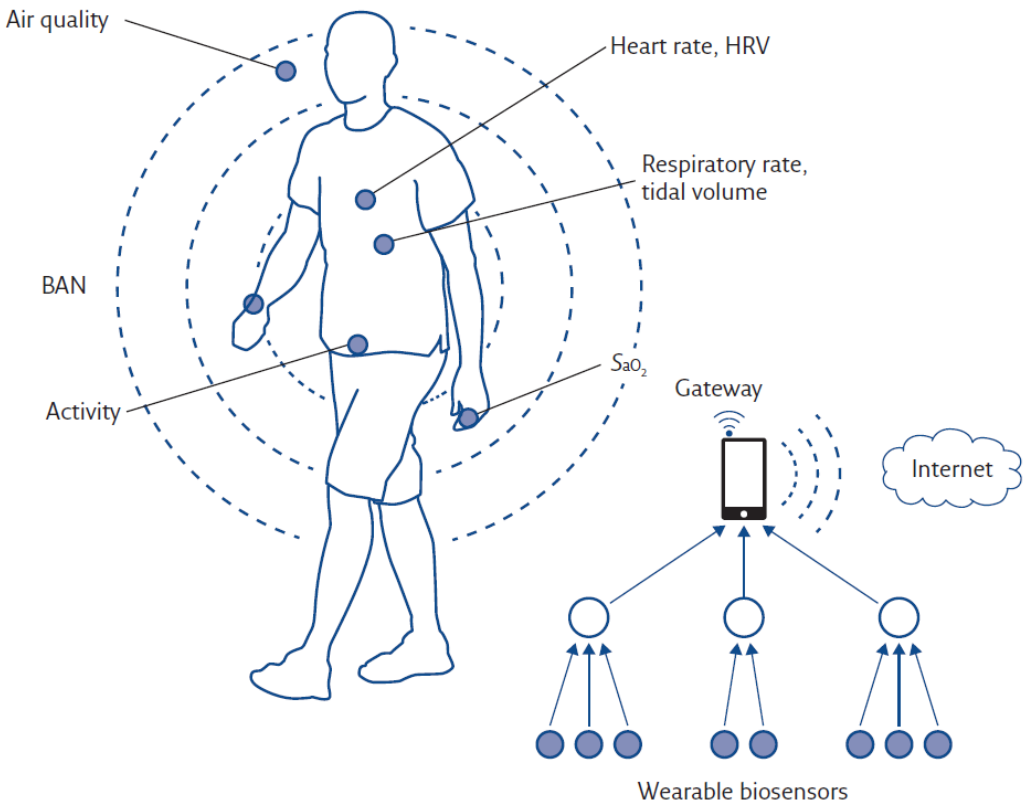


Figure 1: BAN architecture with sensors possibilities.

Sensors on the body of the subject communicate wirelessly with stationary gateway devices such as smartphones. Then the measurement can be stored locally or transmitted to a medical centre.

Wearable sensors are intended to be used not only for ill patients, but they can be helpful also for healthy subjects. For instance, they can be used to track trends and improvements in sport activities, or to study body kinematics. Because of all these considerations, the wearable sensor is a core part of the new telemedicine paradigm designated to support the perception that quality healthcare delivery services will improve through the utilisation of effective information and digital health devices [4].

1 | State of the Art

In this chapter a brief explanation on the respiratory system is presented, followed by an introduction to the main CO₂ sensing techniques. Then, CO₂ measurement techniques in the biomedical field are listed, providing also insights on currently developed devices.

1.1. The Respiratory System

The respiratory system is a network of organs and tissues devoted to breathing. It serves the role of supplying the body with oxygen and removing carbon dioxide. This is allowed by four processes that are [3]:

- **Pulmonary ventilation:** it is a process that moves air inside and outside the lungs, and it is only a part of the complete process of respiration.
- **External respiration:** it represents the gas exchange between the lungs and the blood.
- **Transport:** it is the transport of oxygen from lungs to tissues and of carbon dioxide from tissues to lungs.
- **Internal respiration:** it is the gas exchange between the systemic blood vessels and the tissues.

The first level is ventilation, that is provided by the ventilatory system. There is a conductive zone, where air is conducted from inside to outside the body and vice versa. In addition, air is also filtered and moistened. Then there is the respiratory zone, where gas exchange occurs. It consists of bronchioles, alveolar ducts and alveoli.

The overall flow of air is provided by a set of pressure gradients between different sides and by the conductance of the membrane that is considered.

For instance, if oxygen is considered, the inrush of air from the ambient to the lungs is due to the difference between the partial pressure of oxygen in the inspired air P_I and the partial pressure of oxygen in the expired air P_E. Similarly, the oxygen exchange at the level of the capillaries is due to the partial pressure of oxygen in the alveoli P_A and the

capillary partial pressure of oxygen P_b as shown in Figure 1.1.

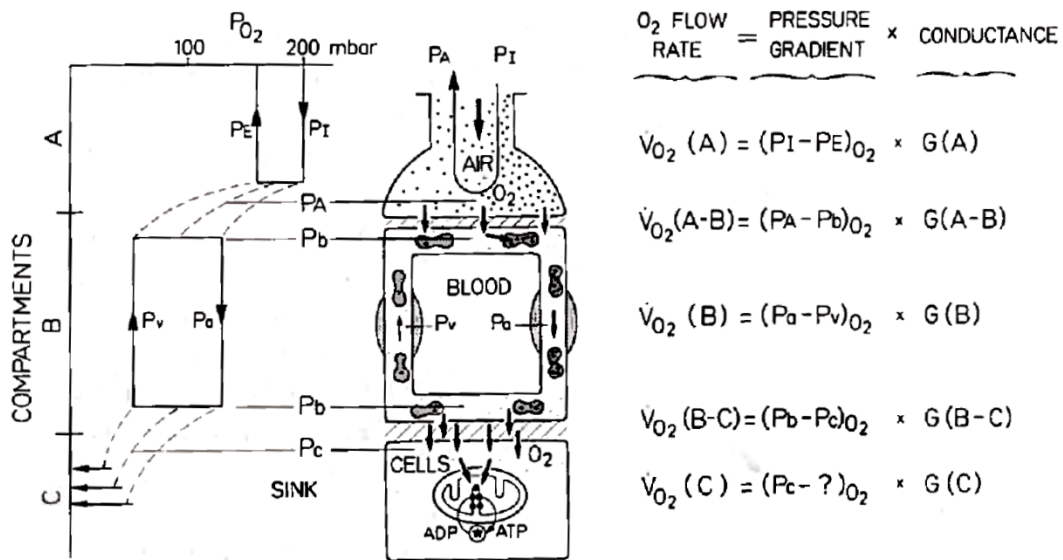


Figure 1.1: Model of the respiratory system and cascade of pressure gradients from [25].

The ventilatory system is also composed by an active part, the respiratory muscles, aimed at providing respiration. Their activation is regulated by the central pattern generator.

1.1.1. Gas exchange and carbon dioxide production

The site for gas exchange between air and blood is the respiratory membrane, which is mainly composed by the alveolar wall and capillaries. It consists of three layers: alveolar epithelium, fused basal laminae and capillary endothelium. The respiratory membrane has a specific thickness and surface area, and these two factors influence the effectiveness of the gas exchange. In fact, oxygen and carbon dioxide are required to diffuse from one side (the alveoli) to the other (the capillaries) and vice versa, and the diffusion is directly proportional to the surface area, and inversely related to the thickness. Also, the diffusion coefficient of the chemical species plays a role. Since the solubility of carbon dioxide is higher than oxygen, theoretically the gas exchange should be dominated by CO₂. But the diffusion coefficient depends also on the molecular weight, so overall the two diffusion coefficients for oxygen and carbon dioxide are very similar, permitting a balance in the gas exchange.

Pathologies such as lung edema increase the thickness of the alveolar wall, resulting in an oxygen deprivation. On the other hand, in case of emphysema, the surface area is reduced because walls of adjacent alveoli break through.

Furthermore, the capillaries attached to the alveolar wall reach their minimum diameter in the respiratory zone, allowing the passage of one red blood cell at a time. At low velocity they tend to get closer, moving one behind the other in formations called rouleaux. This reduces the speed of the blood flow so that gas exchange is optimal.

The steep gradient in pressure allows oxygen and carbon dioxide partial pressure to reach equilibrium if time through the pulmonary capillary is from 0.25 s to 0.75 s. If the exposure time is smaller than 0.25 s the blood is not sufficiently oxygenated, and the intake of CO₂ in the alveoli is not sufficient.

In the venous blood the partial pressure of oxygen is 40 mmHg, and in the alveoli is 104 mmHg. Conversely, for CO₂ the partial pressure is 40 mmHg in the arterial blood and in the alveoli, and of 46 mmHg in the venous blood. The fact that the pressure for CO₂ is the same in the alveoli and arterial blood is because it is not wanted an exchange of carbon dioxide at this level, whereas it is needed between the alveoli and venous blood.

Once oxygen is transferred from the alveoli to blood, the circulatory system is devoted to bringing it to tissues and cells. At cell level, still the gradient in pressure drives the intake of oxygen inside the cell and the outtake of carbon dioxide. Because of this process, the partial pressure of oxygen decreases up to 40 mmHg in the venous blood, and the partial pressure of carbon dioxide rises to 46 mmHg.

It is important to mark that oxygen mostly travels in blood bonded to hemoglobin (oxy-

hemoglobin), while only 2% is dissolved in plasma. Conversely, 70% of CO₂ is transported in the form of bicarbonate HCO₃⁻, 23% is bonded to hemoglobin, and 7% is dissolved in plasma.

Then, cells use oxygen in cellular respiration; the aerobic cellular respiration reacts glucose and oxygen to create energy. In glycolysis, glucose is converted into pyruvate, and two molecules of adenosine tri-phosphate (ATP) are generated in this process. Pyruvate is then further broken into loose carbon and hydrogen, which can combine with oxygen to create carbon dioxide and NADH. If oxygen is not present the pyruvate experiences fermentation and lactic acid is produced. The produced ATP is then degraded into ADP to produce energy.

1.1.2. Regulation of ventilation and respiratory failure

The respiratory process is regulated by the central pattern generator, constituted by pons and medulla oblongata, which sends efferent fibers to the respiratory muscles to control respiration. It also receives afferent signals with the purpose of determining the breathing rate and amplitude.

The biological sensors that are sending signals are the chemoreceptors, and they are divided in central chemoreceptors and peripheral chemoreceptors. The formers are located within the central nervous system, usually in the brain stem or in the hypothalamus, and measure the amount of carbon dioxide in the cerebrospinal fluid. In fact, the cerebrospinal fluid is collecting CO₂ from cerebral capillaries; when the carbon dioxide passes the so-called blood/brain barrier, it reacts with water and generates bicarbonate and hydrogen, according to the reaction in Figure 1.2.

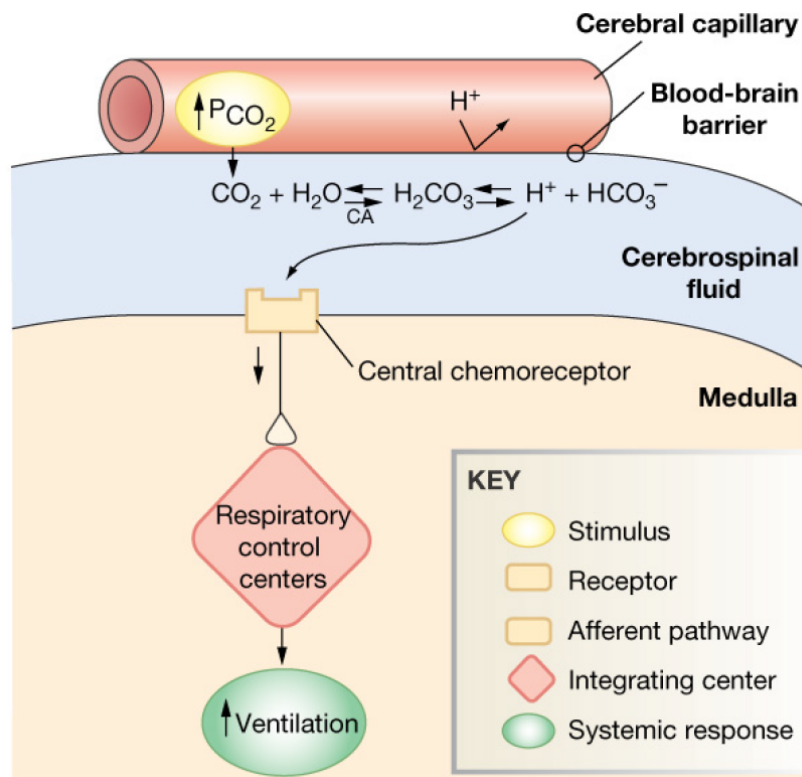


Figure 1.2: Schematic description of central chemoreceptors' role and CO₂ sensing [3]

Properly, central chemoreceptors are not directly sensible to CO₂ concentration, but to H⁺ concentration, which closely depends on the amount of CO₂. For instance, in case of increase of partial pressure of carbon dioxide in blood, the concentration of H⁺ in the cerebrospinal fluid will rise, hence the central chemoreceptors will send to the central

pattern generation the request for increasing ventilation to reduce the amount of CO₂ in blood.

As for the peripheral chemoreceptors, they are located outside the central nervous system, usually in the wall of a blood vessel (e.g. aortic body and carotid body). They are capable of sensing changes in oxygen and CO₂ content and pH of the blood in order to help the control of cardiovascular and respiratory functions.

If the respiration is not properly performed, two main consequences can be observed, that are hypoxemia and hypercapnia. Hypoxemia refers to a low oxygen content in blood, and it can be due to hypoventilation, mismatches in the ventilation-perfusion rate or alteration in the diffusion process. Hypercapnia is a condition in which the carbon dioxide content in blood is excessively high; disfunctions in organs that cause hypoventilation are the main causes of hypercapnia. An excess of carbon dioxide in blood leads to respiratory acidosis, central nervous system depression and eventually coma.

Another possible condition that can affect the carbon dioxide levels in blood is hyperventilation. During hyperventilation, the respiratory rate is increased, and this leads to a faster CO₂ removal from blood with the consequence of a decrease in carbon dioxide partial pressure and a condition of respiratory alkalosis. Alkalosis is associated with different symptoms, such as headache and loss of consciousness.

1.2. CO₂ measurement sensors

In medical practice, the measurement of blood gasses, particularly oxygen and carbon dioxide, provides a respiratory and circulatory insights on the health condition of the patient.

The gold standard to retrieve the values of partial pressure of CO₂ and O₂ consists in arterial blood sampling, a process that is painful and risky, requiring expensive analyzers and experienced staff. Moreover, blood samples need to be further analyzed immediately upon collection, eventually adding logistical constraints.

To overcome these issues, the development of non-invasive oxygen and carbon dioxide measurement techniques has been observed in the last decades. Among the possible solutions, CO₂ can be monitored in the exhaled breath by means of a technique called airway capnometry, which provides the measurement for end tidal CO₂ partial pressure, the petCO₂.

However, in case of increased anatomical dead space or ventilation-perfusion mismatch, this technique is not reliable enough.

The other possible solution lies in transcutaneous CO₂ partial pressure measurement, PtCO₂ (also called EtCO₂). The underneath idea is to trigger local subcutaneous blood arterIALIZATION to enhance carbon dioxide diffusion, and then to measure its concentration.

According to [7], devices aimed at measuring CO₂ can be divided, based on the exploited physico-chemical properties of the carbon dioxide molecule, in four groups:

1. Hydration of dissolved CO₂ into carbonic acid
2. Reduction of CO₂ into CO₂⁻ and CO₃²⁻
3. Acoustic properties of gaseous CO₂
4. Infrared absorption of CO₂

In the following, only type 1 and type 4 sensors are briefly introduced.

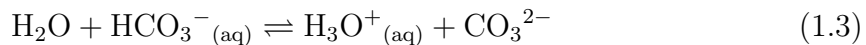
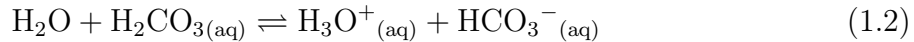
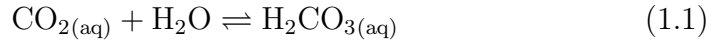
1.2.1. Hydration of CO₂ into carbonic acid

In an aqueous medium, gaseous CO₂ dissolves into carbonic acid (H₂CO₃), that then differentiates into bicarbonate (HCO₃⁻) and carbonate (CO₃²⁻). As a consequence, CO₂ dissolution lowers the pH of the medium and, in addition, dissolved ions vary the conduction of the solution. The former principle is used in the Stow-Severinghaus electrode and ISFET (Ion-Selective Field-Effect Transistor) sensor, while the latter in conductometric CO₂ sensors.

The Stow-Severinghaus electrode

Currently, this sensor represents the state-of-the-art measurement technique for transcutaneous carbon dioxide measurement. It consists of a pH meter plunging in an electrolyte and covered with a thin membrane (Figure 1.3).

CO₂ dissolved in the sensing medium diffuses in the sensor's electrolyte through a CO₂-permeable membrane. pH is lowered by CO₂ dissociation according to the following equations:



The change in pH is measured with a pair of electrodes, the glass electrode and the reference electrode. The glass electrode usually consists in an Ag/AgCl electrode, while the reference electrode is Pt or AgCl. The main drawback of this type of sensor is the lack of long term stability; in fact, drifts in the measured values can verify, making it necessary to recalibrate the sensor from time to time depending on the target accuracy.

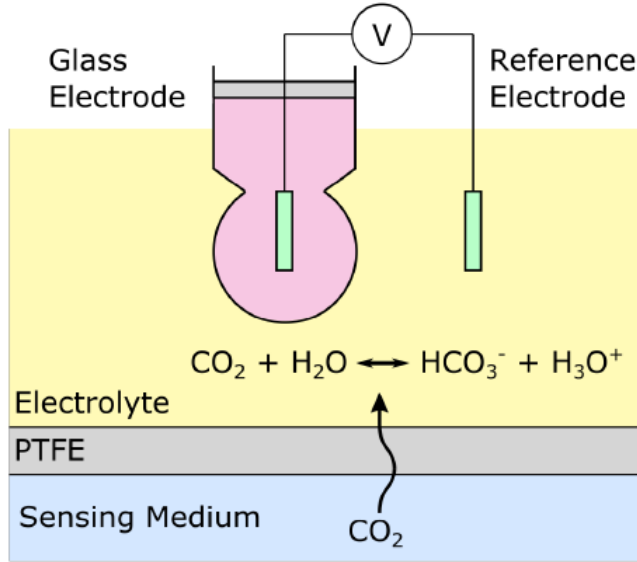


Figure 1.3: Illustration of a state-of-the-art Stow-Severinghaus electrodes [7].

ISFET sensor

ISFETs are MOSFETs whose gate is no more metallic but manufactured in a way that is H_3O^+ sensitive. The need of developing ISFETs sensor sensitive to CO_2 lies in the limited miniaturization of the Stow-Severinghaus electrode.

As for the structure, a reference electrode is placed in the electrolyte where CO_2 diffuses, and the gate of the ISFET is covered with a layer of insulator, silicon dioxide. When hydrated, the gate insulator exchanges protons with the surrounding electrolyte, thus changing the potential at the level of the gate and acting as a pH meter.

The sensitivity to CO_2 is achieved by covering the electrolyte with a CO_2 -permeable membrane that prevents other ions to pass through (Figure 1.4).

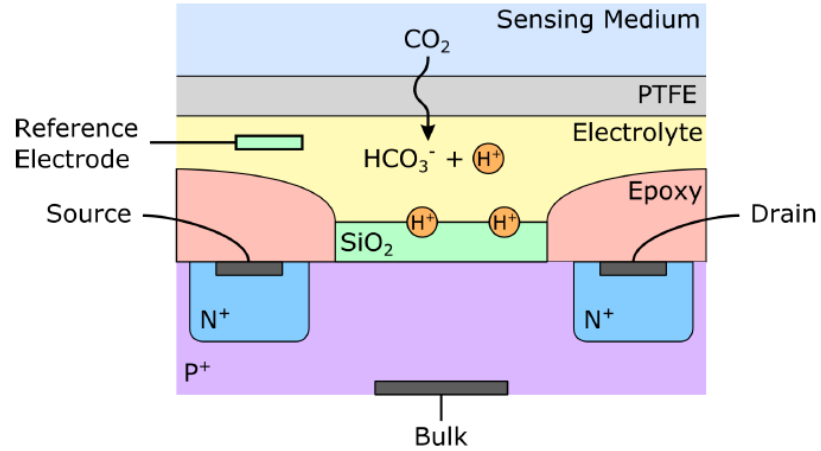


Figure 1.4: Illustration of an ISFET sensor [7].

1.2.2. Infrared absorption of CO₂

Non Dispersive Infra-Red (NDIR) sensor

NDIR CO₂ devices rely on Lambert-Beer's law of absorption. The peak of absorption for gaseous CO₂ is at 4.26 um, with the typical sensor structure that is the following.

An infrared source is located on one side of a cavity containing a gaseous mixture, whereas an infrared receptor is placed on the opposite side. Given a specific wavelength λ , the light flux $\phi_{mes}(\lambda)$ measured by the photodiode (the typical infrared receptor) is function of: the emitted light flux from the source $\phi_0(\lambda)$, the geometry of the sensor k , the light path l and CO₂ concentration and its absorbance (χ_{CO_2} and $A_{CO_2}(\lambda)$, respectively).

$$\phi_{mes}(\lambda) = k \cdot \phi_0(\lambda) \cdot \exp(-l\chi_{CO_2}A_{CO_2}(\lambda)) \quad (1.4)$$

To avoid interferences from other gasses than carbon dioxide, a reference channel is often used together with the measurement channel. The purpose of the reference channel is to compensate for variations in the light source intensity that can be due to power issues or temperature variations, for instance. Typically, the reference channel has a bandpass filter in the 3.8 to 4.1 um region, where no gas is normally absorbed. Conversely, the measurement channel has a bandpass filter in the 4.3 um region, to retrieve the information only on CO₂ concentration (Figure 1.5). The response time of a NDIR sensor depends on the gas flow rate in the sensing chamber, whereas the sensing range is limited by the light path length. LEDs (Light Emitting Diode) are used as light source for this type of sensors, while the receiver is typically a photodiode or a thermopile, miniaturized as a MEMS (Micro Electro-Mechanical Systems) sensor.

This technology is the one on which the CozIR® sensor deployed in this work of thesis is based.

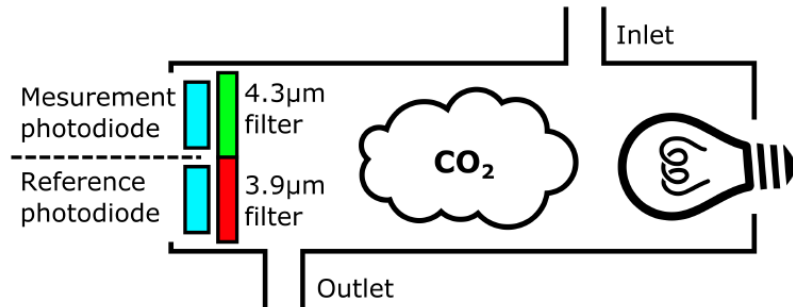


Figure 1.5: Schematic representation of combined reference and measured channels in a NDIR sensor [7].

Photoacoustic sensor

This type of sensor is composed by a sensing chamber, a light source and a microphone. It is still based on the Lambert-Beer law of absorption; a light source periodically illuminates with infrared light the sensing chamber and if carbon dioxide is present in the gas mixture, it absorbs the infrared radiation and it heats up, consequently dilatating. As soon as the illumination is stopped, the analyte cools down and hence compresses. The alternate switching on and off by the light source determines alternates compression and tensile forces that generate an acoustic wave. Depending on the amplitude of the wave it is possible to gain CO₂ concentration (Figure 1.6).

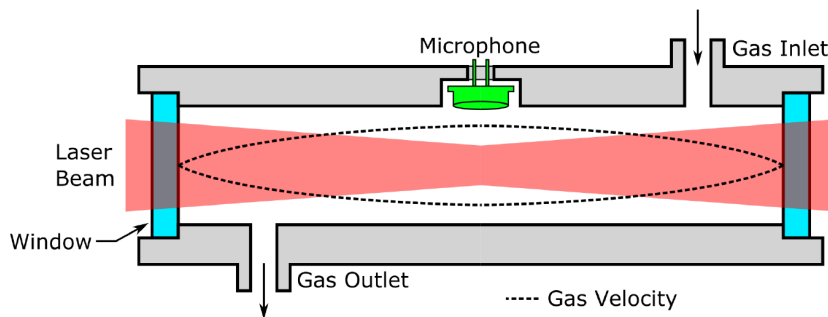


Figure 1.6: Schematic representation of the working principle of a photoacoustic sensor sensor [7].

1.3. CO₂ measurement techniques in the Biomedical field

Homeostasis first definition belongs to Claude Bernard (1878), which defined it as “the fixity of the milieu interne, which is the condition of free and independent life”. Changes in the surroundings determine internal disturbances. When these disturbances are produced, the human system works to keep them within narrow limits according to homeostatic mechanisms [6]. For instance, respiratory homeostasis regulates blood gas composition to maintain a cellular homeostasis.

Homeostasis requires many variables to be considered, such as ion balance, fluid balance, temperature balance and hydrogen-ion concentration (pH) balance.

Since carbon dioxide is mainly transported in blood in the form of bicarbonate, the value of pH is highly influenced by the amount of CO₂ present in blood. Depending on HCO₃⁻ concentration, pH can be determined with the Henderson-Hasselbach equation:

$$\text{pH} = 6.1 + \log \frac{[\text{H}_2\text{CO}_3^-]}{0.03 * p\text{CO}_2} \quad (1.5)$$

A physiological arterial partial pressure of CO₂ equal to 40 mmHg and an amount of bicarbonate equal to 24 mEq/L must be maintained to keep pH in a predefined physiological range. As can be seen in equations (1.2) and (1.3), when carbon dioxide partial pressure rises a condition of respiratory acidosis verifies, with a pH lower than 7.35. Conversely, a pH higher than 7.45 may occur in case of respiratory alkalosis [5].

Since it is a product of humans' metabolism, CO₂ is abundant in human body and its regulation is of paramount importance to maintain homeostasis. Many mechanisms compensate for perturbations, among which:

- Buffer systems in body fluids: with an acid-base tampon body fluids compensate for excessive pH changes.
- Respiratory center: according to the previously introduced consideration on the central pattern generator, they regulate ventilation to washout CO₂ or increase the intake of oxygen.
- Kidneys: associated to a slow response that eliminate acids or bases in excess.

As a consequence, carbon dioxide monitoring has a key role in clinical care. CO₂ measurement can be done in three locations, according to recent techniques:

- In subject's body with blood sampling.
- In subject's exhaled air with capnometry.
- On subject's skin with a transcutaneous approach.

1.3.1. Blood Gas Analysis

It is the gold standard for the assessment of body CO₂ content. The arterial partial pressure of carbon dioxide provides insights on the hemodynamic status of the patient and on its metabolism and homeostasis.

Typically BGA is performed with a painful and potentially risky arterial puncture; because of this, other sampling techniques have been tried, such as arterialized capillary blood sampling, considered a good surrogate for arterial blood sampling [31].

To evaluate pCO₂, two different methods can be used in BGA framework. Either it can be measured in situ with a sensor directly inserted in the blood vessel to continuously monitor the values with a latency given only by the sensor latency, or blood samples are collected and later analyzed. In this second scenario, blood sampling must be performed every time pCO₂ information is needed, and the sample has to be analyzed immediately after the collection, leading to further logistic difficulties.

1.3.2. Capnometry and petCO₂

Capnometry refers to the measurement of carbon dioxide in the exhaled air. In the image (Figure 1.7) it is represented a capnogram, which displays the pCO₂ in the exhaled air as a function of time.

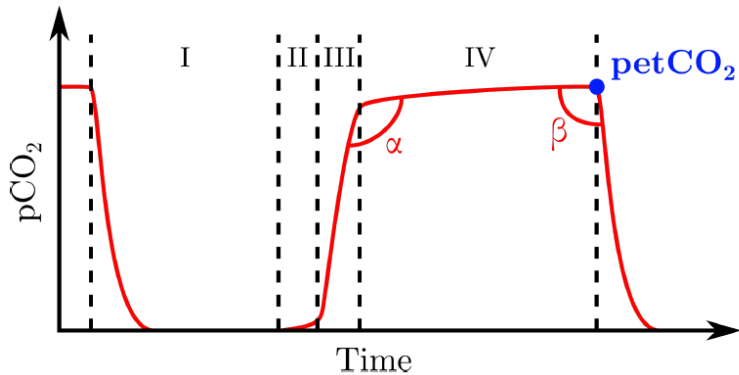


Figure 1.7: Typical expected representation from a Capnogram with the four different phases clearly underlined [22].

Four different phases can be identified when observing a capnogram [22].

1. In phase I inspiration is performed and ended. Theoretically the measured value for petCO₂ (end-tidal CO₂) should be 0, since no expired air is present.
2. Expiration:
 - II. Early exhalation in which CO₂ mixes with air in the dead space volume.
 - III. Dead space and alveolar gas (which contains CO₂) mixed, and the plot has a sharp increase.
 - IV. Expiratory plateau. At the end of this phase end tidal CO₂ (namely petCO₂ or EtCO₂) is computed.

The capnogram can be used to detect ventilation/perfusion mismatches, Chronic Obstructive Pulmonary Disease (COPD), apnea. It also provides information on CO₂ production and elimination, respiratory airflow and many more.

Despite being petCO₂ proved to be a reliable surrogate for paCO₂ (arterial carbon dioxide pressure), the correlation between the two is poor in case of elevated anatomical dead space or ventilation/perfusion inadequacy. Moreover, capnometry is difficult to be used on neonates because of the small amount of exhaled air they are capable of produce.

In the classical implementation of capnometry (*mainstream capnometry*) the patient is

intubated and the whole breath of the patient passes through the CO₂ sensor, placed in the main airway. Because of this configuration it is possible to gain real-time capnogram plots and instantaneous petCO₂ measurements. Instead, in the so-called sidestream capnometry, there exists a delay due to the fact that only a fraction of the patient's exhaled air is taken into analysis through a small diameter sampling tube.

The purpose of capnometry is to measure petCO₂ (also referred as EtCO₂), which is the partial pressure of CO₂ in the expired air at the end of expiration, and it is a good indicator to evaluate the effectiveness of ventilation and possible disfunctions in the respiratory or cardiac systems. For instance, elevated values of EtCO₂ but with physiological cardiovascular and respiratory system functioning can indicate an increase in CO₂ production (hypermetabolic state) or inadequate ventilation. In fact, high values of EtCO₂ are almost always linked with an increase in PaCO₂. On the other hand, low EtCO₂ is linked with decrease in CO₂ production, decrease of pulmonary blood flow or excessive ventilation [16].

EtCO₂ monitoring is a good procedure, but it has the main limitation that cannot be used in patients with respiratory disorders and non-intubated patients.

1.3.3. Transcutaneous CO₂ measurement

Capnometry and BGA usually require bulky and expensive equipment, and external interventions to perform calibration procedures. For these reasons, their usage outside the hospital is impractical.

In this regard, the development of a portable, low-cost and non-invasive solution for transcutaneous CO₂ monitoring becomes of primary importance.

Severinghaus was the first to describe how to measure pCO₂ on human skin. As previously mentioned, PtCO₂ measurement is based on carbon dioxide diffusion through the body tissue and skin, being then detected by a sensor. When the skin is heated, vasodilatation is triggered, increasing the diffusion of CO₂ because of the increase delivery of arterial blood to dermal capillary area. Typically, to promote arterialization, the sensor heats the skin up to 42°C and 44°C.

Cutaneous pCO₂ is a mixture of venous, arterial and capillary carbon dioxide partial pressures. Heating the skin to the previously mentioned values enhances the contribution of the arterial blood flow, having PtCO₂ that closely approximates arterial CO₂ tension (namely, artPCO₂ or paCO₂) [19].

Nowadays, Stow-Severinghaus electrochemical sensor dominates the PtCO₂ measurement techniques, with emerging technologies that are instead based on NDIR sensing. In this regard, a PtCO₂ sensor should fulfill two purposes to be effective:

1. It must cope with patient's changes in hemodynamic values.
2. It must measure PtCO₂ values that reflect patient's state.

To achieve these objectives, it is important to assess the correlation between PtCO₂ and artCO₂ and understand the exhalation rate of CO₂ from the skin to the sensor, that internally determines the latency with which the sensor responds to CO₂ changes.

artCO₂ and PtCO₂ correlation

Correlation between PtCO₂ and artCO₂ is well existing for temperature greater or equal than 42°C, but the procedure of heating patient's skin exposes potential safety problems, thermal injuries and strict requirements in term of power design of the measuring device. In fact, Food and Drug Administration (FDA) recommends not to expose the skin to 44°C for more than four hours [10].

For this reason there is the need of working with lower temperature values, although still maintaining a desirable artCO₂ and PtCO₂ correlation. In a study [29] it was found that,

even at temperature around 37°C a good correlation seems to exist.

CO₂ emission and diffusion

The carbon dioxide that is present in blood vessels can pass through the skin creating a volumetric flow of gaseous CO₂ in a process called cutaneous respiration. Two milestones must be considered when speaking about cutaneous respiration:

1. Humidity of the skin can change carbon dioxide exhalation.
2. Increasing the temperature determines an increased CO₂ exhalation rate.

The latter justifies the procedure of heating the skin when taking PtCO₂ measurements. Hence CO₂ exhalation rate is the most important parameter to be considered when designing a transcutaneous CO₂ sensor.

In [7] a closed-chamber sensor design is presented. The skin is treated as a membrane with a certain thickness e and diffusivity D with respect to CO₂; pCO₂ is assumed to be constant and equal to PtCO₂, while the sensor consists of a contact area S_{se} , a height H_{se} and an internal pressure of carbon dioxide $P_{se}\text{CO}_2$. A condition with no leakages is considered.

According to Fick's law (1.6), diffusion flux of carbon dioxide depends on its concentration.

$$J_s = -D \cdot \frac{dC(x)}{dx} \quad (1.6)$$

Integrating over the membrane thickness, the response of the sensor in terms of measured partial pressure of CO₂ ($P_{se}\text{CO}_2$) is:

$$P_{se}\text{CO}_2(t) = Pt\text{CO}_2 \cdot (1 - e^{-\frac{t}{\tau}}), \quad (1.7)$$

It is trivial to recognize an exponential time-dependent function where the time constant depends on thickness of the skin, the diffusivity of CO₂ and height of the sensor. Acting on one of these three parameters changes the response time of the sensor.

For instance, increasing the temperature of the skin increases the diffusivity, reducing the time constant and hence the response time of the sensor. At the same time, in order to properly sense CO₂ variations without excessive latency, also the dimensions of the sensor's chamber must not be increased too much.

1.3.4. Currently developed devices

Context of application

The main target for wearable devices is to detach from clinical care and allow the possibility of monitoring the health status of the patient also in a different environment. In fact, BGA equipment is bulky and not suitable for a different context of application rather than in the hospital.

Moreover, even in a clinical contest, using a wearable device can decreased the occupied space because of the absence of wires and because of the small size.

Together with these perspectives, a wearable device for PtCO₂ measurement can also be used for monitoring in working environment. There may verify situations in which the operator is equipped with instrumentation that constitutes a barrier to ventilation, such as in metallurgic or chemical companies.

Furthermore, with the ongoing COVID-19 pandemic face masks have become an everyday life personal widget to prevent virus transmission, to be worn almost always. Investigating their impact on systemic CO₂ might be interesting.

As a final possible application, a wearable device can be implied in sport practice, especially in situations where the training environment is completely different with respect to the normal one. For instance, depending on the altitude, human respiration and circulation adapts to the different pressure conditions. Exercising at high altitudes where the oxygen partial pressure is lower can result in increased CO₂ production and easier fatigue.

In literature and on the market it is possible to find different examples of devices to detect PtCO₂, either with an electrochemical or optical working principle.

Electrochemical devices

In literature are present examples of electrochemical devices to measure carbon dioxide partial pressure used together with optical means to measure oxygen partial pressure [27], and the typical commercially available sensor to measure PtCO₂ uses the Stow-Severinghaus electrode.



Figure 1.8: Sentec Digital Monitor.

SenTec Digital Monitoring System (SDMS) in Figure 1.8 is a digital monitor for the continuous non-invasive monitoring of carbon dioxide and oxygen tension, together with saturation. Its usage is suggested in clinical environment and hospitals, while to be used at home it requires a medical prescription.

Moreover, it is a bulky and expensive device, making it unusable for home care and wireless wearable purposes. The working principle is the one of the electrochemical sensor; the skin is heated to promote local arterialization, CO_2 and O_2 diffuses and they are measured.

Data are then displayed on a digital monitor integrated in the device. It is not implemented any type of wireless connectivity with, for instance, a custom application or software to read interactively the collected data. In fact, in order to retrieve data and analyze them, it is necessary to connect to the device with a USB-RS232 cable. This wired connection can also be used to set the parameters of the SDMS and synchronize it [23].

The main limit in using an electrochemical approach for PtCO_2 sensing is the need of regularly reposition, re-membranization and calibration of the sensor. Therefore, this approach is not suitable in a telemedicine framework, requiring qualified staff to perform the mentioned procedures.

Optical devices

In 2005, Salzmann et al. designed a system using optical principles for gas sensing [9]. It consists of a spiral guide made of silicon nitride where CO_2 accumulates, together with a laser diode modulation spectrometry system. It represented a new sensing technology with respect to the already existing electrochemical one. In the same year, Kim et al. published an article where pCO_2 is measured adapting Lambert-Beer's law [18].

Later in 2016, Finci and Salzmann deposited a patent for a sensor for non-invasive measurement of pCO_2 in the skin of humans [11]. The sensor includes, in terms of macro

components: a housing, a gas measuring chamber where gas flow is supposed to be perpendicular with respect to the direction of incident light, a light source and two photodetectors. Infrared light is generated by the source (a LED), split with a beam splitter and sent to two photodetectors. The first photodetector is optimized for sensing light in a spectrum where it is absorbed by the CO₂ (4.26 um), while the second is designed to receive light in a spectrum where no gases absorb light (3.9 um). Subtracting the signal from the two detectors allows to retrieve the amount of CO₂ in the chamber.

In figure Figure 1.9 it is drawn the scheme of the sensor, where 18 indicates the two chimneys for carbon dioxide diffusion, 21 the light source, 15 the detectors, 23 the measuring chamber.

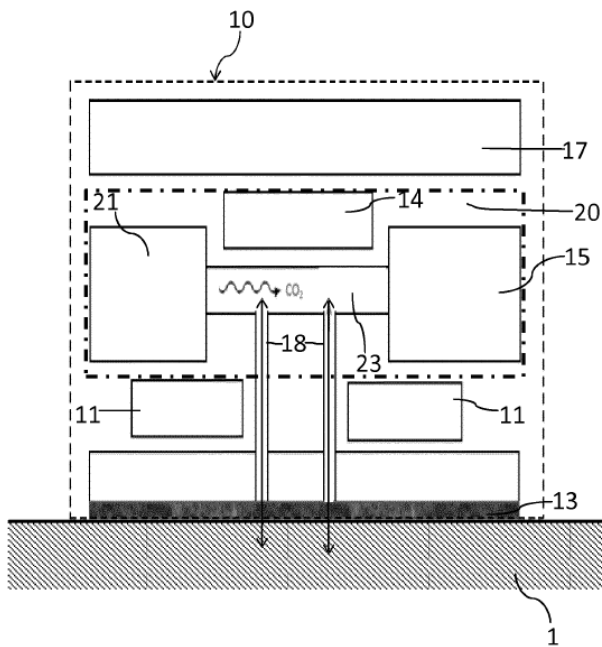


Figure 1.9: Schematic representation of the sensor created by Salzmann [11].

A more recent device has been designed by Tipparaju et al. in 2021 [26]. The device detects CO₂ by measuring infrared absorption at a wavelength of 4.26 um, according to Lambert-Beer's law. The CozIR® NDIR sensor is used for this scope, and also a hydrophobic membrane is deployed to prevent water molecules to interfere with the sensor, having conversely a high permeability to carbon dioxide. Furthermore, a sealing O-ring is added to the device to prevent leakages between the skin and the device's measuring chamber. However, this it doesn't heat the skin to promote arterialization and facilitate CO₂ diffusion.

Moreover, the device lacks of a in-situ microcontroller, with the data that are collected simply by connecting the CozIR sensor to a UART-USB interface.

Nonetheless, the device has been validated against EtCO₂ asking the subject to perform normal tasks such as sitting down, resting and normally breathing. It is observed that the CO₂ detected by the sensor reaches a plateau after a certain time interval, and variations in the plateau value correlate well with changes in EtCO₂ values. For instance, when the subject consumes black coffee, both PtCO₂ and EtCO₂ displayed a quick rise, even with a delay of 5 min circa between the two readings (EtCO₂ is more immediate). Conversely, during a hyperventilation maneuver, both transcutaneous CO₂ and end-tidal CO₂ show a decrease.

In [14] Grangeat et al. present a device for monitoring PtCO₂ in home healthcare applications. Measurements are performed using a differential measurement at two different wavelengths. 4.26 um is the wavelength to evaluate CO₂ absorption, while 3.91 um to get a reference signal. Moreover, the chamber for CO₂ collection has been implemented as a channel such that gas transportation occurs in it according to convection and not diffusion (Figure 1.10). The collection cell is in contact with the heated skin and collects CO₂ and fresh air coming from outside; the measurement cell includes a black body as a light source and two light detectors with the corresponding light filters selective to the specific wavelength; the evacuation cell let the gas flowing out to the environment. The device uses a BLE protocol to exchange data.

A first evaluation of the so-called CAPNO device during cardiopulmonary exercise test (CPET) shows a good behaviour of the device with respect to Sentec sensor, decreasing the fluctuations in measured PtCO₂. In a later study [15], the same authors tested the device in hypo and hypercapnia conditions. The response time of CAPNO is longer than Sentec device, and moreover it has been observed a strong influence on the ambient air CO₂ content on the detected CO₂ concentration.

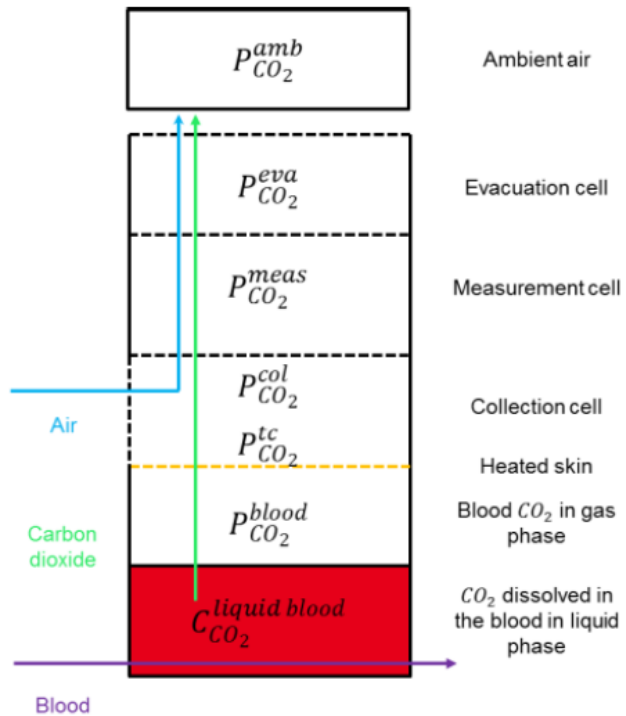


Figure 1.10: Schematization of the different chambers and fluid flux in the CAPNO device

2 | Materials and Methods

In this chapter the technical characteristics of the developed devices are presented. Moreover, firmware description is provided, together with the implementation of an application for smartphone devices able to connect to the previously mentioned device.

2.1. Device realization

The PCB has been developed on EAGLE CAD, an open-source software offered by AUTODESK. In designing the PCB, a peculiar attention has been given in trying to minimize as much as possible the sizes of the components so that they could fit properly in a small case. Indeed, in order to easily fit the board in a printed case, the dimensions have been chosen not to exceed, in terms of length and depth, the sizes of the 3D printed case.

In fact, dimensions of the case where to place the CozIR® sensor, the valve and the PCB can be decreased up to the point where there is still room to position the CozIR® sensor and the valve in a perpendicular fashion. Given that the valve has a length of 20.00 mm, and the sensor has a size of 31.00 x 19.50 mm, the case dimensions can not be decreased, without losing mechanical stability, further than 57.00 x 37.00 mm, arms not included.

These considerations allow to establish maximal dimensions for the PCB, knowing that it must fit in the case, and taking into account the possibility of further reducing the sizes due to safety margins to be accounted for if a closure to the case is also added.

The main components used for the PCB-based device are:

- Arduino Nano 33 BLE.
- NDIR CozIR sensor.
- Normally Open (NO) solenoid valve.
- N-channel transistors and voltage regulator
- Thermistors
- NiChrome wire

- 3.7V Lithium-Ion battery
- Momentary switch and tactile switch

2.1.1. Arduino Nano 33 BLE

This is used as microcontroller for the whole device. It is chosen because of the possibility of connecting it to other instruments via Bluetooth® Low Energy technology. By the same token, also an Arduino Nano 33 IoT can be used, that also adds the WiFi connectivity alongside the BLE one.

In the device the Arduino Nano 33 BLE is used in place of the Arduino Nano 33 BLE Sense. Both belonging to the ‘Nano’ family, they share the same pinout (as for the 33 IoT), but the 33 BLE is chosen over the 33 BLE Sense only because of the smaller price. Indeed, the only distinction between the two Arduino lies in some sensors (a motion sensor, a microphone, an optical module and a temperature sensor) already soldered on the PCB of the Arduino. Since these sensors are not useful in this work of thesis, the 33 BLE is the one selected for the previous consideration.

Beside this, a remark must be done also on the microcontroller directly placed on the Arduino board. For the 33 BLE and 33 BLE Sense it is the same, a 32-bit ARM® Cortex®-M4, the nRF52840 from Nordic Semiconductors. As for the 33 IoT it is the ARM® Cortex®-M0 32-bit SAMD21, whereas the WiFi and Bluetooth® connectivity is performed with a module from u-blox, the NINA-W10, a low power chipset operating in the 2.4GHz range.

All the three types of Arduinos can be easily programmed via Arduino IDE, the Arduino open-source software used to write code in C language and upload it on the Arduino board. However, choosing the 33 BLE or the 33 IoT results in different register-based programming of the microcontroller chip on the Arduino. For example, a timer interrupt is used to handle the sampling of the data coming from the CozIR® sensor; its byte-to-byte setting strongly depends on the chosen Arduino board.

Either way the source code is written both for the nRF52840 controller and for the SAMD21 one.

The nano 33 family is characterized by having 8 analog I/O pins and 14 digital I/O pins, also featuring UART, SPI and I2C communication protocols. The UART communication protocol is of paramount importance because it is necessary to dialogue with the CozIR® sensor.

The UART (Universal Asynchronous Receiver Transmitter) communication protocol does not require, differently from the USART, a common clock line to be shared between two devices that are transferring data. Hence it is necessary to select the same baud rate both for the Arduino and the sensor, so that there is an agreement on the data transfer.

With two different baud rates between the two devices it would be impossible to exchange meaningful data. Since the UART does not require a clock line to be shared, it features only 4 channels: a power supply line, a common ground and the transmitter and receiver lines, used to exchange data. Indeed, the information is unidirectional on the data line; the Arduino communicates to the sensor via the transmitting line, and receives data from the sensor on the receiving line. Hence the TX (transmitter) pin of the Arduino ends in the RX pin of the sensor, viceversa the RX (receiver) pin of the Arduino is connected to the TX pin of the CozIR® sensor. This is a consideration of paramount importance when designing the PCB.

The operating voltage for the Arduino board is of 3.3V, with each pin capable of providing at maximum 15mA of current. This current value is not sufficient to properly heat up the NiChrome wire and drive the solenoid valve, so two n-channel MOSFETs are used.

2.1.2. NDIR CO₂ Sensor

The sensor present in the device is the CozIR®-LP, a low power NDIR (Non-Dispersive Infrared) CO₂ sensor using solid-state LED optical technology provided by GSS. It has a typical measurement accuracy of 30 ppm, UART control and data interface and built-in auto-zeroing.

It is a compact and light device, that makes it ideal for a wearable device. It is ultra low-power consuming and it has a simple data communication interface, based on a UART protocol. Moreover, it is compatible with battery-powered devices, allowing the device to be used also in wireless equipments.

The dimensions of the sensor are 19.5 x 31.0 x 12.2 mm. The operating voltage is of 3.3V, compatible with the output voltage of the Arduino, with a maximal current consumption of 16mA during data acquisition. Since the output current from a pin of the Arduino is of 15mA, also the power supply of the CozIR sensor is attached to the output of the voltage regulator, hence having a current directly taken from the battery power supply.

It is based on a solid state NDIR LED optical technology and it has 6 pins to which the user can connect: power supply, ground, transmitting line and receiving line, while the last two pins are not connected.

When powered on, the typical time needed to obtain a valid measurement is of 3.3 s, compatible with the purpose of the overall device.

It has 3 modes of operation:

- Mode 0, command mode: the sensor is in sleep mode, waiting for commands. No measurements are made.
- Mode 1, streaming mode: this is the factory default setting, according to which measurements are reported twice per second. No polling operation is required by the user.
- Mode 2, polling mode: the sensor provides the data only when asked by the microcontroller. In the background, the sensor is still acquiring data, but their transmission is suppressed until a request for data comes.

The gas chamber has a LED with a nominal emitted wavelength of 4.25 um, and the light signal is received by a photodiode. The sensor has a built-in digital filtering, and the digital filter settings can be varied to cope with the requirements.

2.1.3. Solenoid valve

The valve serves the purpose of impeding or allowing the passage of the air between the outside environment and the chamber formed between the skin of the subject and the case of the device in the region where the sensor is placed.

In fact, during the time interval in which the skin is heated up before the measurement, the valve is left open to let air recirculate. Then, as soon as the skin has reached the correct temperature, the valve closes, blocking any possible exchange with the outer air. In this way it is possible to create a partially isolated system in which transcutaneous CO₂ can eventually accumulate and be sensed by the sensor.



Figure 2.1: Parker® Solenoid Valve.

The chosen valve is the PND-05A by Parker (Figure 2.1). It is a normally open (NO) valve, which means that, with no voltage provided to it, air is allowed to pass. As soon as a voltage is given, the valve closes. It is also a two-way valve, meaning that air can hence move from outside to inside or viceversa, depending on the pressure or concentration gradient across the valve. The PND-05A has a nominal operating voltage of 3V and it can withstand up to 250'000 life cycles. No requirement concerning the maximal input current is provided by the datasheet but, in order to be sure of its correct functioning, its pins are connected to the external battery of 3.7V with 5000mAh and a discharge current of 0.2 C₅A, hence more or less 1A at maximum. An *n*-channel MOSFET is used as a switch to drive the valve's function down resistance to keep the gate voltage fixed to 0V when the Arduino is not providing any voltage. In parallel to the

Moreover, a diode (D1) is placed in antiparallel to the valve to allow for the recirculation of current when the valve is switched off and prevent damages. The diode is kept in TH (through hole) configuration also on the PCB because easier to be eventually de-soldered

and re-soldered if burnt.

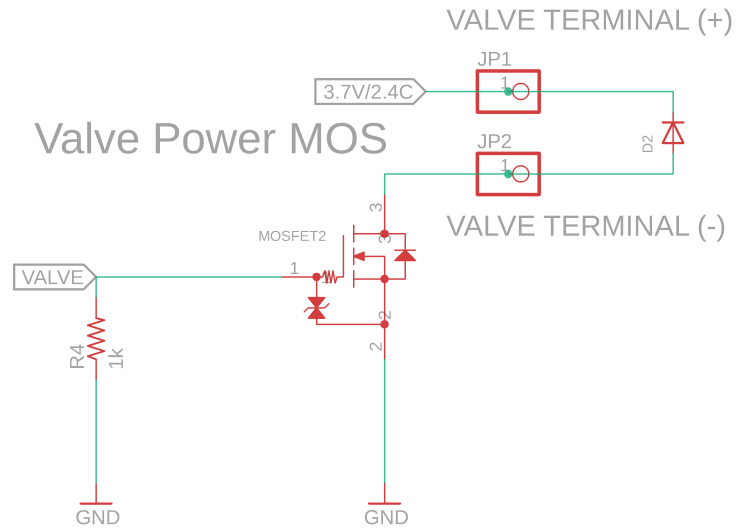


Figure 2.2: Solenoid Valve conditioning circuit.

2.1.4. N-channel MOSFETs and voltage regulator

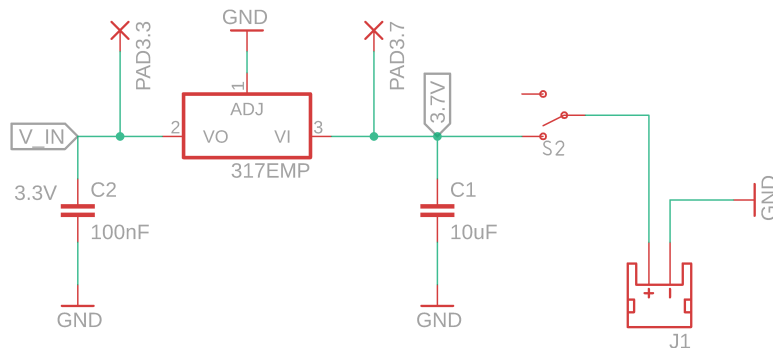
For what concerns the voltage regulator, the component chosen is belongs to the LD1117 series and it is produced by STMicroelectronics. Considering the source of the regulator put to ground, it can withstand $\pm 20V$ on the gate, and the output voltage depends on the package. A first choice was the LD1117V33, which has an output voltage of 3.3V and it comes in TO-220 configuration. This package is not ideal for a PCB implementation, so it has been changed to LD1117S33TR, which has a SOT-223 footprint.

One of the important features of the voltage regulator is the low dropout voltage, that is the smallest difference between the input and output voltage the regulator can provide, that is in this case less than 1V.

In fact, the highest voltage with which the whole device works is the 4.2V coming from the battery. Since the dropout voltage is smaller than 1V, having 4.2V is still acceptable to be converted in 3.2V in output from the regulator (value measured with a voltmeter), being also able to provide up to 800 mA of output current. Other voltage regulators might be used, but if the dropout voltage is higher, the output voltage from the regulator will be also lower than the one defined on the datasheet.

The output voltage from the regulator is then provided to the 3.3V of the Arduino to power it. Theoretically, the Arduino has a pin that can be used to input a voltage, but its input voltage range is between 6V and 20V, so it can not be practically used.

In order to keep stable the output and input voltages, two capacitors are added in parallel to the regulator. The output capacitor is of 10uF, while the input capacitor is of 100nF, as can be seen from Figure 2.3.

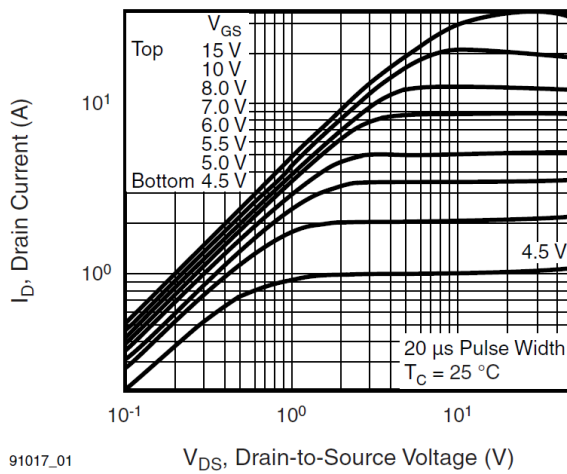


3.7V Battery Power supply

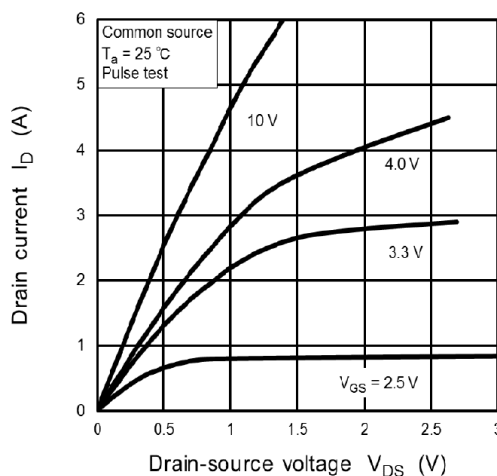
Figure 2.3: Voltage regulator conditioning circuit.

As for the N-channel MOSFETs, as previously mentioned, they are two and used as switches to drive both the valve and the Nichrome wire. A first choice of MOSFETs were the IRF520, with TO-220 footprint. The most important feature that must be considered when selecting the transistor is the drain current that passes given a specific gate-source voltage and drain-source voltage.

Keeping in mind that the maximum voltage that the Arduino can provide between gate and source, given that the source is put to ground, is of 3.3V, looking at the datasheet, if the drain is put to the 4.2V of the battery, the IRF520 allows almost 600mA (Figure 2.4a).



(a) IRF520 V_{DS} vs I_D characteristic curve.



(b) SSM3K2615R V_{DS} vs I_D characteristic curve.

Figure 2.4: Comparison between IRF520 (a) and SSM3K2615R (b) on the drain-to-source voltage (V_{DS}) versus drain current (I_D) relationship at 25 °C.

In order to miniaturize these transistors, the choice was the SSM3K2615R produced by Toshiba.

Besides the smaller dimensions because of the SOT-23F footprint, this N-channel MOS-FET features also good electrical characteristics. If the allowed drain current is compared with the V_{GS} and V_{DS} , it is noticeable that already with 3.3V the allowed current is more than 1A (Figure 2.4b).

One side note must be done concerning heating issues. Indeed, during its activation, the IRF520 was showing an increase in temperature due to the current passing through it. This was a major issue mainly because the transistor was placed outside the case, and hence an eventual contact with it could have resulted in a burn. The same issue, even though more reduced, is still present with the SSM3K2615R. However, its position in the PCB is under the Arduino, hence preventing possible contacts. Moreover, the whole PCB is integrated in a plastic case, further reducing this risk.

2.1.5. Thermistors and resistances

The thermistors are used to measure the temperature of the Nichrome wire and of the skin. They are NTC (Negative Temperature Coefficient), meaning that the resistance of the sensor decreases as the temperature increases. Since they are made from semiconductors, the decrease in resistance is due to the higher presence of charge carriers, coming from the valence band, in the conduction band, due to thermal promotion.

The chosen thermistor is the NXRT15WF104FA1B040 by muRata Electronics; it is in through hole configuration with a resistance of 100 kOhm at 25°C. The size of the cap is of 0.5 x 0.4 mm. This is a choice performed to decrease the thermal resistance of the cap and be more sensitive to the temperature of the skin.

The TH configuration is necessary because one thermistor must be placed in contact with the skin, and one in contact with the Nichrome wire, and both are far from the PCB.

As for the readout circuit, the thermistors are simply placed in a voltage divider configuration with another resistance of 100 kOhm. Theoretically, to achieve better sensitivity and linearity, a quarter Wheatstone bridge would be better, but since measuring the exact temperature with high sensitivity is not strictly necessary, a simple voltage divider is preferred, also because it saves space on the PCB.

One final note concerning the resistors. All the resistors soldered on the PCB are SMD (Surface Mounting Device) resistors, with the 0603 footprint. This is a footprint still sufficiently large to perform, in case of need, de-soldering and re-soldering, if one's resistance value has to be changed.

2.1.6. Nichrome wire and Lithium-Ion battery

The Nichrome wire is characterized by a resistivity of 5.755 Ohm/m.

The length of the wire is of 18 cm, resulting in an overall resistance provided by the wire of 1 Ohm, so small that with an applied external voltage the wire was seen as a short circuit instead of a proper resistance. This is also the reason why it is needed to have a very high V_{GS} voltage for the MOSFET driving the switch. The higher the V_{GS} , the higher the amount of drain current that can even reach values of 1A. This also explains the self-heating phenomenon observed in the MOSFET driving the wire.

For what concerns the battery, it is a lithium-ion battery with nominal voltage of 3.7V. Despite this, when fully charged, the battery is able to provide up to 4.2V. The choice of Li-Ion battery lies also in the possibility of recharging. The capacity for the selected battery is of 5000 mAh, and since the discharge current can be up to $0.5 C_5 A$, it means

that it can provide up to 2.5A. This is useful because the battery provides voltage and also current to the wire, creating an external loop whose activation is driven by a signal on the gate of the MOSFET connected to an Arduino pin. Thus, both issues concerning the maximal output current from the Arduino and voltage across the wire to develop a significant current are overcome.

It is important to underline that the voltage drop across the wire is not exactly the battery voltage when the switch is closed. Indeed, of the 4.2V battery voltage, only 1.3V fall on the wire (tested with a voltmeter). This is due to the fact that, even if the source of the MOSFET is put to ground, the PCB traces themselves are resistive, subtracting voltage due to the resistive divider occurring between the PCB trace between power supply and the wire, the wire itself, and the trace between the wire and ground.

To reduce this problem wires with higher resistivity per meter has been tested, resulting in an overall worst performance because of the incapability to properly heat up.

This is not a problematic issue, because already 1.3V over a 1Ohm resistance are sufficient to generate enough current to correctly heat the wire up.

The wire driving circuit is the same seen for the valve with the only difference that the diode is missing (Figure 2.5). JP3 and JP4 still represent the terminals to which the Nichrome wire should be attached, but it cannot be directly soldered on the PCB. Hence normal copper wires are soldered to the PCB, and then the two free extremities are wounded around the Nichrome wire to create an electric contact without the need of soldering.

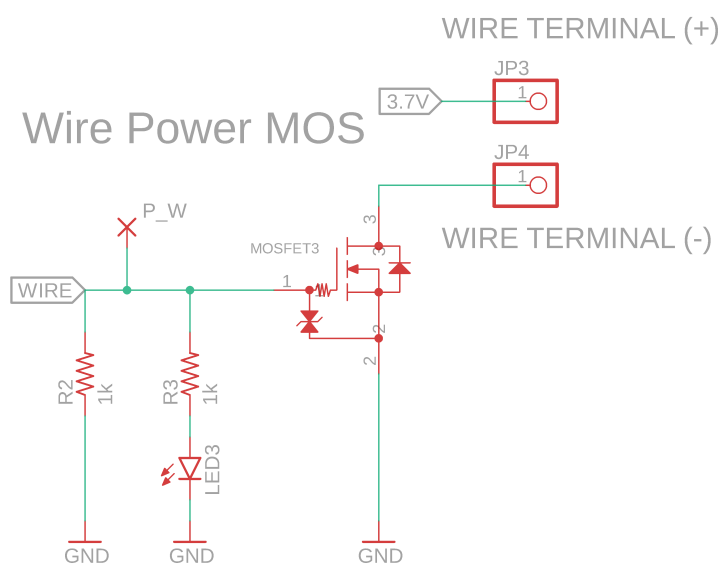


Figure 2.5: Nichrome Wire conditioning circuit.

2.1.7. Momentary switch and tactile switch

The momentary switch is used to drive the functioning of the Arduino. With the switch is actually possible to start the measuring process, stop the heating of the wire or stop the measurement. It is in pull-up configuration, meaning that as soon as the switch is pressed, the value read by the Arduino is a logic ‘0’, whereas normally it reads a logic ‘1’ (i.e. 3.3V). Moreover, an hardware low pass filter is implemented on the line connecting the switch and the Arduino with the purpose of preventing the bouncing of the signal.

The tactile switch is used to connect or disconnect the battery power supply from the PCB. Its pins are connected to the battery, ground and in input to the voltage regulator.

The overall device schematic is presented in Appendix A: PCB Version 1.

2.2. PCB Design

In this section it is explained how the PCB has been designed and the choice of the components' layout.

2.2.1. Software and tools

The software used to design the PCB is Eagle, provided by Autodesk. This choice also allows to render the PCB in a 3D fashion thanks to the interconnection with Fusion 360, a CAD software still belonging to Autodesk.

The size of the PCB is of 46.00 x 31.60 mm (Figure 2.6), hence sufficiently small to be easily placed in a plastic case of 57.00 x 37.00 mm. Most of the SMD components are placed under the Arduino board. In fact, the two green piles of 15 pins each represent the footprint for the Arduino, that will be soldered on the PCB with a 0.50 cm gap with respect to the surface of the PCB; this placement leaves room for SMD components to be placed under it, i.e. in the middle of the board between the Arduino footprint.

The two thermistors for measuring wire and skin temperatures are in the upper part of the PCB, but their position in the PCB area doesn't have to fulfill any particular requirement, because the electrical link can be eventually extended with copper wires.

The same reasoning does not apply for the valve, wire and sensor pins. The valve's pins have to be located as close as possible in the valve region of the plastic case, so that the wiring is not complex. As for the sensor's pins and wire's pin, they must be placed over the sensor area. In fact, the housing for the sensor in the case has to be covered with a closure to seal the chamber, and to avoid difficult wirings it is better to place the pins in the PCB in the region that is just over the aperture for wires in the plastic closure.

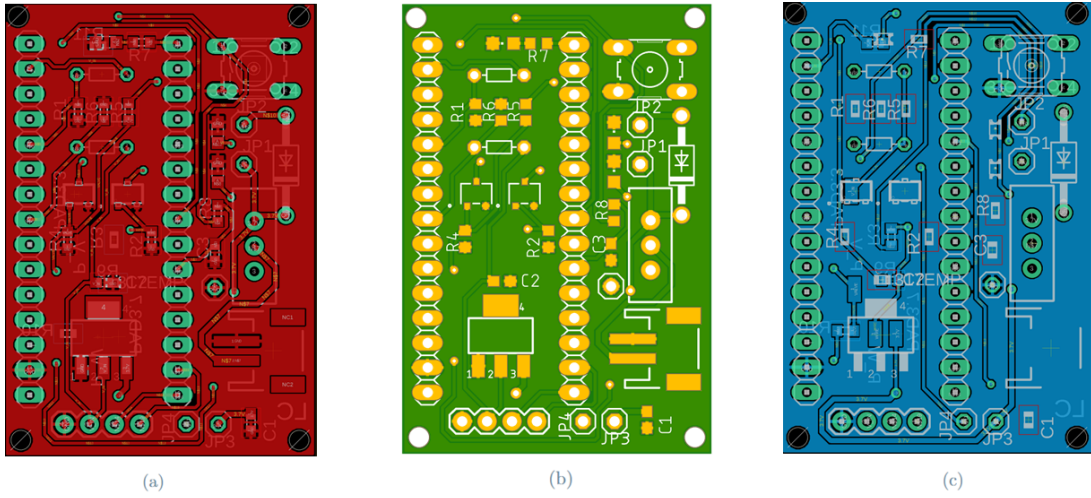


Figure 2.6: Board Panel. (a) is the Top Layer, (b) is the Manufacturing Preview, (c) is the Bottom Layer.

Furthermore, the battery connector has to find a place as close as possible to the PCB border, otherwise plugging the battery in to power the device would be difficult.

The components are placed both on the top and bottom layers, using a trace width of 0.3 mm to connect all the component except for the traces connecting the battery, the wire, and the transistor, where the width has been increased up to 0.5 mm, to decrease the trace resistance.

Also, LEDs indicating the activation of the wire and the valve are not placed below the Arduino, otherwise their blinking would not be observed. In fact, their activation is still noticed even if an overall closure for the PCB is implemented because the upper surface of the closure is made so thin that light can still be seen through.

2.3. Further PCB Improvements

If other features needed to be included in the circuit, a possible improvement of the device design could be the following. Besides the components already present in the first PCB design, it is possible to add:

- A Micro-USB recharge module.
- MOSFET temperature sensing.
- Battery level monitor.
- A DC Brushless motor fan

2.3.1. Micro-USB recharge module

In the first PCB design no recharge module was included, differently from the first prototype. Hence, any external LiPo battery charger can be used to charge the battery.

However, also the possibility of directly recharging the battery without unplugging it might be interesting. In a further PCB development, a LiPo recharge module can be added. The possible choice is the MCP73831 by Microchip. It is specifically designed for charging circuits for LiPo batteries, it has an output voltage of 4.2V and a programmable charge current between 15mA and 500mA that can be selected by connecting a proper external resistor.

Given that the used battery has a capacity of 5000mAh, a recharge current of 500mA would be ideal.

The MCP73831 employs a constant-current/constant voltage charge algorithm that is also capable to detect when the battery is fully charged and stop the charging.

As for the external connector, a micro-USB connector can then be used to attach the device to a socket for recharging.

2.3.2. MOSFET temperature sensing

The major issue observed when activating the MOSFET switch that drives the heating of the wire is the transistor's self-heating. This was due to the high amount of current forced to pass through the transistor.

In order to limit the possibility of reaching very high temperature for the MOSFET and for the board to which it is soldered, one idea is to place a temperature sensor close to it to sense the variation of temperature. To achieve this goal, a NTC thermistor in SMD

configuration is placed next to the MOSFET on the PCB; the idea is that, as soon as the temperature sensed by the thermistor exceeds a given value, a proportional decrease of the gate voltage on the transistor is provided. It is a negative feedback loop in which the temperature of the MOSFET is kept within safe levels regulating the gate-source voltage solely on the basis of the temperature sensed by the thermistor.

The conditioning circuit for the thermistor is a simple voltage divider with a 10kOhm resistance, because the thermistor resistance at 25°C is of 10kOhm. Again, the consideration about the Wheatstone bridge done in section 2.1.5 still holds.

2.3.3. Battery level monitor

As it is now, the device is not capable of understanding the remaining battery during its usage. To overcome this problem, a simple voltage divider can be used to track the nominal voltage the battery provides to the PCB. Since the analog pins of the Arduino Nano can receive in input 3.3V as maximal sensed value, having 3.8V or 4.2V in input from the battery to the pin would be indistinguishable. Because of this, the battery voltage is read out at the middle point of a voltage divider consisting of a 1kOhm resistance and 220Ohm resistance.

2.3.4. Motor Fan

A DC motor fan can be introduce to washout the CO₂ from the chamber to prevent saturation when an excessive amount of carbon dioxide accumulates. The fan has to be compact to be easily included in the case, with small operating voltage and current to be compatible with the power supply of the already existing device.

One possible choice is the Axial Motor Fan produced by Sunon®. It has a weight of 0.56 g and the dimensions are 10 x 10 x 3 mm. It has an operating voltage between 2.0 and 3.5VDC, with a rated current of 96mA. Certainly, since the require current exceeds the output current from an Arduino pin, it is necessary to connect the fan to the battery power supply and drive its activation with a switch, as it is done for the valve and the nichrome wire.

In Figure 2.7 is presented a possible PCB implementation. More details on the device hardware connections are present in Appendix B: PCB Version 2.

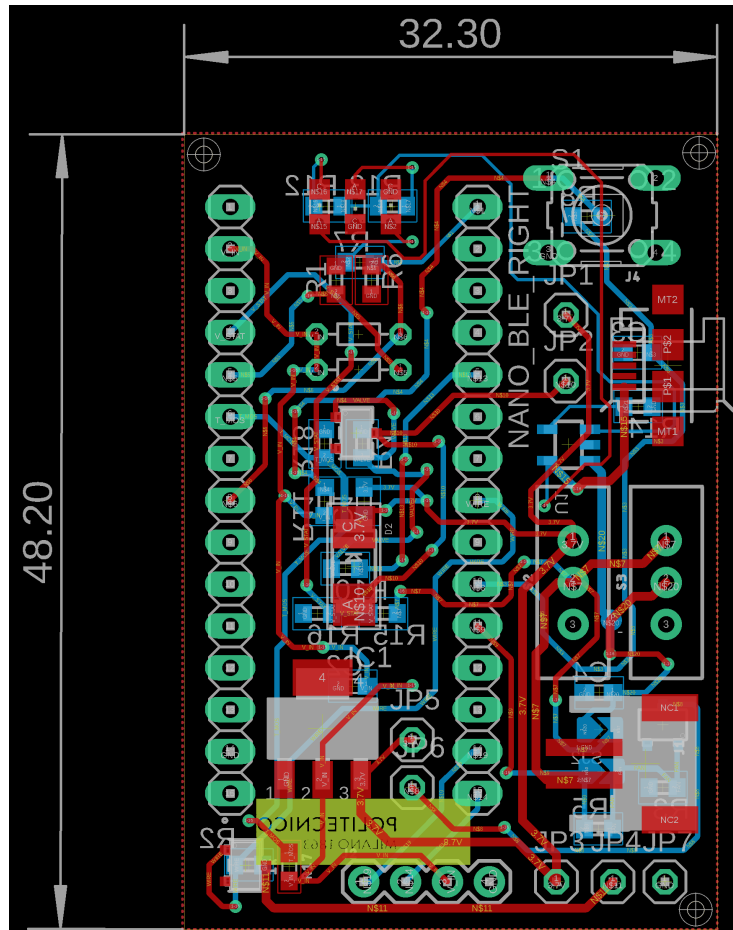


Figure 2.7: PCB tracks, pads, pins, vias and components positioning of the second version of the device. The ground plane is not visible for the sake of transparency with respect to the components.

2.4. Case

The 3D-printed case is designed in Fusion 360. The case has a dimension of 57.22 x 37.00 x 35.97 mm, closure included.

The material used to print the case is the *VeroGrayTM*, which has a tensile strength of 50 – 65 MPa, and a glass transition temperature $T_g = 54^\circ\text{C}$.

The device is not printed with classical printing filament material such as ABS, which has a T_g between 61.9°C and 76.9°C . Having a lower glass transition temperature is not an issue in this case configuration. Indeed, thanks to the placement of the wire, it is impossible to exceed a given temperature, that is decided as 42.0°C (this specific value will be clarified later).

The 3D print is not with a fused-filament technique, but the case is obtained by polymerization. According to this process, layers of polymer are deposited one over the other, leading to a final result that has an overall resolution typically better than the one of the fused-filament technique.

When being printed, the *VeroGrayTM* needs also layers of supporting material in the empty regions of the case. They need to be subsequently removed via NaOH at 1% bath. Eventually, since the air channel that connects the chamber with the external environment may be difficulty reached by the NaOH, using also an air-compressed jet might be practical to free the duct form the supporting material.

The overall case can be divided in 3 main parts. A base, that has to host the valve, the sensor, the wire and the PCB; a cover to hermetically close the sensor area; a bigger closure that must compose with the base to encapsulate the PCB.

The CozIR® sensor is placed perpendicularly with respect to the case longitudinal direction, 3 mm over the bottom of the base. Between the sensor and the base, room is created to host the wire. Indeed, instead of placing the wire inside the sensor area and separate it from the skin with a layer of polymer belonging to the case, in this new version the layer of polymer is separating the sensor and the wire, with the wire completely immersed in a thermal paste that is then in contact with the skin.

In this way it is ensured that the temperature of the wire sensed by the thermistor that contact with it, of the thermal paste that covers the wire and the thermistor, and of the skin, is exactly the same, because the problem of transferring the heat across the plastic of the case is not existing anymore.

This workaround makes also obsolete the use of a second thermistor to sense the temperature of the skin.

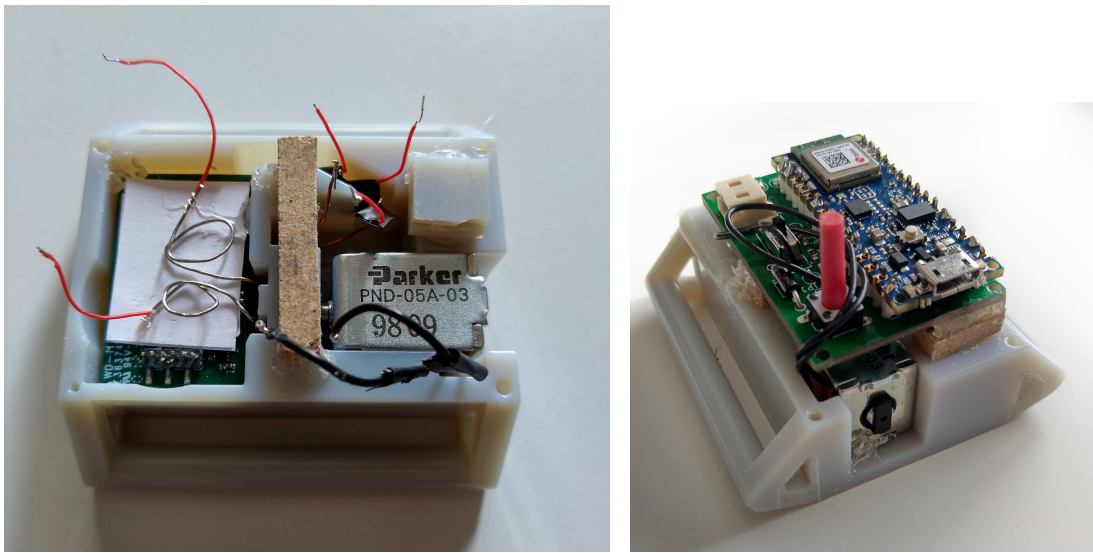
Although the housing for this second temperature sensor is still included in the case design, its use is not necessary. In fact, given that the second thermistor is not exactly in the region where the heated skin is, that is the region where the chamber to accumulate CO₂ generates, the temperature that it measures is not exactly the skin temperature, but it is the skin temperature minus a variation in temperature due to the thermal resistivity of the skin in the path between the heating region and this second sensing region.

Since now the wire is directly heating the skin, of course through the thermal paste, the overall temperature that the wire's thermistor senses is also the temperature of the skin. For this reason, exceeding with temperatures higher than a prefixed threshold, e.g. 37.5°C, is impossible, because the Arduino would sense through the thermistor the increase in temperature and deactivate the MOSFET that drives the wire.

The valve is positioned in a perpendicular fashion with respect to the CozIR® sensor with the purpose of allowing or impeding the passage of air through the duct that links the chamber generated above the skin with the external environment out of the case.

Then, the sensor area is covered with a closure that has a small hole for the passage of wires. This is needed to seal the sensor in a closed environment, preventing leakages that could have altered the measurement. Theoretically, once the valve is closed, no air can pass in the duct, and no air hence exits from the chamber.

A detailed description of the case and the 3D rendering are provided in Appendix C: Case 3D rendering and dimensioning.



(a) Bottom of the case and components inside. (b) PCB anchored to the bottom of the case.

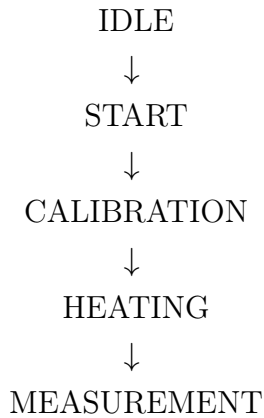
Figure 2.8: (a) Components inside the device; it can be seen the solenoidal valve, the NiCrome wire, the CozIR sensor. (b) Assembled device with the bottom part of the case and PCB.

2.5. Firmware

The firmware is written on Arduino Software (IDE), a cross-platform application (for Windows, macOS, Linux) that is based on functions from C and C++.

The firmware is designed as a state machine with three central main states: ambient CO₂ measurement, heating and skin CO₂ measurement.

The following is a very simplified overview of the five different states in which the firmware is subdivided.



Paring with a Bluetooth device is not necessary to run the hardware. In fact, connection with a custom BLE application is required only if data needs to be displayed on a smartphone. Otherwise, cable connection with a PC is sufficient. Moreover, this firmware version supports both cable connection and BLE connection at the same time or one independently from the other.

A detailed schematic configuration of the firmware is presented in Figure 2.9.

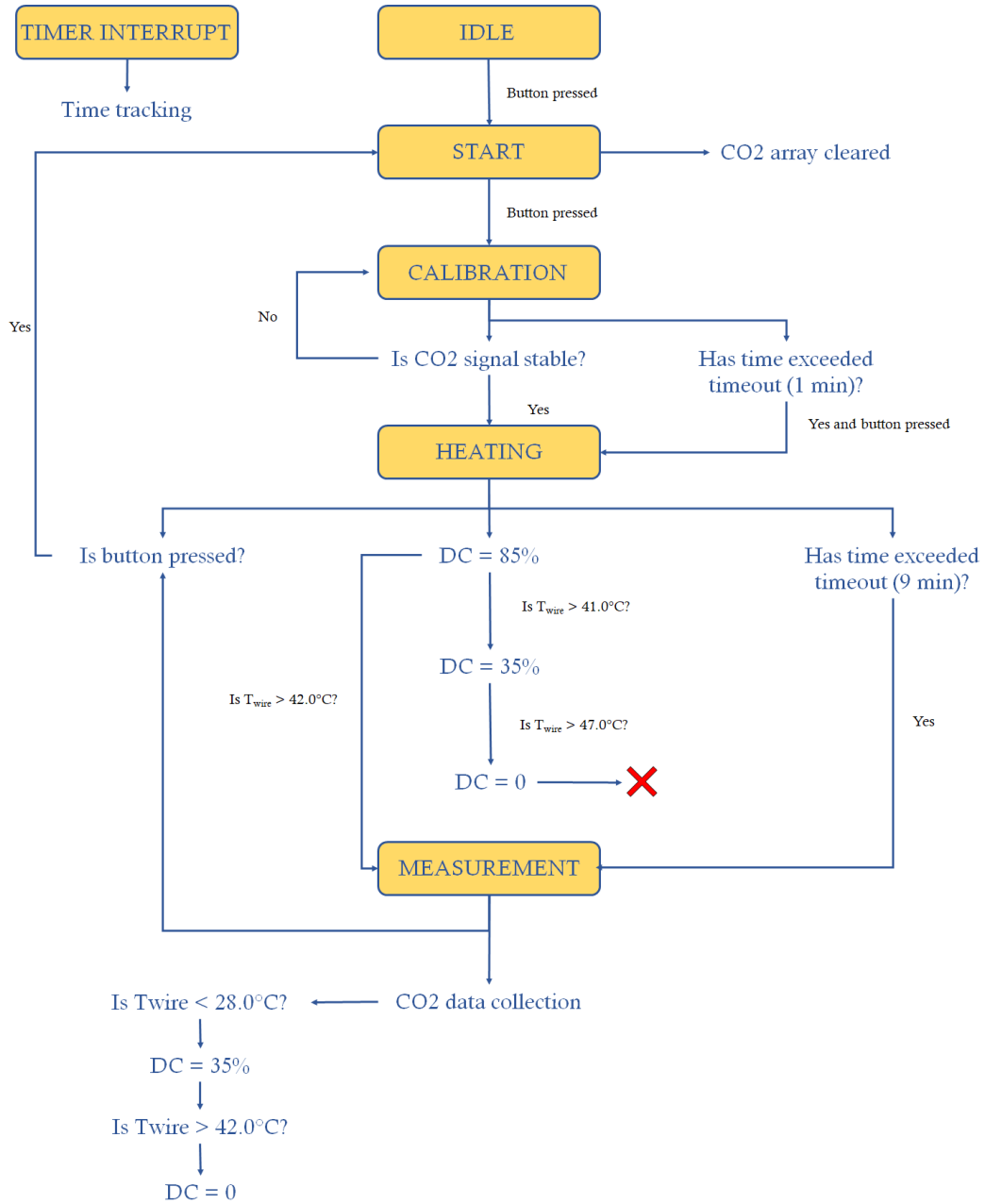


Figure 2.9: Workflow of the firmware. When powered on, the device is in the IDLE state. By pressing the user-button the state moves to START, where previously stored data are cancelled. If the button is pressed again, CALIBRATION begins and, when the signal is stable or the user-button is pressed after 1 min, the state changes to HEATING. Here the duty cycle (DC) is regulated so that temperature of the skin reaches 42.0 °C without harming the subject. When the target temperature is reached, the valve is closed and MEASUREMENT state begins.

2.5.1. Timer Interrupt

An interrupt is an asynchronous interruption of the normal workflow of the processor in order to carry out different tasks. A timer interrupt is introduced to track time and regulate sensor's sampling, and it is set on a time interval of 1 s.

Its simple implementation is needed to provide the firmware some timers that check the elapsed time. In fact, the timer interrupt is used during the calibration phase to verify if the calibration is lasting more than 1 min. Similarly, it is also used during the heating phase to check if 9 min are passed. In order to have a proper time base, also during the measurement phase the timer interrupt tracks time.

Moreover, in the Timer Interrupt flags to regulate the sampling of data are managed. Flags are three: one for the calibration phase, one for the heating phase and one for the measurement phase when data are collected. In this way it is possible to get rid of delays existing in the previous version of the device, which represent a waste of resources for the microprocessor. Furthermore, having a timer interrupt allows to have data collected at specific time instants, without having variable delta times between consecutive samples.

2.5.2. Idle State

This state is introduced in order to start the hardware in a known configuration, without any specific task to be performed by the microcontroller. In the idle state the CO₂ values are not sampled, nor the skin is heated.

This state can be useful if a device must be connected to the Arduino. Since nothing is happening at the hardware level, this ensures a connection without any loss of data. Moreover, it also allows to power on the device and wear it.

2.5.3. Start State

In the start state the CO₂ array is cleared, and the device waits for the pression of the button to move to the calibration state. Also in this state no data sampling is performed.

2.5.4. Calibration State

In the calibration state CO₂ data from the sensor are collected and analyzed to check if the signal is stable. The purpose of this state is to find the ambient CO₂ value that will serve as a reference for the computation of the differential signal with the CO₂ value retrieved during the later measurement phase.

CO₂ data are sampled with 1Hz frequency from the sensor (according to the timer inter-

rupt frequency), collected in an array and then evaluated. To assess if the signal is stable, the first and last element of the array are compared, and if the difference between them is smaller than 20 ppm in absolute value the signal is considered stable. If not, the array is shifted, new values are added, and the same procedure is performed with the subsequent 10 samples.

Even if this seems a trivial procedure, it is good enough to check if the signal is not stable due to drift of the value. In fact, when the signal is constantly decreasing and it is not stable, the calibration procedure would continue up to the point where the previously mentioned condition is met.

Concurrently with the calibration procedure, a green LED on the PCB is toggled every second. When it is permanently switched on the calibration has ended and by pressing the user button the firmware moves to the heating phase.

During the calibration procedure, if the user wants to stop it before the signal is actually stable, it is possible to wait 1 min and then eventually press the button to pass immediately to the heating phase. If the button is pressed and the signal is neither stable nor the time has crossed 1 min, nothing will happen.

2.5.5. Heating State

In the heating phase the skin of the user is heated. The heating process starts by setting the Duty Cycle (DC) of an output pin of the Arduino to 85%. Since the output voltage of an Arduino nano pin is of 3.3V, the average voltage that will be seen by the gate of the n-MOSFET used as a switch to drive the nichrome wire is of 2.85V.

The current flowing in the nichrome wire will heat the metallic filament, resulting in an increase of temperature. The temperature of the wire is measured with a thermistor and sampled with a frequency of 1 Hz.

In the current version of the device, the wire, the thermistor and the skin are experiencing the same temperature, because they are all in contact with the same medium, that is the thermal paste. Even if the case is still designed to host a possible second thermistor to measure skin temperature in another site, at firmware level its value is not sampled. In fact, theoretically knowing the temperature of the thermistor in the thermal paste should be sufficient to also know the temperature of the skin.

As soon as the temperature reaches 42.0°C the heating phase ends, the DC is set to 0 and the device automatically passes to the measurement phase.

Even if theoretically a feedback control over the temperature of the wire is not strictly

needed, for safe reasoning it is decided to reduce the DC to 35% if temperature exceeds 41.0°C, and to 0 if temperature exceeds 44°C. The feedback loop is not needed because in this new configuration there is not the risk for the wire to cross the 37.5°C threshold, because as soon as this happens, the device autonomously moves to the measurement state, preventing further heating of the skin.

Also in the heating state a timeout of 9 min is set. If in 9 min the temperature of the skin does not reach 37.5°C the heating state is automatically ended, and the device shifts to the measurement phase.

2.5.6. Measurement State

In the measurement phase the valve, that has been open for all the previous phases, is closed.

Data are sampled from the sensor in polling mode with a sampling frequency of 1 Hz. If the button is pressed, the measurement state ends and the device returns to the start state.

In this phase there is also a check over the skin temperature. If temperature goes below 28°C the heating process is started alongside the measurement one, up until the temperature crosses 42.0°C.

2.6. Software

In this section it is presented a short insight on the Bluetooth® and Bluetooth Low Energy (BLE) connectivity and the functioning of the developed application.

2.6.1. BLUETOOTH® AND BLUETOOTH LOW ENERGY

General description

In the field of healthcare, an increasing urge to develop wireless system to monitor the health status of the patient is observed. Until now, there are four main wireless technologies: Wi-Fi, ZigBee, Bluetooth® and Bluetooth low energy [20]. Despite the technology chosen, the wireless communication should fulfill some requirements:

- **Interoperability:** ensuring that products from different manufacturer can interact one with the other.
- **Low-power operation:** this is done in order to reduce maintenance and running costs.
- **Customized software** for medical applications.
- **Compatibility:** to ensure the coexistence between other radio services without causing electromagnetic interference.
- **Secure transmission of data**

The Bluetooth® technology is a short-range communications system aimed at replacing the fixed electronic devices and connecting cables, and meets all the requirements thanks to its key features that are robustness, low power consumption and low cost.

There exist two forms of Bluetooth technology, that are Basic Rate (BR) and Low Energy (LE). Both systems include device discovery, connection establishment and connection mechanisms.

The great advantage of BLE with respect to Bluetooth BR is the lower complexity and lower cost, including also features specifically designed for products that require low current consumption.

In order to have communicating devices, it is necessary to have both the protocols implemented. BLE and Bluetooth BR can not interface directly [30].

Despite the protocol, the Bluetooth core system consists of a Host and one or more Controllers. The former is a logical entity defined as all the layers above the Host Controller Interface (HCI), while the latter is still a logical entity defined as all the layers below the

HCI. The HCI is a thin layer which transports commands and events between the Host and Controller elements of the Bluetooth protocol stack.

So far, devices that implement a Bluetooth protocol can be divided in two classes: single-mode devices, that implement only Bluetooth BR or BLE, and dual-mode devices, that implement both classic Bluetooth and BLE.

Bluetooth Low Energy

Bluetooth Low Energy is developed by Bluetooth Special Interest Group for short range communication [12]. Like in classic Bluetooth, the BLE protocol stack is composed of two main parts: the Host and the Controller, as previously mentioned.

The Controller includes the Physical Layer and the Link Layer, and it is normally implemented as a small System on Chip with an integrated radio. Instead, the Host runs on an application processor and includes more sophisticated functionalities, like the Attribute Protocol (ATT), the Generic Attribute Profile (GATT) and the Generic Access Profile (GAP) (Figure 2.10).

Physical layer For what concerns the physical layer, the BLE operates in the 2.4 GHz band and defines 40 radio frequency channels with 2 MHz spacing. The types of channels are two: advertising channels and data channels. The former are used for device discovery, connection and broadcast transmission, whilst the latter are implied in bidirectional communication between connected devices.

Overall, the coverage of the BLE is of various tens of meters.

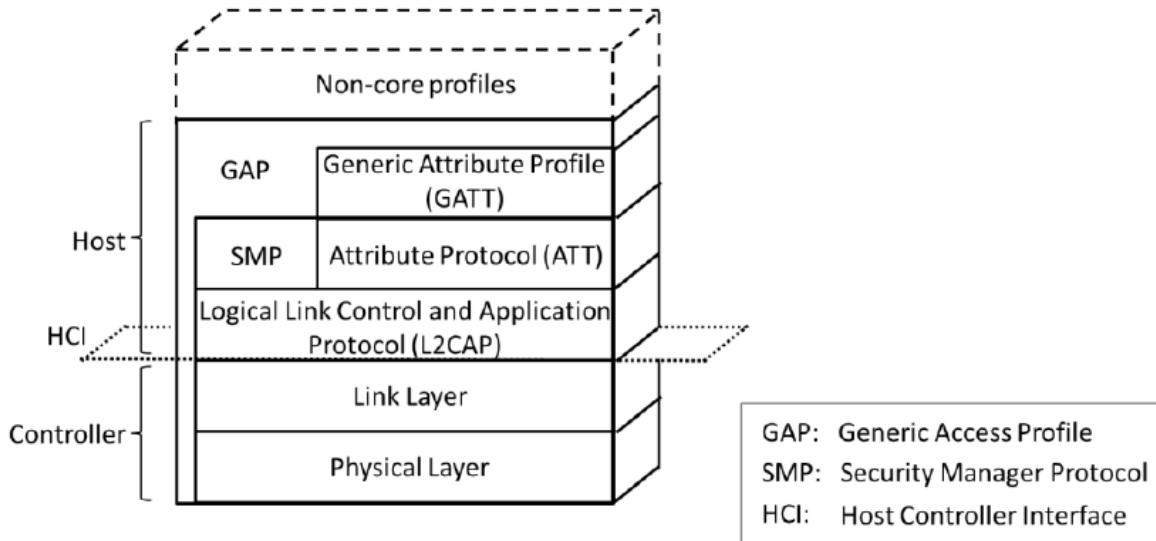


Figure 2.10: BLE protocol stack from [12].

Link layer Two types of communication can occur when using the BLE technology: broadcast data transmission and bidirectional data transmission.

In the case of broadcast communication, only a device needs to send data and it transmits them in the form of packets through the advertising channel. Any device that transmits these packets is called advertiser. The other devices only aim at receiving data, and are called scanners.

As for bidirectional data communication, this occurs between two devices that must be in connection one with the other.

The connection between two devices is an asymmetric procedure according to which the advertiser communicates through the advertising channels that other device can connect to him. As soon as a device listens such advertisements, it sends a connection request to the advertiser in order to create a point-to-point connection. This communication happens in the physical layer.

For the created connection, at the level of the Link Layer, BLE defines two device roles: the master and the slave. The first initiates the connection, while the second sends the connection request.

A master can have several concurrent connections with various and different slaves, but a slave can connect only to one master.

One of the main features of BLE lies in the communication between the master and the slaves. In fact, in order to save energy, slaves are normally in sleep mode and wake up from time to time to receive possible packets from the master.

Once the connection exists, the physical layer is subdivided into non-overlapping time slots named *connection events*. Inside one connection event all the packets are transmitted. There is a control of the flow in the sense that if the slave gets a packet, it must also send a packet to the master in response. However, the master is not required to send a packet when one from the slave is received.

In order to detect possible losses of connection, a supervision timeout is used. Since the time the last packet is received, a counter checks if the elapsed time exceeds the *supervision timeout*, that is in the range between 100 ms and 32 s. When time passes over this selected value, the connection is lost.

2.6.2. The Smartphone Application

In this subsection it is described how the developed application works and the choices done to optimize data acquisition and visualization.

Plug-ins

In order to manage the Bluetooth® technology, the generation of CSV data with the acquired information from the BLE peripheral and the creation of charts, some plug-ins are added in the *pubspec.yaml* file of the application.

Packages included are:

- **flutter_blue 0.8.0**: to manage BLE connections.
- **syncfusion_flutter_charts 19.4.56**: to generate data charts.
- **csv 5.0.1**: to create and export files in CSV format.
- **path_provider 2.0.9**: to manage CSV files download.
- **permission_handler 9.2.0**: to manage permissions.
- **file_picker 4.5.1**: to manage access to stored file and data.
- **external_path 1.0.1**: to retrieve internal smartphone paths and write to them.
- **wavelock 0.6.1**: to handle smartphone's lock screen.
- **firebase_auth 3.3.13**: to manage Google Firebase authentication modules.
- **firebase_storage 10.2.11**: to manage Google Firebase storage modules.
- **firebase_core 1.14.0**: to manage Google Firebase plug-ins.
- **provider 6.0.2**
- **email_validator 2.0.0**: to validate email addresses.
- **url_launcher 6.0.20**: to allow URL addresses opening in the browser.
- **syncfusion_flutter_pdfviewer 19.9.56**: to open PDF files inside the application.
- **flutter_local_notifications 9.4.0**: to generate push notifications from the application.
- **dio 4.0.6**: to manage internet connections.

- **google_sign_in 5.3.0**: to manage Google log in method to the application.
- **open_file 3.2.1**: to open files with smartphone's predefined application. This package is intended to be used together with the file_picker package.

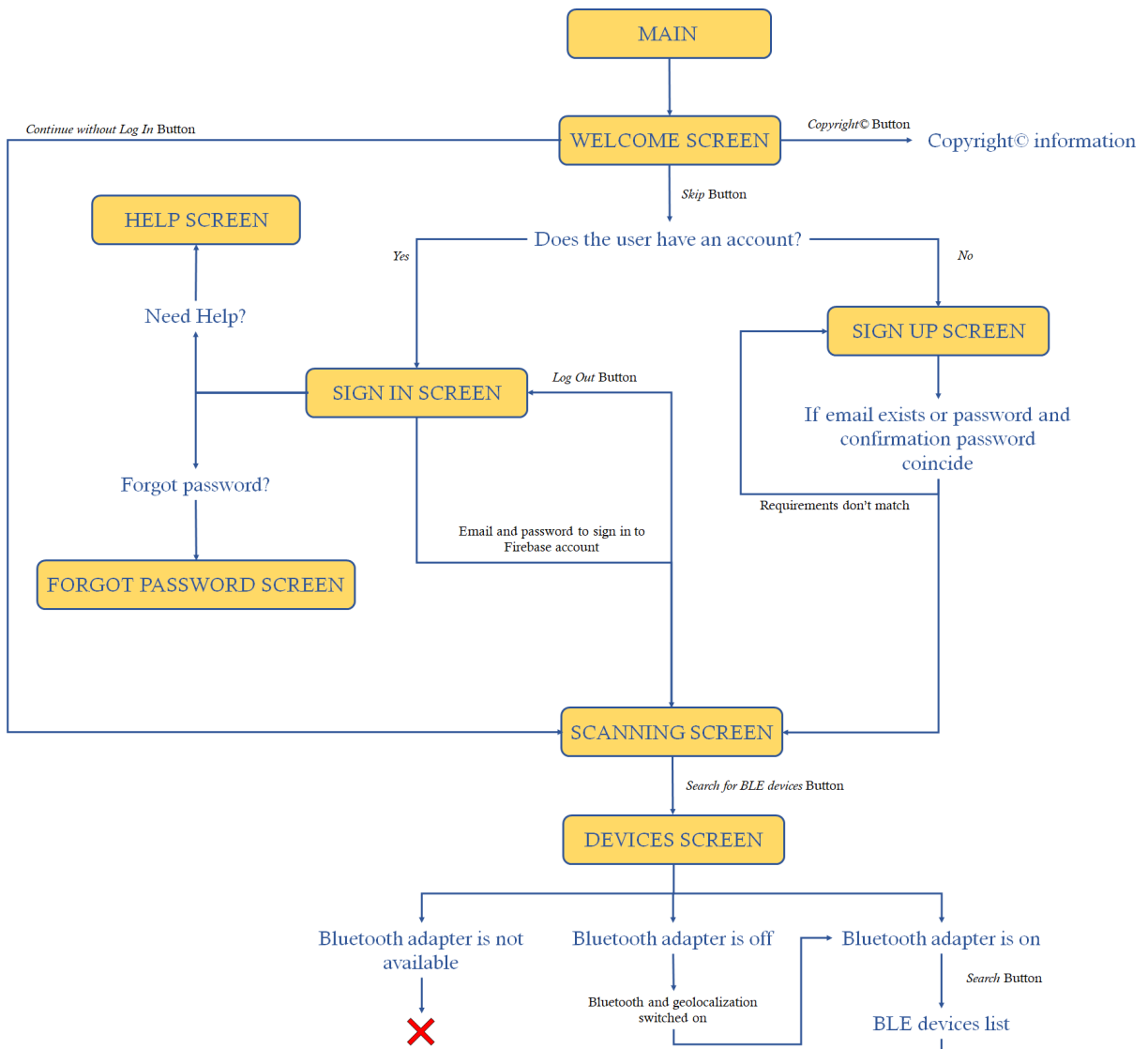
These packages are created by other developers, verified by Google and available on <https://pub.dev>, the official package repository for Dart and Flutter apps.

The application has been developed on Microsoft® Visual Studio Code® in Flutter, an open-source framework by Google that allows to build multi-platforms applications from a single codebase. Flutter is powered by Dart, a language optimized for fast apps on any platform. Because of this, this application can run on both Android and IOS devices.

2.6.3. Workflow

The application has been developed on Microsoft® Visual Studio Code® (also named VS Code) in Flutter, an open-source framework by Google that allows to build multi-platforms applications from a single codebase. Flutter is powered by Dart, a language optimized for fast apps on any platform. Because of this, this application can run on both Android and IOS devices.

The application follows a linear workflow consisting of seven different screens, and the passage from one screen to the other is mediated with buttons or the satisfaction of a specific condition (e.g. successful log in or sign in).



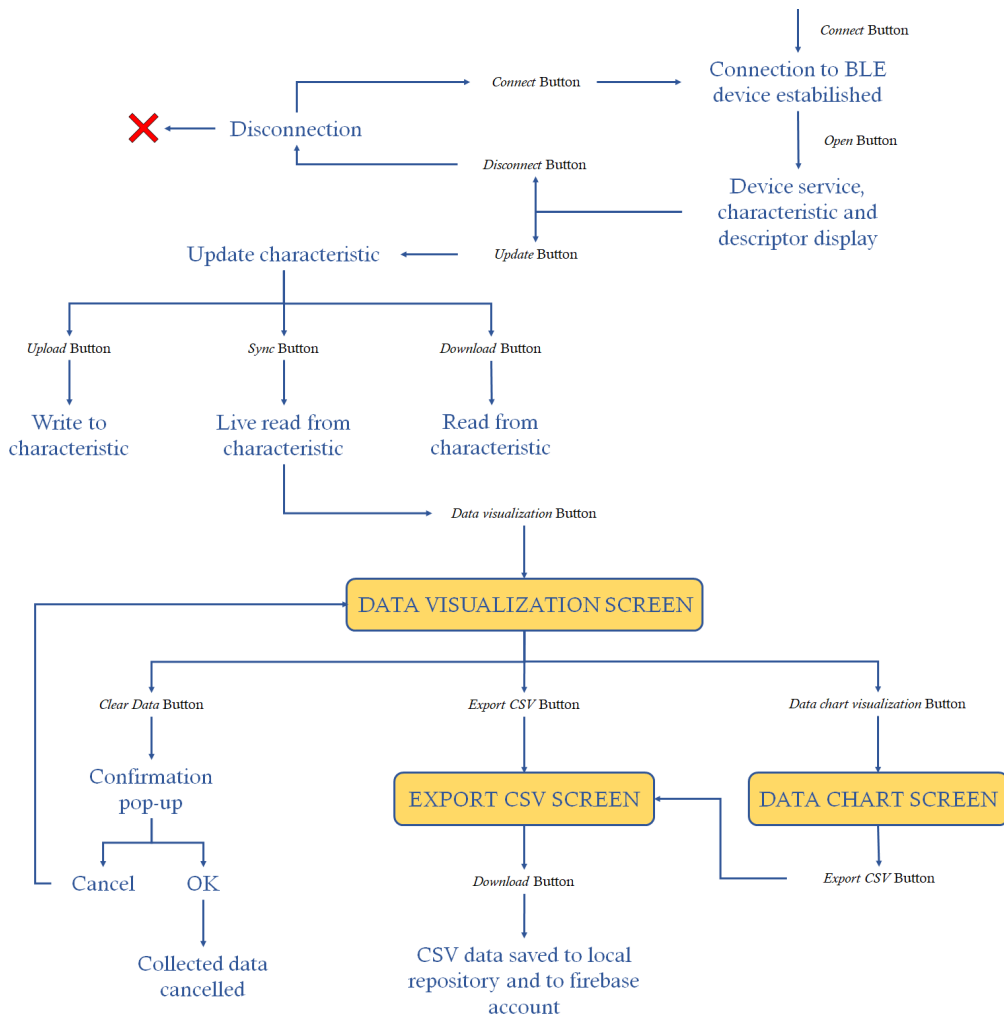


Figure 2.11: Simplified flowchart representing the application functioning described in Section 2.6

2.6.4. Google Firebase

Firebase is a backend service provided by Google that enables developers to develop iOS, Android and Web apps.

Firebase provides a set of services that normally a developer should build on his own, hence shifting the effort of the developer in creating the app itself rather than the services.

Firebase products have components that are fully maintained and operated by Google.

In this Android application the following services are used: Firebase Authentication and Firebase Storage.

Firebase Authentication

A key feature for most apps is the user authentication. Knowing the user's identity allows the application to provide a personalized experience and also to securely save user's data [13].

Firebase supports authentication using password, phone number and popular federated identity provider like Google, Facebook and Twitter.

- **Anonymous auth:** this type of authentication registers the user without asking for signing in by creating a temporary anonymous account. Then, if the user decides to sign in or log in, the anonymous account is changed with a regular account.
- **Email and password auth:** the user is authenticated with his/her email and password. Firebase authentication SDK provides tool to create emails to be sent to the user to register to the app, but also to eventually reset the email, if forgotten.
- **Phone number auth:** it authenticates the user by sending a message to its phone.
- **Federated Identity provider auth:** Firebase Authentication SDK provides methods that allow users to sign in with their Google, Facebook, Twitter, and GitHub accounts.

After a successful sign in, it is possible to access user's information and control user's access to other Firebase products, such as Firebase storage.

In the developed application, email and password authentication and Federated Identity provider authentication are implemented. Moreover, if the user does not want to have a personalized app, it is also possible not to log in and use the application without being registered to Firebase. However, this choice prevents data collected from the device to be stored on Firebase Cloud, but only locally on user's smartphone.

For this project, the following functions are used, from Firebase documentation:

- *authStateChanges()*: Notifies about changes to the user's sign-in state (such as sign-in or sign-out).
- *signInWithEmailAndPassword(String email, String password)*: Attempts to sign in a user with the given email address and password. A *FirebaseAuthException* may be thrown if the user signs in with an invalid email or if the user is disabled.
- *sendEmailVerification()*: Sends a verification email to a user.
- *createUserWithEmailAndPassword(String email, String password)*: Tries to create a new user account with the given email address and password. A *FirebaseAuthException* may be thrown if the user signs in with an invalid email or the email is already used.
- *signInWithCredential(OAuthCredential credential)*: Asynchronously signs in to Firebase with the given 3rd-party credentials (e.g. a Facebook login Access Token, a Google ID Token/Access Token pair, etc.) and returns additional identity provider data.
- *signIn()*: Starts the interactive sign-in process.
- *signOut()*: Signs out the current user.
- *sendPasswordResetEmail(String email)*: Sends a password reset email to the given email address.

Firebase Storage

Firebase Cloud Storage is used to store user-generated content, such as files and photos; all types of files can be either uploaded or downloaded. Moreover, Firebase Storage integrates with Firebase Authentication, so it is possible to control accesses to groups of files and make them public or private depending on the necessities.

All transfers to or from Firebase Storage are performed under a secure connection, and are defined as *robust*, meaning that they will automatically resume in case the connection is broken. This is an essential feature to transfer large files over a poor or unstable connection.

For this project, the following functions are used, from Firebase documentation:

- *ref(String path)*: Returns a new path.
- *putFile(File file)*: Uploads a file from the filesystem. The file must exist.

2.6.5. Application Icon

The application has a specific icon that has been designed in Adobe Illustrator®, a vector graphics app that allows the creation of logos, icons and drawings. Illustrator allows to create multi-levels design to specifically met user's wishes; this icon is a one level design. Background color is set to (60, 191, 240) in RGB code, with a diagonal shade up to (38, 53, 135) from upper left to lower right corners. Over the background, the CO₂ symbol is written using *Myriad Pro characterm*, with a white color. On the top of this, a gray shadow using the fusion tool is created to give a more dynamic aspect to the logo. Because of how the icon is exported from Illustrator and imported in VS Code, it easily adapts to smartphones settings, making it changing shape depending on user's smartphone icons settings.



Figure 2.12: Application Icon designed on Adobe Illustrator.

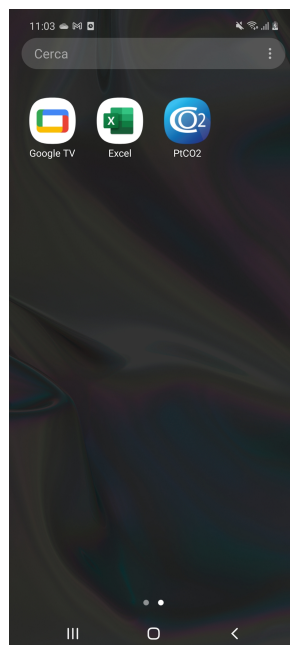


Figure 2.13: App logo and appearance on the smartphone.

2.6.6. Main, Welcome Screen and Wrapper structure

The main.dart file handles all the initialization for the correct functioning of the application.

In this file, the *Workmanager* is activated, so that the app can properly turn on. Moreover, Google Firebase set up is also called with the function *initializeApp()*.

When the application is started, it displays the so-called "Welcome Screen". It is a simple screen with a white background and the Politecnico di Milano logo together with the name of the application. Once the 'Login' button is pressed the user is moved to a *Wrapper* structure.



Figure 2.14: Welcome Screen.

A Wrapper is a *stateless widget* (as well as most of the application screens), i.e. a widget that does not change when the user interacts with it. On the other hand, it is possible to encounter also *stateful widgets*, that instead change when the user interacts with them. Also, a widget is an immutable description of part of a user interface. Hence, when designing an application, widgets are for example Column or Row layouts, buttons, texts and anything that composes what the user sees on the screen.

In this context, the Wrapper is used to differentiate between two possible conditions. In the first case, the user is already logged in from a previous registration; in this situation, the application directly passes to the *Scanning Screen*. The other possibility is that the

user is not registered to the application, nor logged in. In this case the application will move to the *Authentication Screen* or *Registration Screen*.

2.6.7. Authentication and Registration Screens

Depending on being already registered to the application or not, the user will face two different screens. If it is the first time that the application is launched or the user is changed, the registration screen in Figure 2.15 will appear.

Three fields have to be filled with email, password and the confirmation of the password. Internally, the application checks if the email is valid with the *email_validator* plug-in and if the password has at least 8 characters and 2 numbers. Then password and confirmation password correspondence is verified.

Finally, the "Register" button allows the user to be registered via email and password on Google Firebase.

Another possibility is to press the "Continue without Log in" button, that prevents user's registration.

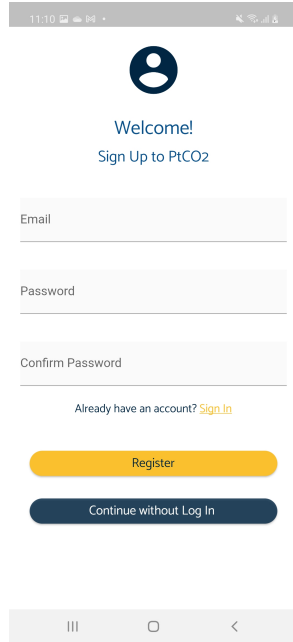


Figure 2.15: Registration screen.

Conversely, if the user is already registered, it is possible to shift to the Authentication Screen by pressing the "Log in" rich text (a rich text is a clickable part of text).

The Authentication Screen is very much similar to the Registration Screen. Still, email and password fields are present, but now the user has to insert the credentials with which

the first registration was performed (Figure 2.16a).

Otherwise, it is also possible to bypass the "email and password" authentication technique and use a personal Google account. In this case, a pop-up will appear, where it is possible to select the account for the authentication procedure as shown in Figure 2.16b.

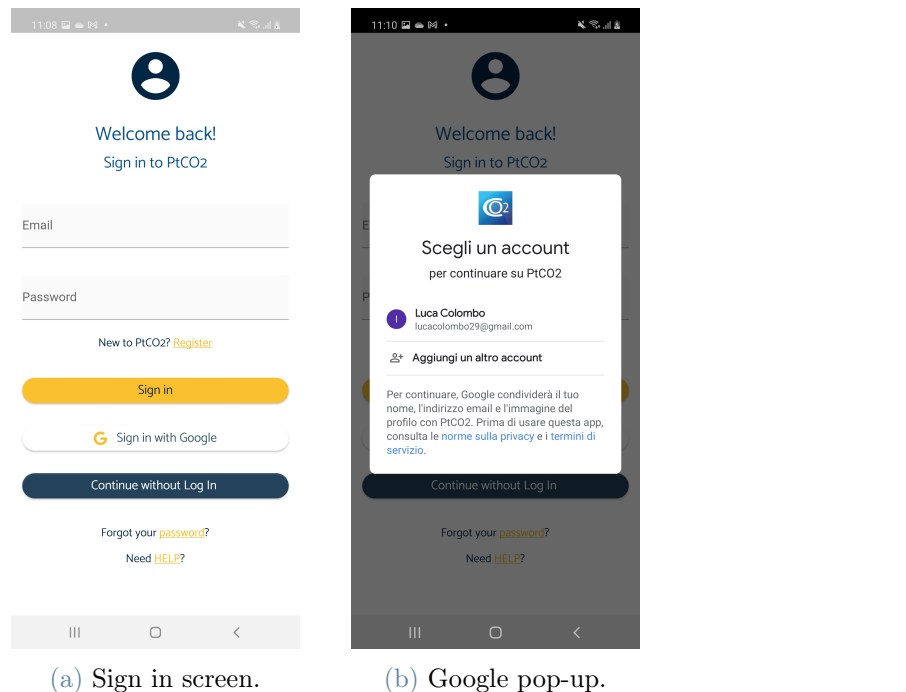


Figure 2.16: Authentication screen and Google Sign in pop-up

Also in this screen it is present the '*Continue without Log in*' button.

Moreover, three rich text fields are implemented:

- *Register*: if pressed, the application displays the Registration Screen.
- *HELP*: if pressed, the user is brought to a screen where developer's contactS and a user's guide are present.
- *password*: if pressed it is possible to restore the password, if forgotten (see Section 2.6.7).

Forgot password

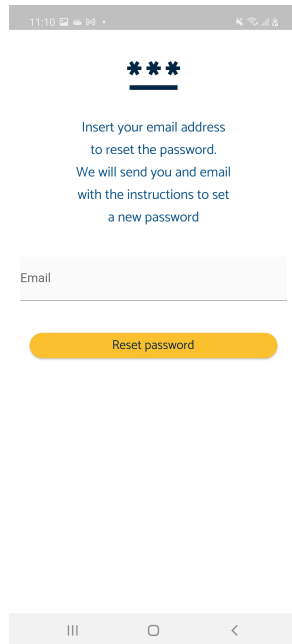


Figure 2.17: Forgot email screen.

If the user needs to reset the password, using the email with which he/she signed up, the application automatically sends an email containing a link that can be used to create a new password. This is done by calling the function `sendPasswordResetEmail(String email)` seen in Section 2.6.4. An example of the email is in Figure 2.18.

Once the user has successfully registered, is logged in or has decided to continue without logging in, the application displays a screen where Copyright© information and a disclaimer on device usage can be found. Depending whether the user is signed in or not, the email address will be displayed or not. This procedure is also done to ensure a correct log in procedure (Figure 2.19).

Reset your password for PtCO2 App  Posta in arrivo x

 **PtCO2** <noreply@ptco2-a0353.firebaseio.com>
a me ▾

 inglese ▾ ➤ italiano ▾ [Traduci messaggio](#)

Hello,

Follow this link to reset your PtCO2 application password for your lucacolombo29@gmail.com account.

https://ptco2-a0353.firebaseio.com/_/auth/action?mode=resetPassword&oobCode=VwfPJMbns08taj9Hc297g1EtUAlzaSyCoQJfi899n0sKQgDDC5gvdk2FloJtLWKo&lang=en

If you didn't ask to reset your password, you can ignore this email.

Thanks,

Your PtCO2 app team

Figure 2.18: Example of the received mail when the user asks for a password reset.



Figure 2.19: In yellow the user email. In blue the disclaimer.

2.6.8. Scanning Screen

In this screen it is handled the Bluetooth® connection and synchronization with the device. The first thing that the application does is checking if the smartphone is equipped with a Bluetooth® adapter. If the Bluetooth® is not available, the application can not run further, and it will be displayed the string “Bluetooth adapter is not available”. In this case, the application can not search and connect to BLE devices, so it can not be used unless a Bluetooth® adapter is connected to it.

Otherwise, if the Bluetooth adapter is available, two possible situations can occur. If both the device’s Geolocation and Bluetooth are switched off, the screen will display the string “Bluetooth adapter is off”. As soon as the Bluetooth is enabled in the phone’s settings, the application will be able to search for devices to which connect. However, with the Geolocation off, this procedure is not performed.

This open the path for the second possible situation, in which both the Bluetooth and Geolocation of the smartphone are enabled. In this case the application can search and find BLE devices.

It is important to remark the fact that the application scans only for Bluetooth low energy devices. Hence, an eventual peripheral implementing a classical Bluetooth BR/EDR will not be detected.

Moreover, in order to connect to a peripheral with a BLE protocol, also the smartphone must be equipped with both classical Bluetooth and BLE adapter. Having just the Bluetooth BR/EDR is not sufficient to run the application.

Once the Geolocation and Bluetooth are enabled, by pressing the bottom right search button (Figure 2.20a), it begins the quest for BLE peripherals to which connect. When pressed, the button turns red and by pressing it again the search is stopped. The time window for devices’ discovery is of 2 seconds. As soon as a device is found, it will be displayed on the screen. Each row of the list displays the name of the available peripheral, the signal strength in terms of decibel (it varies with distance) and the device identification sequence (ID) as a subtitle of the device’s name (Figure 2.20b).

When the ‘*Connect button*’ is pressed, connection between the central (phone) and the peripheral (device) is established. Note that, coherently with the implementation of the firmware, the built-in LED of the Arduino should switch on at this time, and eventually turn off when the connection is voluntarily stopped.

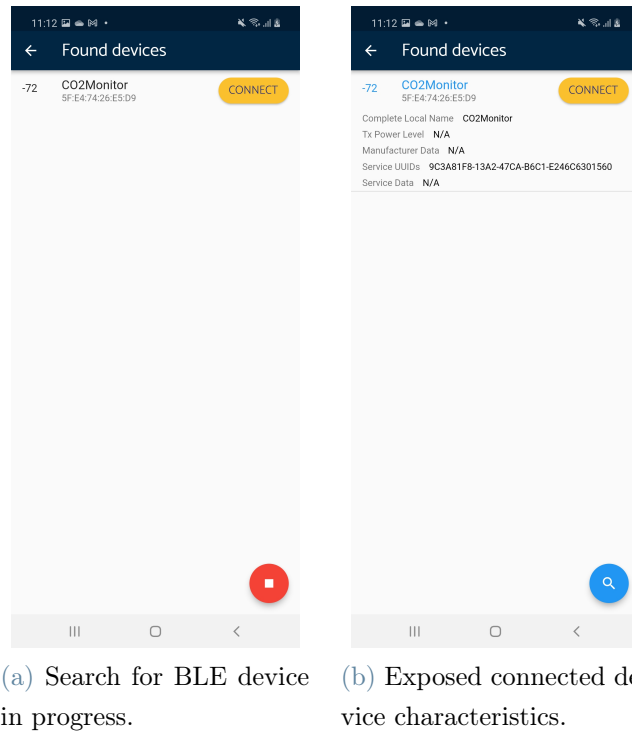


Figure 2.20: During the search for BLE devices in the neighbourhood of the smartphone, found devices will be displayed in brief with their characteristics.

When the connection is performed, the application moves to a sub-screen of the main “Scanning Screen”.

In this new screen it is shown the status of the device, i.e. if it is connected or not, the Maximum Transmission Unit (MTU) size, i.e. the maximum length of an ATT packet, and the list of available services from the connected device.

In the upper right corner there is the ‘*Disconnect button*’; when pressed, connection between the central and the peripheral is ended. However, by pressing again the ‘*Connect button*’, connection is re-established.

When pressing the ‘*Go-back button*’, either from the Appbar or from the phone command palette, the application moves back to the screen where the devices search is performed. If the ‘*Search button*’ is pressed once again, the quest for BLE devices begins again, without loosing the existing connection with the previously selected device. Indeed, the connected device will appear at the top of the pile of possible available devices, and the ‘*Connect button*’ is substituted with a green ‘*Open button*’.

If instead connection with another devices has to be performed, it is possible either to keep the connection with the previous device and initialize a new one, i.e. having two peripherals connected to the same central, or close the previous connection and initialize

a new one with a different device. The choice is up to the user.

If the device is connected, by pressing the ‘*Update button*’ in the upper right corner of the screen, it appears the list of available services for the selected device. By clicking on the service, also the characteristic of the device is displayed. With the ‘*Upload button*’ it is possible to write values to the device, while with the ‘*Download button*’ is the device that is sending data to the smartphone every time the button is pressed.

Another possibility is to press on the ‘*Sync button*’; this establishes a continuous communication between the device and the smartphone, with the phone that is just collecting data from the device without the need of polling for them manually by the user.

It can also be remarked that under the “Characteristic” tab is shown the current data received from the device. It is written in the form [x, y, z, p], where x, y, z and p are 8-bit integers, i.e. spanning from 0 to 255, because the data exchanged between the central and peripheral are of 32-bit size.

When the “Characteristic” is pressed, a “Descriptor Tile” opens, showing the value for the descriptors associated to each characteristic. If the ‘*Data Visualization button*’ is pressed, the application switches to a new screen, where the data collected from the device are displayed.

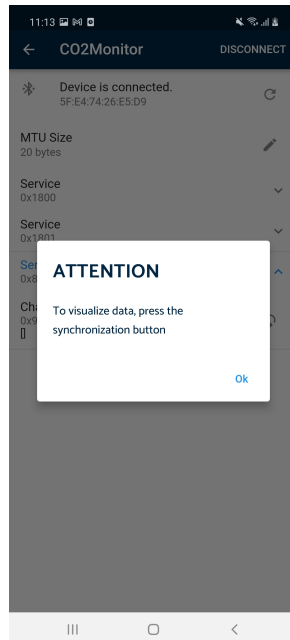


Figure 2.21: Attention Pop-Up when "Data Visualization" button is pressed before pressing the synchronization button. In the background the complete characteristics of the connected device can be seen.

2.6.9. Data Visualization Screen

On this screen all the information sampled by the sensor inside the device are displayed. It is of paramount importance, before pressing the ‘*Data Visualization button*’ in the “Devices screen”, to press the ‘*Sync button*’ and make sure that the characteristic value is correctly updating. Theoretically, since a new value is sent by the device every second, the characteristic value should also update every second.

If the ‘*Sync button*’ is not pressed, when moving to the “Data visualization screen”, the current value from the sensor won’t be updating, because the BLE receiver (i.e. the smartphone) is configured in manual polling mode.

Once the ‘*Sync button*’ is pressed and the user is in the “Data visualization screen”, the current value from the sensor will be updating automatically.

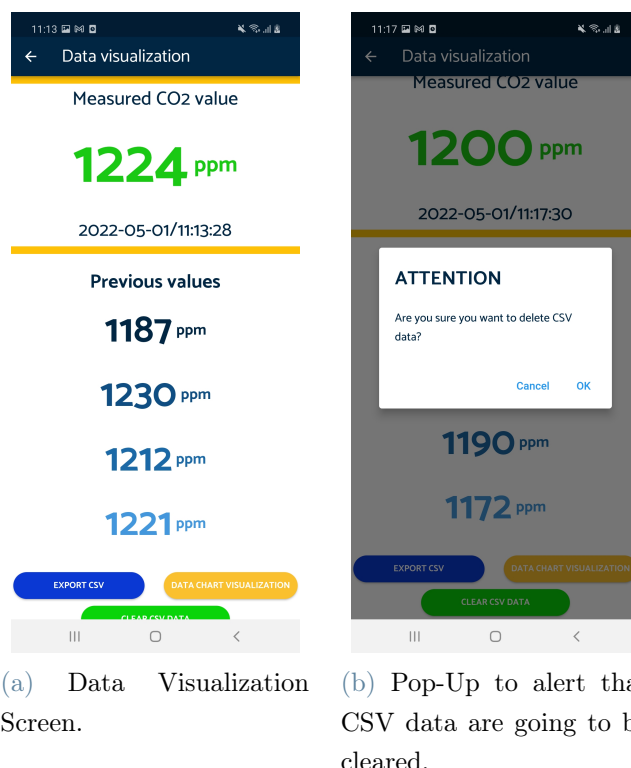


Figure 2.22: Data Visualization Screen features three buttons to clear collected data, export collected data and visualize a real time plot of the collected data.

In this screen layout (Figure 2.22a), the green color highlights the current value received, while the other values shown are the previously collected data. The date and time are also displayed. At the bottom of the page, the user can interact with three different buttons. If the ‘*Export CSV button*’ is pressed, the user is brought to the “Export CSV screen” in

which there is a list of available CSV files that the user can download. Indeed, as soon as the user is brought in the “Data visualization screen”, all the data received from the peripheral are collected and converted in a CSV file ready to be downloaded later.

The CSV file has a simple structure; on one column it is saved the date and time of the arrived data, while on the contiguous column, in the corresponding row, the value of the arrived data.

If the ‘*Download button*’ is pressed, collected data are saved locally in the smartphone download folder, and online on Firebase Cloud Storage, if the internet connection is on and the user is logged in.

If the ‘*Clear CSV data button*’ is pressed, a pop-up dialogue window is generated. This pop-up warns the user if the CSV must indeed be cancelled. If the user presses the ‘*Cancel*’, the CSV data are not deleted, otherwise if ‘*Ok*’ is pressed the array is cleared. (Figure 2.22b).

If the ‘*Data chart button*’ is pressed, the user is brought to the “Data chart screen”, where a plot is displayed with all the values collected up to the present time instant and stored in the CSV file. The plot, that is real-time updating, has on the y axis the CO₂ value expressed in parts per million (ppm), while on the x axis it is shown the elapsed time, expressed in seconds. From this screen it is also possible to move to the “Export CSV screen” by means of the ‘*Export CSV button*’ (Figure 2.23).



Figure 2.23: Real time data chart representing the CO₂ values sampled from the sensors.

2.6.10. Widgets

Alongside the different screens, a series of widgets is defined to provide functionalities. Widgets are Dart classes with a specific function, and theoretically a single widget could be used to create an entire screen in the application.

- **ScanResultTile:** in the “Scanning screen” (Section 2.6.8) this widget provides, once the name of the device is pressed, the following attributes:
 - Complete local name, that shows the complete name of the device, if available.
 - Tx power level, that specifies the strength of the signal that the device produces during the times it transmits. By default it is 8 dBm meaning that all of the advertisement packets and data packets will be transmitted with this power level. If the information is not available it will be displayed ‘N/A’.
 - Manufacturer data, that provides the information concerning the manufacturer.
 - Service UUIDs, that shows the value of the service; in the specific case, the service value for the device should be: “9c3a81f8-13a2-47ca-b6c1-e246c6301560”.
- **ServiceTile:** in the sub-screen of the “Scanning screen”, this widget creates a list of all the services associated with the connected device.
- **CharacteristicTile:** in the sub-screen of the “Scanning screen”, when a service name is pressed, this widget creates a list of all the characteristics associated with the connected device.
- **DescriptorTile:** in the sub-screen of the “Scanning screen”, when a characteristic name is pressed, this widget creates a list of all the descriptors associated with the connected device.
- **StreamBuilder:** given a device ID value, a service value and a characteristic value, this widget creates a *stream* of data from the connected device to the smartphone. Data are received in a 32-bit configuration in the form [x, y, z, p] previously introduced, and they are converted in the classical ‘readable to the user’ integer form by a designed function. In the same widget, the data is stored in an array together with current date and time, ready to be subsequently converted in a CSV file or plotted in a chart.

2.7. Experimental Campaign

To asses if the device is correctly sensing PtCO₂ variation, an experimental campaign is started. The purpose of the experimental campaign is also to compare the created device (the PCB device) with a gold-standard measurement device, that is the *Sentec Digital Monitor*.

With the cooperation of Centro Cardiologico Monzino, trials on healthy subjects are carried on following a specific test protocol.

The idea is to stimulate CO₂ production in the subject undergoing the test, having thus an increase in arterial CO₂ concentration and, consequently, an increase in PtCO₂ measured value.

In order to trigger carbon dioxide production, a rebreathing maneuver is chosen. This maneuver consists in forcing the subject to breath its own air for a certain period of time, so that CO₂ content in the inhaled air progressively increases, leading also to an increase in arterial CO₂ levels. Then the subject breaths in normal air to balance back the situation.

Thanks to the cooperation with the Centro Cardiologico Monzino, this maneuver is performed under medical supervision, with doctors ready to intervene if needed.

Data are collected with a cable connected from the Computer to the device using **MegunoLink**, that helps to plot real time data.

The subject wears a Electrocardiograph and the Sentec device clip is placed either on the earlobe or on the forearm. Indeed, two consecutive tests on the same subject are performed. In the first one, the Sentec clip is placed either on the earlobe or on the forearm, while in the second one in the other position. The PCB device, instead, is always positioned on the right wrist, as it can be seen in Figure 2.25.

In between the two tests, air in the room is recycled, and a resting time of circa 45 minutes is waited.

Moreover, in between the mouthpiece that the subject holds in his mouth and the rebreathing bag, a flowmeter and carbion dioxide sensor are placed, to detect end exhalation CO₂ values. The same machinery that collects end exhalation CO₂ values also detects saturation levels by means of a ear clip that the subject wears, in addition to the one of the Sentec device.

Then, a three ways valve is used to direct airflow from the patient either in the rebreathing bag or in the open air. This apparatus is depicted in Figure 2.24.

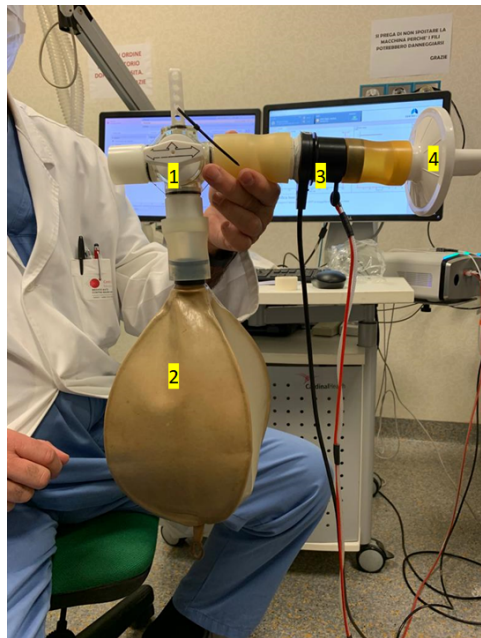


Figure 2.24: Apparatus used to perform the rebreathing maneuver. 1 is the three ways valve, 2 the rebreathing bag, 3 the flowmeter, 4 the mouthpiece.

As for the tested population, it consists of 21 subject aged from 21 years to 55 years. Tested population composition is presented in Table 2.1.

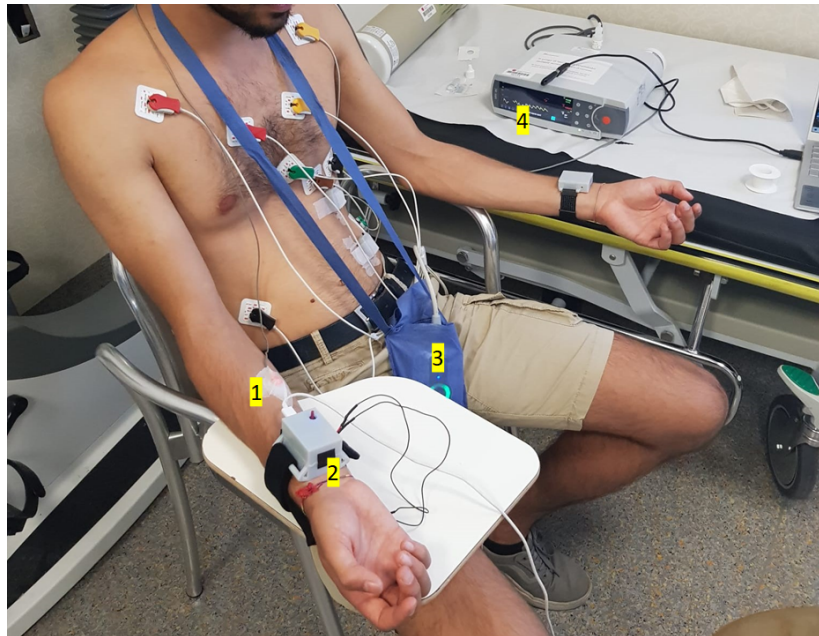


Figure 2.25: Experimental instrumentation. 1) Sentec Forearm sensor. 2) PCB device. 3) ECG. 4) Sentec Digital Monitor.

	Age	Sex
Subject1	55	M
Subject2	32	M
Subject3	26	F
Subject4	26	M
Subject5	26	M
Subject6	24	M
Subject7	24	M
Subject8	23	M
Subject9	24	M
Subject10	25	F
Subject11	26	F
Subject12	25	F
Subject13	33	F
Subject14	27	M
Subject15	21	F
Subject16	25	M
Subject17	46	F
Subject18	24	M
Subject19	24	M
Subject20	29	M
Subject21	24	M

Table 2.1: Tested population

2.7.1. Test Protocol

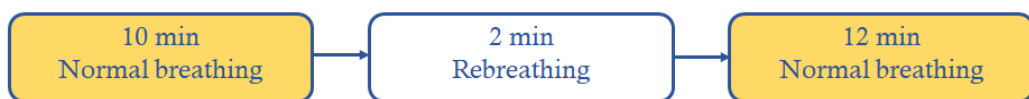


Figure 2.26: Schematic representation of the test protocol

The subject is equipped with an ECG, the PCB device, the the Sentec device and has the mouthpiece in his/her mouth and a nose plug.

Once the PCB device has reached the optimal skin temperature and the Sentec device signal is stable, the three ways valve is in open configuration with the ambient, and the subject is asked to breath for 10 consecutive minutes ambient air.

Then, a 2 minutes rebreathing maneuver is performed. The three ways valve is switched so that the the subject breaths in the bag. When the rebreathing phase is finished, the valve is again positioned open with respect to the ambient and the subject breaths ambient air for 12 minutes (Figure 2.26).

Complete duration of the test is of 24 minutes. PCB device and Sentec device samples subject's data each second, while the CPET machinery measures EtCO₂ with a breath by breath approach.

2.7.2. Questionnaire

Before being tested, each subject agrees voluntarily to the experimental campaign. The subject is provided with an informative module and is asked to sign a informed consent. After the trial, the subject has to compile a questionnaire, in which the following data are collected: Age, Gender, Weight and Height.

Then, 10 questions/sentences have to be answered by the examined subject. The score is from 1 to 5 for each question, where 1 means totally in disagreement, whereas 5 means completely in agreement.

1. The device is easy to be worn and positioned.
2. External help might be needed in handling the device.
3. The device anchoring system makes it easier to be worn and positioned.
4. I would have preferred to remove the device during the test.
5. I think I would be able to use the device autonomously.
6. The anchoring system is uncomfortable.
7. I think I could wear the device for a prolonged time.
8. I think the usage of the device could negatively affect my daily activities.
9. I think I could sleep normally wearing the device.
10. I felt pain and burning where the device is placed during the test.

Aggregated questionnaire results are presented in Chapter 3.

2.8. Statistical methods

In this section the statistical methods used to analyzed collected data are presented. Since data from the PCB device, data from the Sentec device and data from the CPET machinery are saved in different file configurations, a unique dataframe has to be created. To do so, the Python plug-in for VS Code is used, together with MATLAB® software. Data are differentiated depending on having the Sentec device positioned on the forearm or on the lobe, and three dataframes are created in a CSV format. One containing forearm data from the Sentec, PCB device data and EtCO₂ data from the CPET machinery, the other including lobe data from the Sentec, PCB device data and EtCO₂ data. The last dataframe has all the data from the subjects in both forearm and lobe fashion.

2.8.1. PtCO₂ analysis

In order to assess if transcutaneous CO₂ variations have been detected, a series of statistical analysis on collected data is performed.

In first place, normality of the data has to be checked. To do so, *stats* library from *SciPy* [1] is imported in order to use the *scipy.stats.normaltest(array)* on an array of data. The function returns the p-value for the normality test; if the p-value is smaller than 0.05, data has to be considered non-normal. Otherwise, data are normally distributed.

In fact, the normality is verified on the whole array of data collected from a specific subject during the first or second trial in the protocol time window (that is 24 minutes).

It is evident that, since for almost all the subjects data are not normally distributed, parametric tests can not be performed. This assumption automatically excludes the possibility of considering the *Anova test for repeated measurements*, the *Paired t-test* and the *Independent t-test*, because all these tests are based on a normality of the data assumption. Hence, other tests has to be considered.

Kruskal Wallis Test

A first analysis, that can be referred as a *Repeatability Analysis*, considers the **Kruskal Wallis test**. It is a non-parametric test alternative for the one-way Anova, that instead is used for normal distributions. The main objective of the test is to detect whether there is a statistical difference between the medians of at least three (two are sufficient in the Python implementation) independent populations. The Kruskal Wallis test has the

following Null and Alternative Hypotheses:

- **Null Hypothesis (H0):** the median is the same for all the data groups.
- **Alternative Hypothesis (H1):** the median is not the same for all the data groups.

Looking at the results, if the p-value is not less than 0.05, the Null Hypothesis H0 can not be rejected, hence the median is the same for all the data groups. Conversely, if the p-value is greater than 0.05, the Null hypothesis can be rejected, and the Alternative hypothesis H1 holds.

To run all the statistical analysis, raw data from PCB device and Sentec device are pre-processed.

The start of the rebreathing manouver is considered as the origin of a temporal reference system. Then, considering a variable time window, data from the rebreathing time instant going back in time and going forward in time are grouped, as it is shown in Figure 2.27. The time window is variable; knowing that each sample is collected every second, considering 10-samples groups means using also a 10 seconds time window.

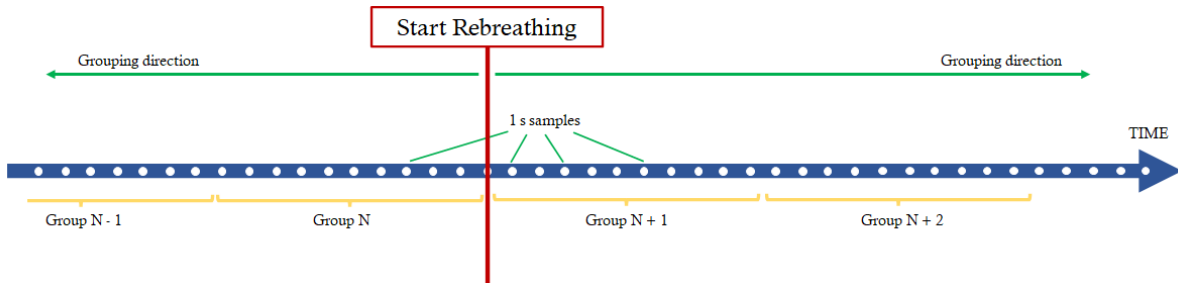


Figure 2.27: The start of the rebreathing manouver is the time origin. White dots represent data samples, collected each second. The grouping algorithm starts from the time origin and moves back in time selecting a number of samples coherently with the chosen time window and creating in this way groups. The same procedure is then performed from the start rebreathing to the end of the test. Groups medians are then saved in an array.

Different time windows have been considered; 1 minute of resolution is too poor to enhance specific variations of the signal after the rebreathing manouver. 10 seconds resolution is instead too detailed, providing an output signal that is almost identical to the raw one both for the Sentec and PCB devices. A good compromise is represented by a 30 seconds time window (remembering that the whole test lasts for 24 minutes). However, both 10s processed data and 30s processed data are used. The former for the Exponential Fitting

described in Section 2.8.1, the latter for the Kruskal Wallis test.

Then, the mean or median value is extracted from each group and saved in an array. In this way, each subject raw data are filtered by extracting the mean or the median grouping samples based on a specific time interval, and data subject itself will be from now on analyzed considering only the generated filtered array.

In particular, arrays to perform the Kruskal Wallis test are further processed. In fact, using `scipy.stats.kruskal(*args, nan_policy = propagate, axis = 0)` [1], two arrays are fed to the function, that in returns provides the p-value for the test. The arrays are two and organized as follows: for each specific time instant, lobe data from all the subjects constitute the first array, whereas forearm data from all the subject constitute the second array. Then, the test is performed iteratively on these two arrays for all the time instants from the start of the rebreathing maneuver.

Wilcoxon Matched Pairs Test

A second statistical analysis is the **Wilcoxon Matched Pairs Test**. It is a non-parametric equivalent of the Paired t-test.

In fact, data to be analyzed with this test are the two arrays composing the lobe acquisition (with respect to Sentec device positioning, that is acquisition 1) and the forearm acquisition (with respect to Sentec device positioning, that is acquisition 2) for each subject. It is performed on the PCB device acquired data, iteratively for each subject considering the two acquisitions. The Wilcoxon test is chosen because with this approach it is clear that acquisition 1 and acquisition 2 are paired, in the sense that they are both related to the same subject, besides being done in two consecutive tests.

Once again, to run this test the SciPy library is used: `scipy.stats.wilcoxon(x, y = None, zero_method = wilcox, correction = False, alternative = two-sided, mode = auto, *, axis = 0, nan_policy = propagate)`.

The Wilcoxon matched pairs test has the following Null and Alternative Hypotheses (that are the same of the Paired t-test):

- **Null Hypothesis (H0):** the true mean difference between the two populations is equal to zero (in other words, there is no difference between the two "populations").
- **Alternative Hypothesis (H1):** the true mean difference between the two populations is not equal to zero (in other words, there is a difference between the two "populations").

Regarding the arrays for the test, the same time resolution used for their creation in the

Kruskal Wallis is also adopted for the Wilcoxon Matched Pairs Test.

The output of the test is the p-value. A p-value smaller than 0.05 allows to reject the Null Hypothesis and embrace the Alternative Hypothesis.

Friedman Repeated Measures Analysis of Variance on Ranks

This test is a non parametric test used to compare three or more groups. Being non parametric means the test does not assume that data comes from a particular distribution (e.g. a normal distribution). It is statistic test used for a repeated measures type of experiment to determine if a particular factor has an effect, in this case, over time. The following are the Null and Alternative Hypothesis:

- **Null Hypothesis (H0):** there is not a statistical difference amongst the different time instants.
- **Alternative Hypothesis (H1):** there is a statistical difference amongst the different time instants.

If the p-value is smaller than 0.05, the Null Hypothesis is rejected and the Alternative one embraced.

Correlation Analysis

The objective of the correlation analysis is to investigate if a relationship between the signal recovered from the PCB device and from the Sentec device exists .

The two signals have to different units of measure, that is mmHg in the case of the Sentec device and ppm in the case of the PCB device. Because of this, direct comparison is not possible and data have to be normalized, to remove the effect of the unit of measure.

The normalization procedure is done subtracting to each sample related to a specific time instant the value of the signal at the beginning of the rebreathing phase and then dividing by the same value, that is again the value of the signal at the beginning of the rebreathing. This procedure is done both for PCB device signals from each subject and Sentec device signals.

As for the tests that can be used to investigate possible correlations, the Independent t-test cannot be used. First of all, because it is suitable for data that are normally distributed, while neither PCB device data nor Sentec device data form each subject are so. Moreover, PCB device signals and Sentec device signals have a completely different waveform, making impossible a direct comparison even using non-parametric tests for non-normal distributions.

To overcome these issues, the Bland-Altman plot and a simple scatter plot is created to detect whether there is a correlation or not. The scatterplot considers on one axis the time delay between the beginning of the rebreathing maneuver and the time instant of the peak of the PtCO₂ signal for the PCB device, whereas on the other axis for the Sentec device.

Exponential Fitting

The exponential fitting is aimed at identifying two parameters representative of the post-rebreathing increase in detected PtCO₂ from the PCB device. Data from all the subjects are individually analyzed, still preserving the differentiation between forearm and lobe acquisitions. No comparison between arrays is performed in this procedure, but post-rebreathing data are fitted with an exponential curve of the following type:

$$y = B \cdot (1 - e^{-\frac{t-t_0}{\tau}}) + A \quad (2.1)$$

Where A , B and τ are parameters, while t_0 indicates the time instant of the start of the rebreathing maneuver.

In order to fit data, SciPy is used once again, in particular the function of interest is:

```
scipy.optimize.curve_fit(f, xdata, ydata, p0 = None, sigma = None, absolute_sigma = False,
check_finite = True, bounds = (-inf, inf), method = None, jac = None, **kwargs).
```

f is the function to be used to fit the data (2.1), $xdata$ the array of time stamps, $ydata$ the array of PCB device measured values related to the corresponding time instant. The other parameters are not of interest for this fitting.

Together with the values of the parameters, this function also returns a matrix of estimated covariance for the computed parameters.

The choice of an exponential fitting is justified by a qualitative analysis of the post-rebreathing curve. In fact, PCB device typically expresses an increasing trend few minutes after the rebreathing maneuver, reaching later a plateau due to a saturation.

The most significant parameter from this analysis is the τ , which indicates the time the PCB device needs to achieve the plateau (or at least a maximum of the signal), depending on the tested subject. Results on this exponential fitting, a table with B and τ values are presented in Chapter 3.

3 | Results and Discussion

In this chapter results on PCB device performance are presented. A first section evaluates the response of the device in comparison with the *Gold Standard*, that is the Sentec device. Then results of the statistical analyses are introduced.

3.1. PCB Device Response

During the 24 minutes of test, data from the PCB device and Sentec device are collected and saved in a unique CSV file for data processing.

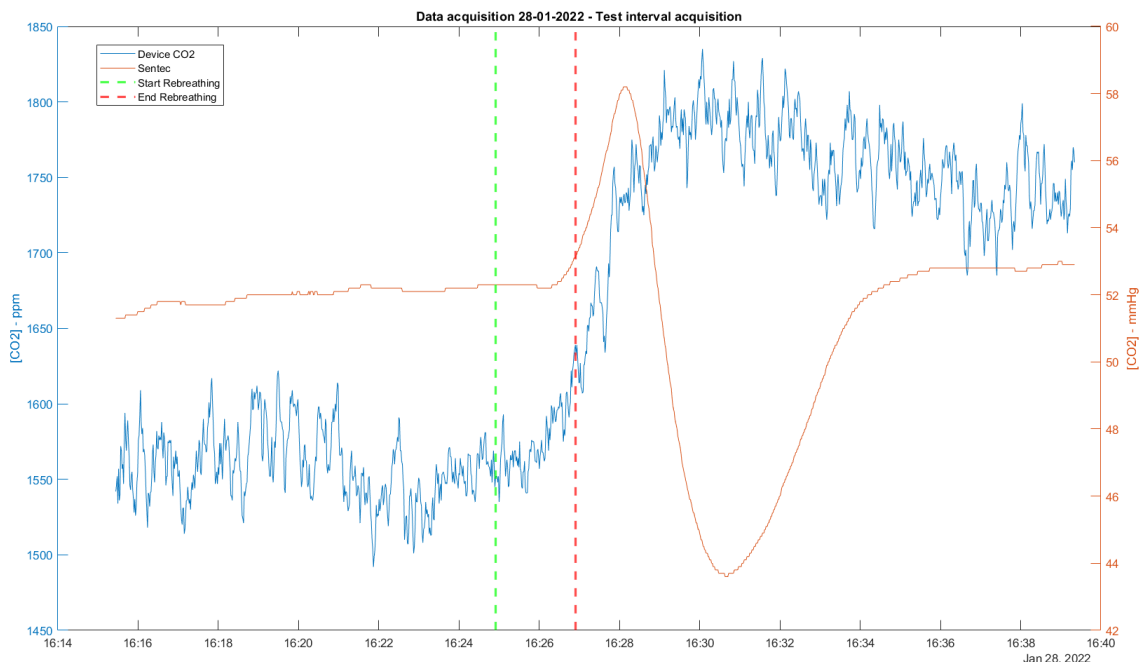


Figure 3.1: In blue raw data from the PCB device, in orange data from the Sentec device. The green vertical line indicates the beginning of the rebreathing maneuver, while the red vertical line the end of the maneuver.

Using MATLAB®, raw data are plotted. Figure 3.1 represents the two output signals from the PCB device and Sentec device. It is important to remark that plotted PCB device data are raw, in the sense that no digital filtering is performed on the data outputted from the CO₂ sensor inside the device. Conversely, Sentec device data is heavily digitally filtered, as the Sentec Digital Monitor datasheet explains. This is the reason why the PCB device blue signal is superposed to a certain level of noise, while the other signal is almost noise-less.

As for the trend of the two signals, some considerations are required. Regarding the PCB device signal, typically during the 10 minutes before the rebreathing maneuver a slight decrease in values is observed, reaching then a baseline before the maneuver. A possible explanation for this behaviour can be found in the CozIR® sensor datasheet [24]. In fact, the operating temperature range is in between 0°C and +50°C. Since this CO₂ sensor is specifically designed for ambient air evaluation, typical operating temperature is around 25°C.

In the current PCB device implementation, however, there is a heating element, that is the Nichrom wire. During the heating phase, the wire reaches temperature of more or less 43°C, that is a value close to the upper limit for the temperature operating range of the sensor. However, after the heating phase, the wire rapidly returns to lower temperature.

Since the CO₂ sensor is separated from the Nichrom wire by a 1mm layer of VeroGray® (Stratasys printing material), it might be affected by the high temperatures of the wire. Because of this, collected values from the sensor immediately after the heating phase, i.e. at the very beginning of the test, can possibly be distorted due to temperature effects. Nevertheless, the 10 minutes wait of the test before the start of the rebreathing phase are specifically introduced in the protocol to allow the sensor to reach a stability in the outputted signal.

As for the signal behaviour during the rebreathing maneuver, typically no significant increase is observed during the 2 minutes of rebreathing, with the signal that instead increases some minutes after the end of the rebreathing. This situation has a trivial explanation; first of all, there is a physiological delay (not known exactly) in between when the stimulus is provided and when the increase in blood CO₂, that occurs in the lungs, travels across the body and reaches the site where the PCB device is positioned, that is the right wrist. In second instance, there is also a so-called *sensor delay*, according to which effective variations in trascutaneous CO₂ values can be detected. In fact, too small variations of PtCO₂ can not be detected because of the noise level.

A sensible variation is PtCO₂ values is usually observed after the end of the rebreathing

maneuver. The signal has an increase whose steepness depends on how much the subject has tolerated the provided stimulus and hence on the subject itself.

After this increase, the signal reaches a plateau and transcutaneous CO₂ value remains almost the same till the end of the test, eventually with a small decrease observed in some subjects.

A possible explanation for this saturation behaviour can be found in the case architecture (Appendix C). In the current design, a chamber is created between the skin of the subject and the sensitive part of the CozIR sensor. This chamber is sealed by the closure of the solenoidal valve at the beginning of the test, just after the rebreathing phase. Since there is no room for the transutaneous CO₂ to leave the chamber, it accumulates in it during all the test. Following this reasoning, theoretically the PtCO₂ detected values should always increase until the end of the test, because CO₂ progressively accumulates in the chamber without being washed out. However, due to small leakages because of the non perfect contact between the skin and the case (sealing is not ideal) and diffusion through the VeroGray® material, CO₂ leaves the chamber. Nevertheless, the intake of transcoutaneous CO₂ is almost equal to the outtake due to the previously mentioned, hence stabilizing the signal to a plateau.

On the other hand, the Sentec Digital Monitor output signal is characterized by a stable signal (in some subjects decreasing) in the 10 pre-rebreathing minutes. As well as the PCB device, also the Sentec device has a response time to the stimulus that depends on a physiological and a sensor delay.

Moreover, depending on having the Sentec sensor placed on the earlobe or on the forearm, the delay between the beginning of the rebreathing maneuver and the detection of a PtCO₂ peak is variable; usually it is higher in forearm positioning.

Sometimes, the Sentec signal has also a local minimum just after the maximum, stabilizing in the end to a PtCO₂ value that is almost always a bit higher than the pre-rebreathing baseline value for the Sentec device.

Note that in Figure 3.1 the y axis has two different units of measure, parts per million (ppm) for the PCB device and millimeters of mercury (mmHg) for the Sentec Digital Monitor.

3.2. PCB Device Evaluation

As introduced in Section 2.7.2, subjects are asked to fill a questionnaire after the test. The score for each question is between 1 and 5, where 5 indicates 'totally in agreement' and 1 'totally in disagreement'. Average results on questions responses are presented in Table 3.1.

	Q1	Q2	Q3	Q4	Q5	Q6	Q7	Q8	Q9	Q10
Average	4.7	2.0	4.2	1.0	4.5	1.4	3.9	2.3	3.5	1.2
Ideal	5.0	1.0	5.0	1.0	5.0	1.0	5.0	1.0	5.0	1.0

Table 3.1: Averages scores for the questionnaire responses, compared with the corresponding ideal values.

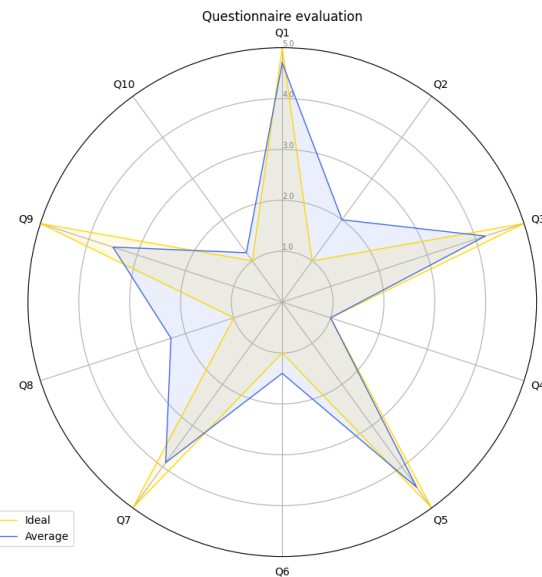


Figure 3.2: Averages values for questions responses compared to ideal values.

The score that deviates the most from the ideal value is the one related to Question 9, that is: *I think I could sleep normally wearing the device.*

In its current version, the PCB Device is used during the test anchored to the wrist with a fabric strap, being also connected with a micro-USB to USB cable to a remote computer. Theoretically, Bluetooth communication could be used to transfer data from the device to the smartphone and then data saved on the connected smartphone. However,

to prevent interferences with other devices that might corrupt the data, cabled connection is preferred over wireless connection. Probably, in answering Question 9, the subject has its judgment influenced by this setup condition. Questionnaire average answers can also be seen in Figure 3.2.

Moreover, dimension of the overall device are smaller than the device version in [5] that was implemented using a prototyping board, but still not as small as a commercially available smartwatch, albeit the latter is not capable to perform PtCO₂ monitoring so far.

3.3. Aggregated Data Analysis

At the current time, the experimental campaign comprises 21 subjects, 8 women and 13 men. The target of the campaign is to reach 30 subjects in total.

However, some preliminary statistical analysis can be performed on collected data, as introduced in Section 2.8.

Collected data, both from the Sentec Digital Monitor and the PCB Device are processed as described in Section 2.8.1; three possible output plots can be represented. One in terms of absolute values, one in terms of delta values, where the delta indicates that to the whole data array of the acquisition the baseline value of the beginning of the rebreathing is subtracted and one in terms of normalized values, where the normalization is performed subtracting to each value the baseline value and dividing by the baseline value again.

It is trivial to conclude that there is no difference in the shape of the signal for the three different representation, because the same processing to retrieve delta or normalized values is done on each sample of the data array.

Moreover, a remark has to be done on the temporal resolution of the x axis. In Section 2.8.1 it is stated that a temporal resolution of 30 seconds is used to retrieve the median value of that time interval, iteratively from the beginning of the rebreathing maneuver going forward and backward in the saved data array. However, time instant displayed are associated to multiple of 15 seconds labels. This is done because ideally the median is in the center of the interval, hence occupying the 15th position in the 30 seconds time window.

Aggregated data for all the subjects in the form of boxplot can be seen in Figure 3.3, considering Lobe and Forearm data, respectively. The differentiation is based on the positioning of the Sentec device on the subject. It can be seen that the trend of the aggregated signal is similar to the one observed on all the subjects (Figure 3.1).

Moreover, plotted data are not in absolute values, but in terms of delta values, considering the start-rebreathing value as the baseline value to be subtracted to all the other time instants.

In Figure 3.3b the Sentec device has some outliers from 14.45 min to 16.45 min; the absolute value for these points is of 0 mmHg, they belong to subject S05, which has suffered a detechment of the Sentec sensor from the forearm during the test.

In Figure 3.4 only median data are plotted.

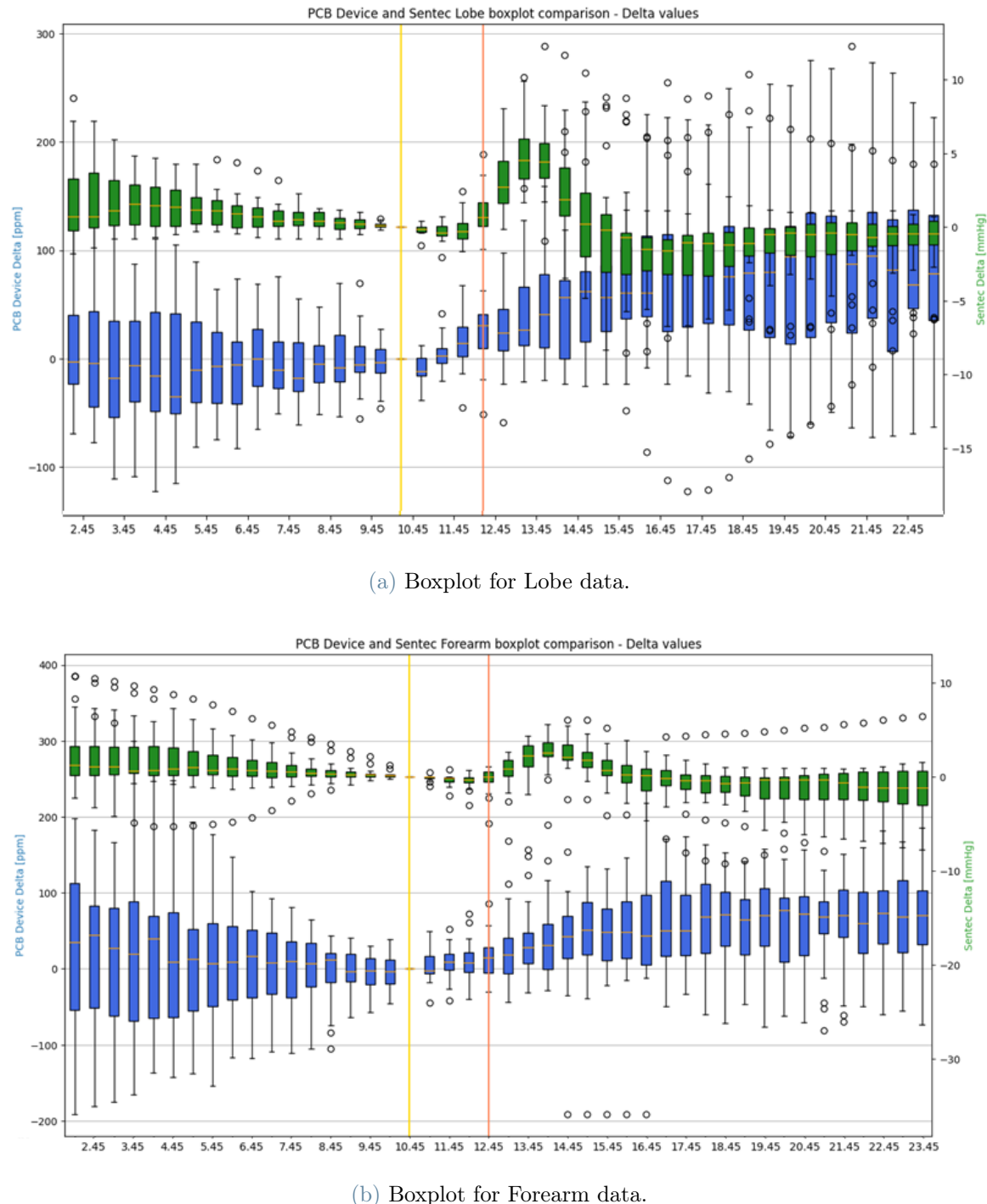


Figure 3.3: Boxplots for aggregated data for all the subjects. The blue color indicates the PCB device, while the green color the Sentec device. The orange small horizontal lines indicate the median values. Vertical yellow and orange lines indicate the beginning and end of the rebreathing maneuver. Boxplots are created using 30s median data, and on the x-axis the time stamp is in minutes.

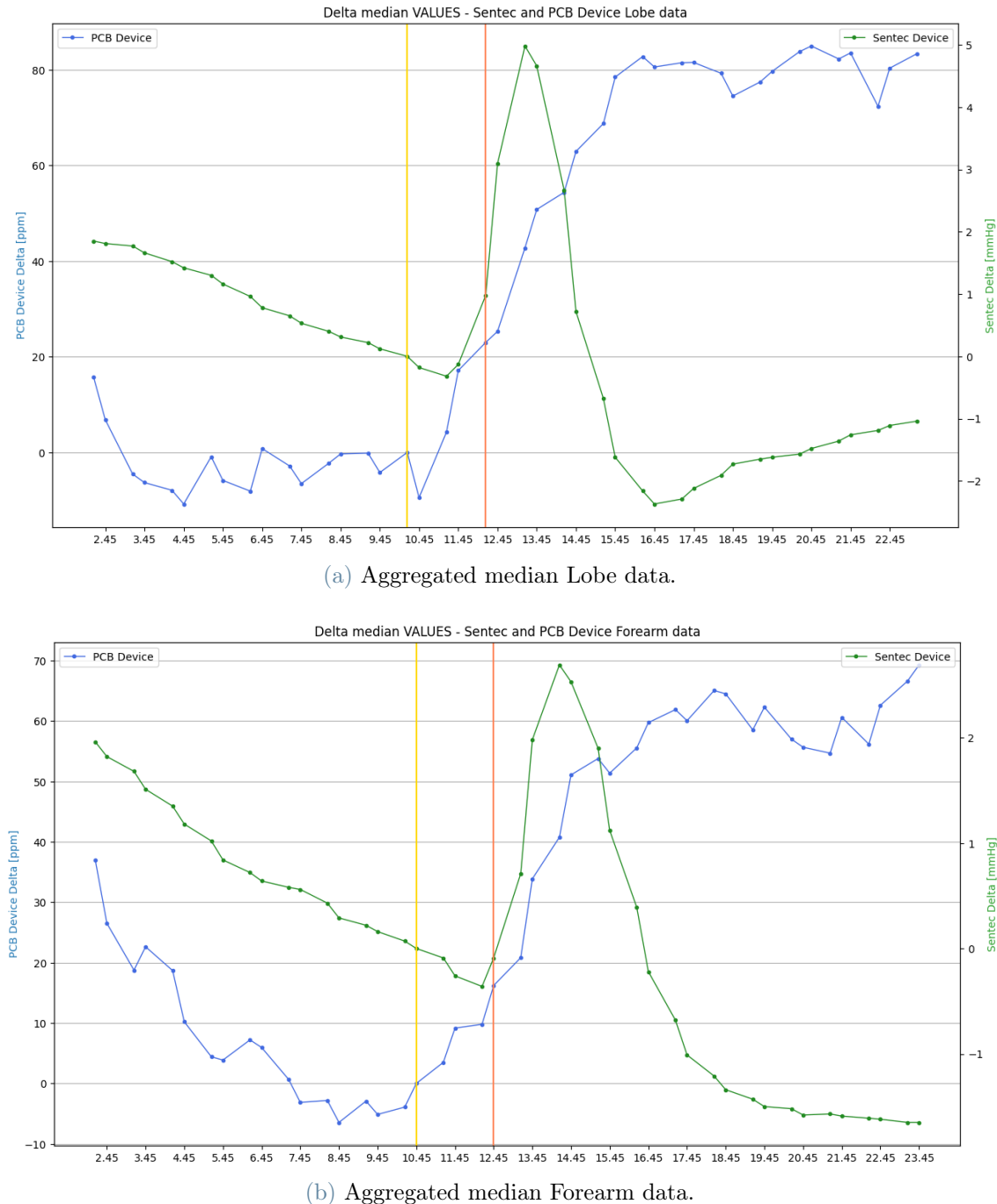


Figure 3.4: Aggregated median data for all the subjects expressed in delta terms with respect to the baseline value. In green the Sentec device, in blue the PCB device, horizontal grid enhances PCB device variations. Vertical yellow and orange lines indicate the beginning and end of the rebreathing maneuver. Plot (b) misses data from subject S05 because Sentec sensor has detached from the forearm of the subject during the test.

3.3.1. Kruskal Wallis test results

The results of the test can be seen in Figure 3.5. It can be seen that the p-value for the PCB device is constantly above the threshold level of 0.05, except for the time instant corresponding to the beginning of the rebreathing. Since if $p\text{-value} < 0.05$ the Null Hypothesis can not be rejected, it can be concluded that the median is the same for all the data groups. Practically, this means that in two consecutive acquisitions on the same subject, the corresponding time instants on the two arrays of collected data show similar values.

This is a good result for the repeatability of the measure over time for different subjects.

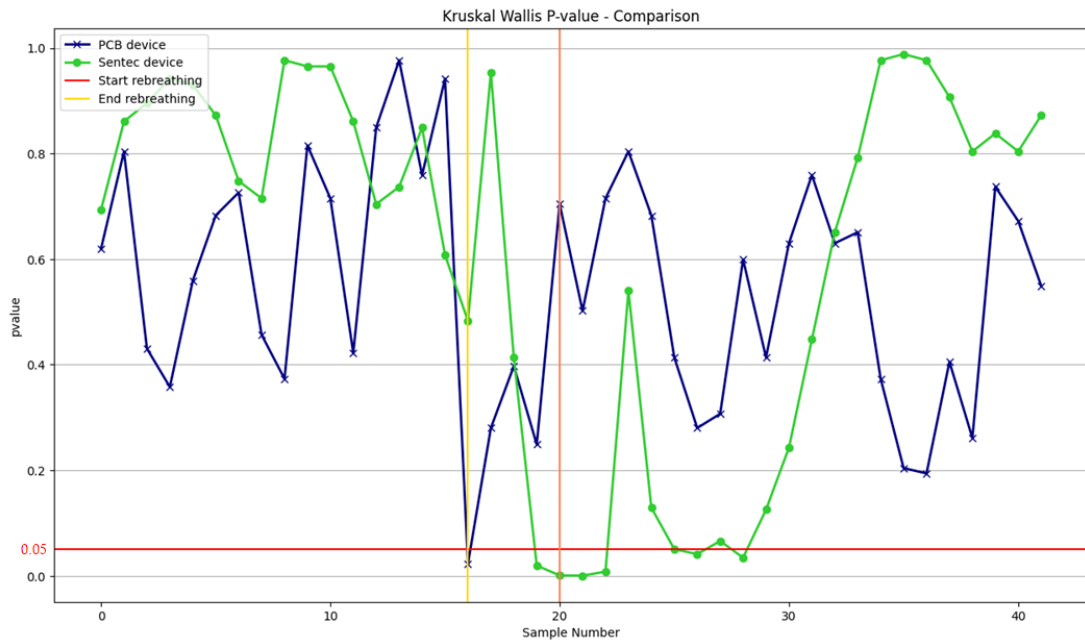


Figure 3.5: Trend of the p-value resulting from the Kruskal-Wallis test. Note that on the x-axis it is indicated the sample number. Between each sample a 30s time passes.

3.3.2. Wilcoxon Matched Pairs Test results

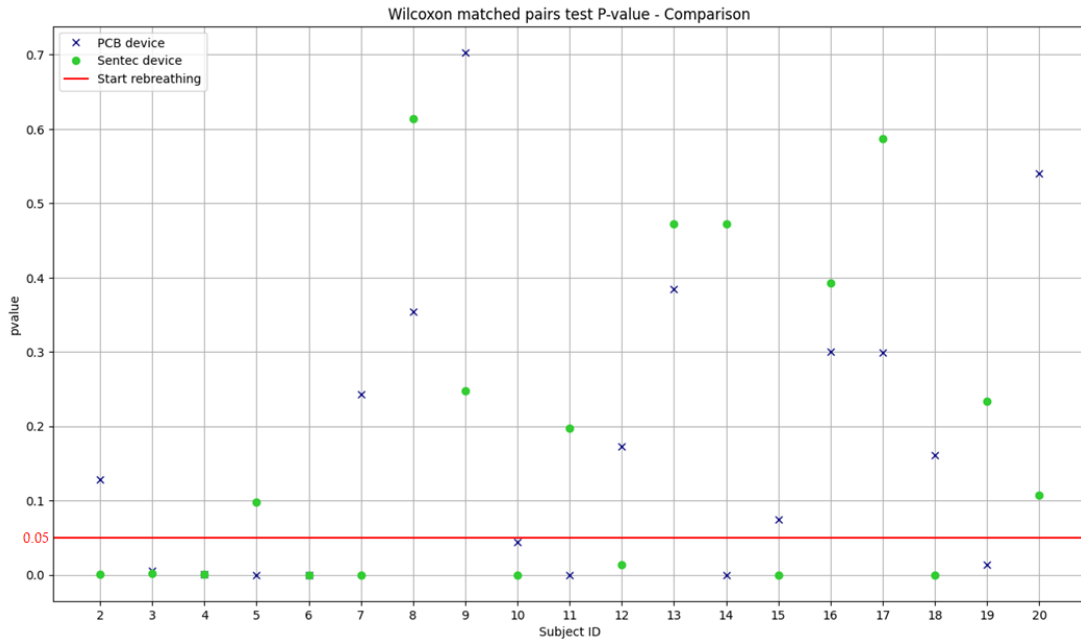


Figure 3.6: Trend of the p-value resulting from the Wilcoxon Matched Pairs test. Note that on the x-axis it is indicated the subject ID.

The Wilcoxon Matched Pairs Test results is used when two samples are under analysis and they are paired. Since the data that undergo this test come from the same subject, beside being collected in two different acquisitions, the test is meaningful. Data used for the Wilcoxon test are the Lobe data and Forearm data for each subject, and in output the p-value of the test is given.

The analysis is performed on 30s median data, and in Figure 3.6 the output is displayed. On the x-axis the subject number, that is the subject ID, is listed, and whenever the $p\text{-value} > 0.05$ the true mean difference between the two populations is equal to zero (in other words, there is no difference between the two "populations"). It is trivial to conclude that for some subjects this consideration holds, while for other subjects not.

However, the important result is that subjects with a p-value greater than 0.05 for the PCB device are often coupled with the same result for data taken from the Sentec device. This indicates a matching of behaviour between the two devices. Moreover, for 11 out of 19 subjects the PCB device validates the test, whereas for the Sentec device this happens for 10 subjects.

3.3.3. Friedman test results

The Friedman test on collected data is performed using SigmaPlot on PCB Device delta and normalized data, considering the 30s median data. The Friedman test is the non parametric alternative to the Repeated Measures ANOVA (RM ANOVA), and it is used because the CO₂ concentration levels are studied over a certain time for the same group of subjects.

The overall dataset passes the Shapiro-Wilk test for normality, despite being the data for each specific subject not normally distributed. However, the Equal Variance Test is failed.

Because of this, the RM ANOVA can not be used, and the Friedman Repeated Measures Analysis of Variance is performed.

The result of the test is that the differences in the median values among the treatment groups are greater than would be expected by chance, and hence there is a statistically significant difference.

To isolate the group or groups that differ from the others a multiple comparison procedure is used, and it is the **Dunnet's Method**. Dunnett's Method compares means from several experimental groups against a control group mean to see if there is a difference. Hence one fixed control group is compared to all of the other samples. To identify the control group it is chosen the group associated to the time instant of the beginning of the rebreathing procedure, that is also the time instant when baseline values are extracted.

In Table 3.2 and in Table 3.3 and the results are listed.

Time instants [min]	
p-value<0.05	5.3, 6.0, 6.3, 7.0, 7.3, 8.0, 8.3, 9.0, 9.3, 10.0, 10.3, 11.0, 11.3, 12.0, 12.3, 13.0
p-value>0.05	5.0
Not tested	0.3, 1.0, 1.3, 2.0, 2.3, 3.0, 3.3, 4.0, 4.3

Table 3.2: Friedman test results after Dunnet's Method for Lobe data. Time stamps refer to the beginning of the rebreathing maneuver

Time instants [min]	
p-value<0.05	5.3, 6.3, 7.0, 7.3, 8.0, 8.3, 9.0, 9.3, 10.0, 10.3, 11.0, 11.3, 12.0, 12.3, 13.0
p-value>0.05	4.3
Not tested	0.3, 1.0, 1.3, 2.0, 2.3, 3.0, 3.3, 4.0, 4.3, 5.0, 6.3

Table 3.3: Friedman test results after Dunnet's Method for Forearm data. Time stamps refer to the beginning of the rebreathing maneuver

Table 3.2 displays Lobe data considering the time instants of the test and the group of all the subjects, as well as for Table 3.3 but for Forearm data. It can be seen that in both cases the statistical significant difference with a p-value < 0.05 is found for all the time instants 2.3 min after the end of the rebreathing maneuver, as it is observed also for individual collected data for each subject.

Time instants just after the rebreathing maneuver are not tested by the algorithm because too similar to the baseline value, whereas also before the beginning of the rebreathing maneuver they are not tested because not of interest. A visual result can be seen in Figure 3.7.

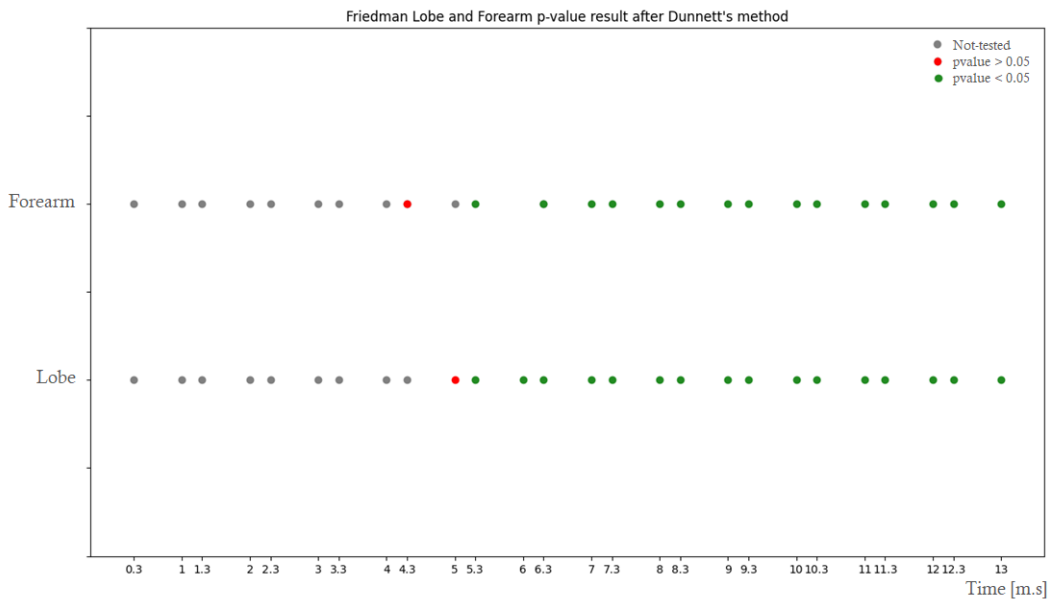


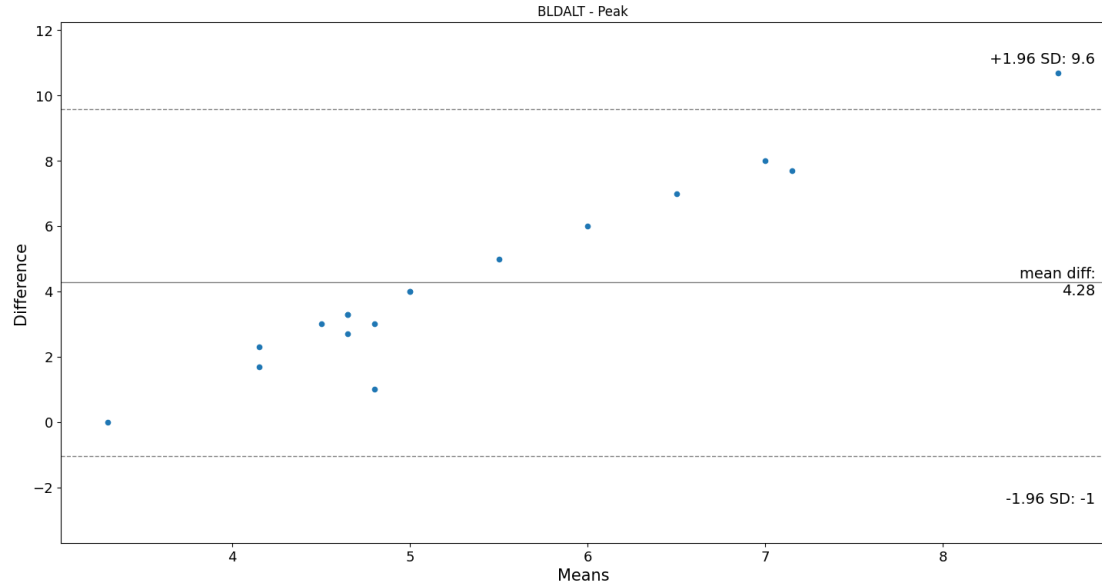
Figure 3.7: Friedman test results. Each dots represents the Friedman test result after the beginning of the rebreathing phase following the application of Dunnett’s Method. According to the legend, all the time instants 3 minutes after the end of the rebreathing maneuver are statistically different from the beginning of the test. This is in concordance with what has been observed from subjects’ data.

3.3.4. Bland-Altman Plots

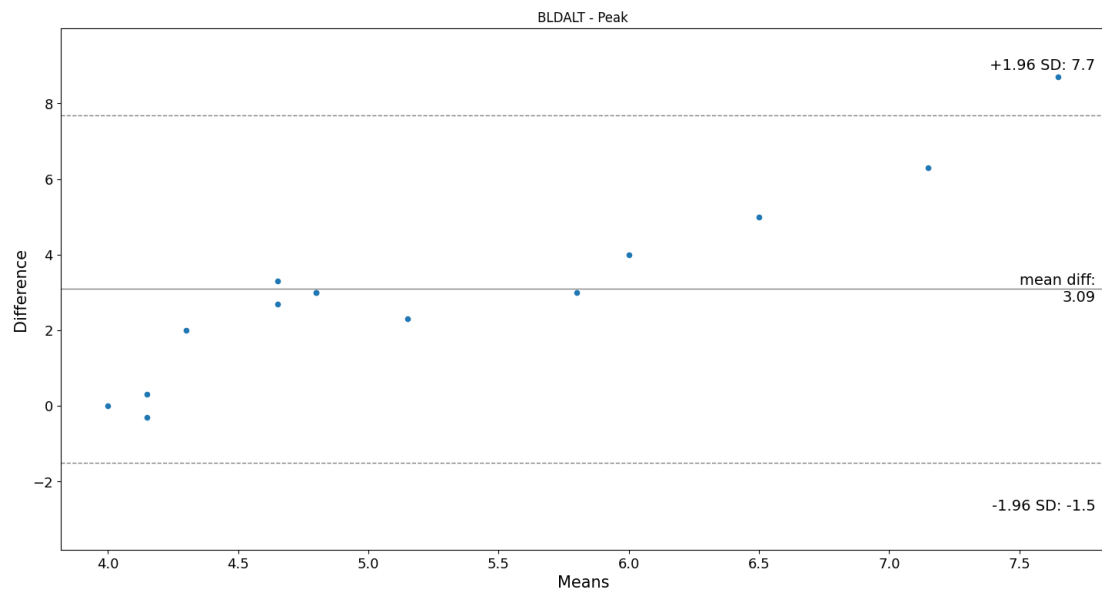
The Bland-Altman plot is used to visualize the differences in measurements between two different instruments or two different measurement techniques, that in this specific case are the PCB device and the Sentec device. It is used to assess how similar a new instrument or technique is at measuring something compared to the instrument or technique currently being used.

Data for the Bland-Altman plot are the 30s median data for lobe and forearm. Since it is impossible to compare time instant by time instant the two devices, because the units of measure of the two devices are different (mmHg and ppm), a workaround has been found. In particular, in Figure 3.8 there it is depicted the Bland-Altman plot for the times needed to reach the peak value for the two devices counting from the beginning of the rebreathing maneuver. Thus the variable compared is the same for the two devices, and it is ‘time’.

Since almost all the points lie between -1.96 SD and $+1.96 \text{ SD}$, there is an agreement between the two devices in terms of time to reach the peak value.



(a) Bland-Altman Plot for Lobe data.



(b) Bland-Altman Plot for Forearm data.

Figure 3.8: The x-axis of the plot displays the average measurement of the two instruments and the y-axis displays the difference in measurements between the two instruments.

3.3.5. Correlation Analysis

Since the Sentec Digital Monitor measure CO₂ values in mmHg whilst the PCB device does it in ppm, a direct comparison using for instance a correlation analysis through a Bland-Altman plot considering each time instant is not possible, as it was seen in Section 3.3.4. Moreover, also the shapes of the two output signals from the two devices are significantly different.

Because of this, to investigate correlation between the two devices a simple scatterplot is used, plotting maximal absolute values for the two devices in correspondence of the peak value of the two signals. Once again, the scatterplots are differentiated depending on having the Sentec device positioned on the Forearm or on the Lobe of the subject.

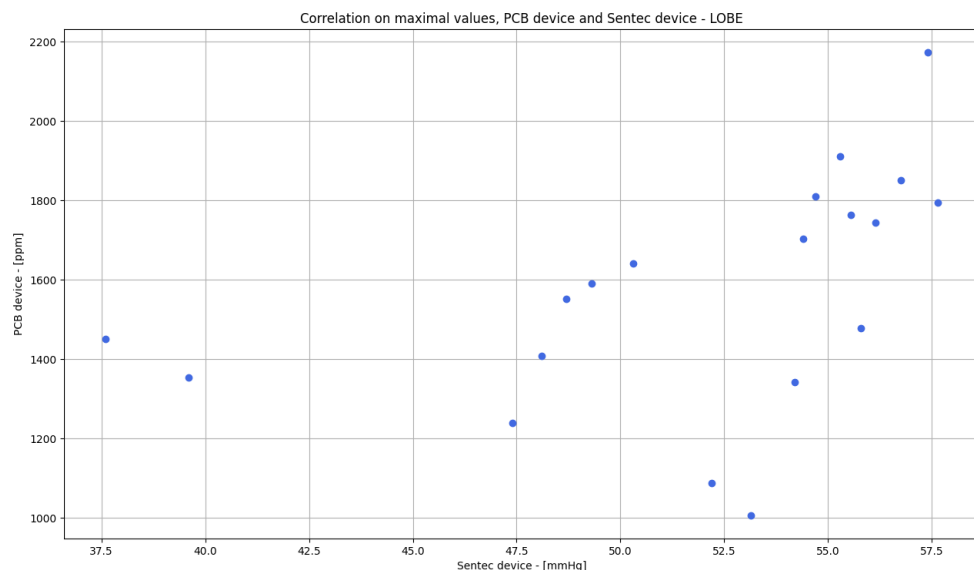


Figure 3.9: Lobe correlation result. The y-axis displays Sentec device absolute values, the x-axis PCB device absolute value.

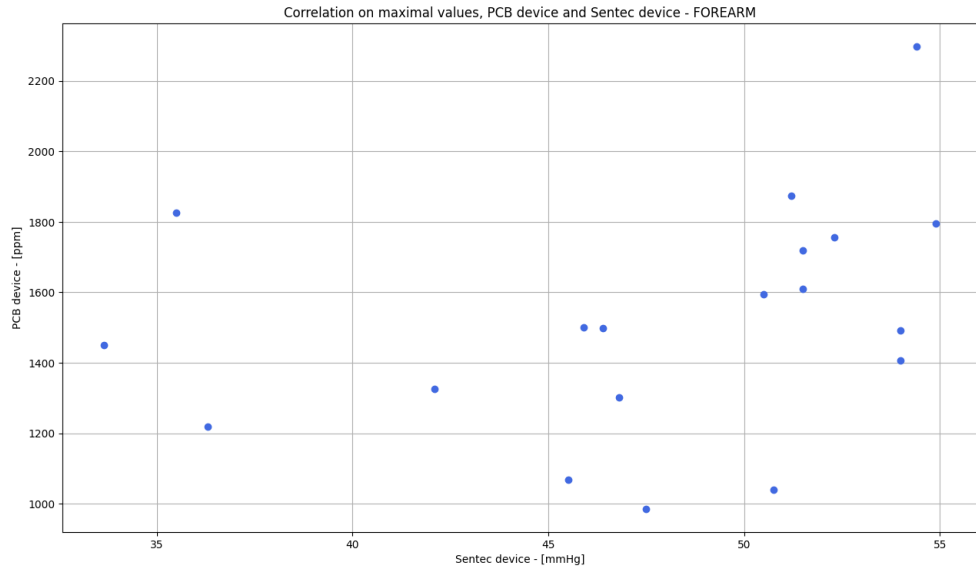


Figure 3.10: Forearm correlation result. The y-axis displays Sentec device absolute values, the x-axis PCB device absolute value.

3.4. Exponential Fitting

The results of the exponential fitting on Lobe and Forearm data can be seen in Table 3.4 and Table 3.5, respectively. The parameters of interest are mainly the time constant of the exponential curve τ , the asymptotic value B , the offset (*offset*) and the fitting goodness R^2 . In addition to these parameter, it is of interest to investigate the time elapsed between the beginning of the rebreathing maneuver and the beginning of the rise in CO₂ detected by the PCB device and Sentec Digital Monitor (*D. PCB* and *D. Sentec*, respectively). Moreover, since sometimes the PCB device responds with a curve that tends to decrease after reaching a certain level of saturation, the exponential fitting is not always performed from the rise of the curve to the end of the test, but an intermediate pre-decreasing value where to stop the fitting is found (End FT). Values in Table 3.4 and in Table 3.5 are retrieved from subject acquired data to which the baseline value of start rebreathing is subtracted. For this reason, they are not absolute values, but values with respect to each subject's baseline (i.e. delta values).

Lobe data present an average of 142.2 ppm for the B parameter with a standard deviation of ± 65 ppm, whereas the τ parameter has an average of 187.2 s with a standard deviation of ± 144 s. Conversely, Forearm data show an average of 101.8 ppm with a standard deviation of ± 51.9 ppm for the B parameter, and an average of 84.3 s with a standard deviation of ± 54.6 s for the τ parameter.

The high standard deviation in the τ value for Lobe data can be explained with the presence, amongst all the subjects, of two set of data, related to subject S08 and S14 with a high τ value. Despite being possible outliers, they are not marked as that because of the fitting goodness R^2 which is still acceptable, in particular for subject S14.

In addition, for what concerns the standard deviation related to the B parameter, it has to be remarked that the fitting is done over data acquired with a NDIR CO₂ sensor with a declared measurement accuracy of ± 30 ppm, hence representing another source of variability in collected data affecting also the overall standard deviation.

Since the PCB device is always positioned on the wrist during the two acquisitions on the subject, if data acquired are considered in-toto, without performing the distinction based on the Sentec device positioning, the B parameter has an average of 121.4 ppm with a standard deviation of ± 61.3 ppm, while for the τ the average is 135.8 s, and the standard deviation ± 119.2 s.

	D. [s]	PCB [s]	D. Sentec [s]	End [s]	FT [ppm]	Offset [ppm]	B [ppm]	τ [s]	R^2
S02	170	180		600	0.0	230.0	76.8	0.88	
S03	190	180		800	-20.0	285.1	117.2	0.96	
S04	120	110		610	-2.0	65.5	128.8	0.50	
S05	120	100		700	0.0	138.4	79.8	0.65	
S06				NA **					
S07				NA *					
S08	110	180		880	-25.0	90.4	425.6	0.42	
S09	150	180		780	-8.0	115.4	154.9	0.77	
S10	210	140		550	-27.0	103.6	73.4	0.74	
S11	120	160		880	-49.0	208.3	163.2	0.81	
S12	130	110		880	-24.0	166.6	153.6	0.76	
S13	200	160		700	-55.0	81.4	101.9	0.42	
S14	120	110		880	-51.0	238.9	568.1	0.83	
S15	100	100		880	-50.0	129.5	125.1	0.33	
S16				NA **					
S17	230	140		700	-4.0	87.2	173.8	0.60	
S18	250	180		880	-37.0	129.0	323.8	0.66	
S19	110	160		500	-40.0	87.9	63.5	0.65	
S20	110	160		700	-52.0	118.0	239.6	0.60	

Table 3.4: Exponential fitting curve parameters for each subject Lobe data.

* Non-exponential behaviour.

** Linear behaviour

Values in Table 3.4 and Table 3.5 are to be intended according to Equation 2.1. For instance, for subject S04, in the case of the lobe acquisition, the exponential takes the following form.

$$y = 65.6 \cdot (1 - e^{-\frac{t-120}{128.8}}) - 2.0 \quad (3.1)$$

Where y is the estimated output of CO_2 partial pressure in ppm. The same reasoning can than be applied to all the subjects.

	D. [s]	PCB [s]	D. Sentec [s]	End [s]	FT [ppm]	Offset [ppm]	B [ppm]	τ [s]	R^2
S02	180	210	700		-60.0	183.5	51.1	0.77	
S03	210	210	600		-45.0	162.4	77.8	0.92	
S04	110	220	800		25.0	112.5	236.7	0.76	
S05	180	220	500		-20.0	220.5	53.0	0.89	
S06	130	230	800		-35.0	99.3	158.3	0.76	
S07	130	190	450		-10.0	38.6	52.5	0.25	
S08	400	190	880		-30.0	60.0	38.2	0.35	
S09	400	190	880		-30.0	62.3	151.8	0.22	
S10	190	160	880		-22.0	70.0	100.2	0.56	
S11	230	160	880		0.0	128.6	196.0	0.71	
S12	250	160	700		-10.0	79.0	63.2	0.33	
S13				NA *					
S14	230	160	700		-52.0	105.5	86.7	0.52	
S15	240	180	550		-77.0	54.6	5.9	0.24	
S16				NA *					
S17	300	180	800		5.0	61.5	108.3	0.42	
S18	120	190	550		-35.0	60.5	61.3	0.22	
S19	140	160	580		-20.0	154.9	138.2	0.67	
S20				NA **					

Table 3.5: Exponential fitting curve parameters for each subject Forearm data.

* Non-exponential behaviour.

** Linear behaviour

The parameters retrieved from the exponential fitting can than be substituted in the Equation 2.1 to draw the exponential curve. Examples of the result can be seen in Figure 3.11 and Figure 3.12. They both display data retrieved from subject S03, piling the capnogram data, Sentec device data and PCB device data. In the last plot, the fitting curve is overlapped to 10s median data from subject S03 (to understand how the 10s median array is build, see Section 2.8.1).

Sentec device data and capnometry data are presented in absolute values, while the PCB device plot is with delta values with respect to the baseline value (because the fitting was

performed on delta data for all the subjects).

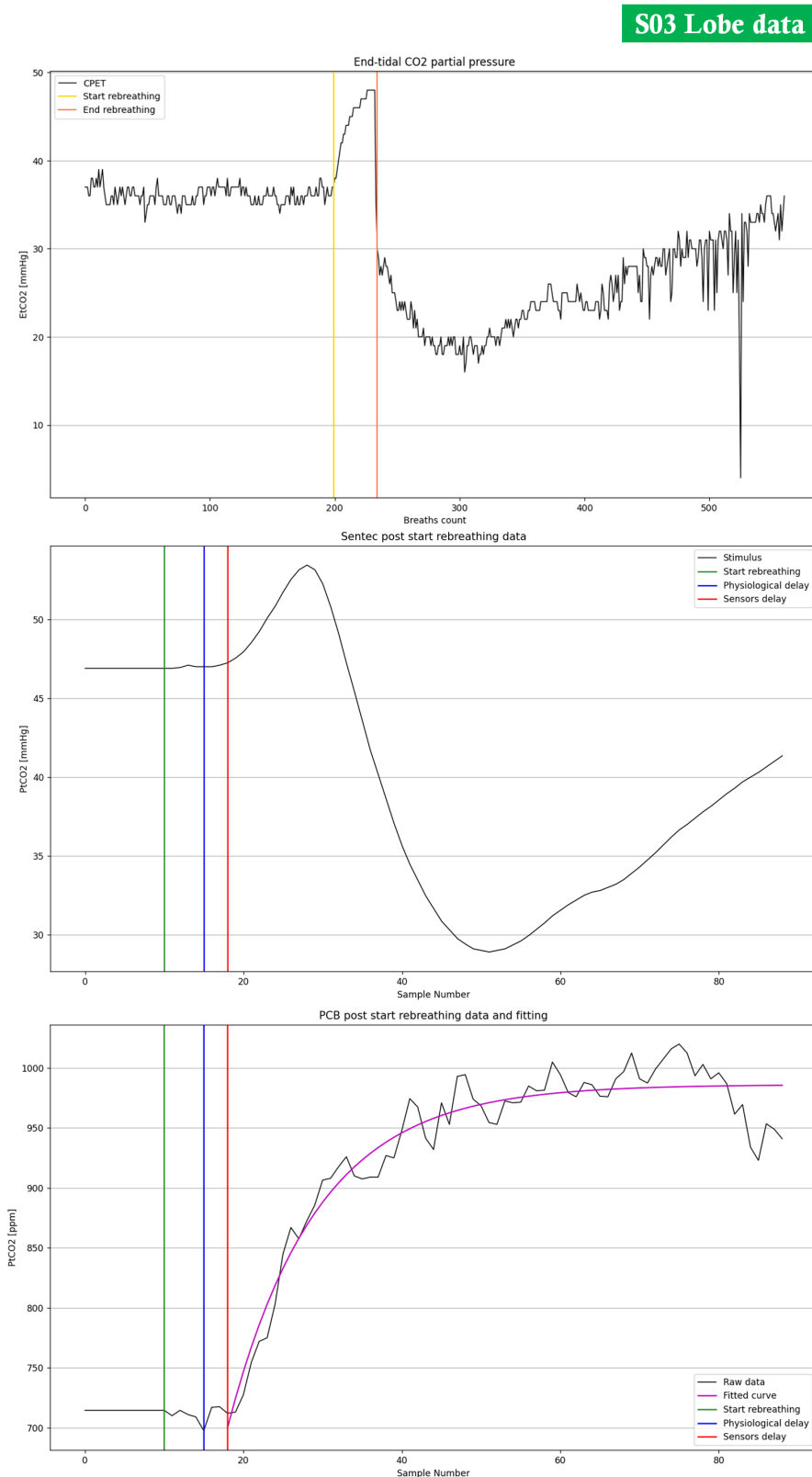


Figure 3.11: The first plot shows breath-by-breath capnometry data of the whole test, the second plot represent the Sentec device data from the beginning of the rebreathing and the third plot the PCB device data from the beginning of the rebreathing.

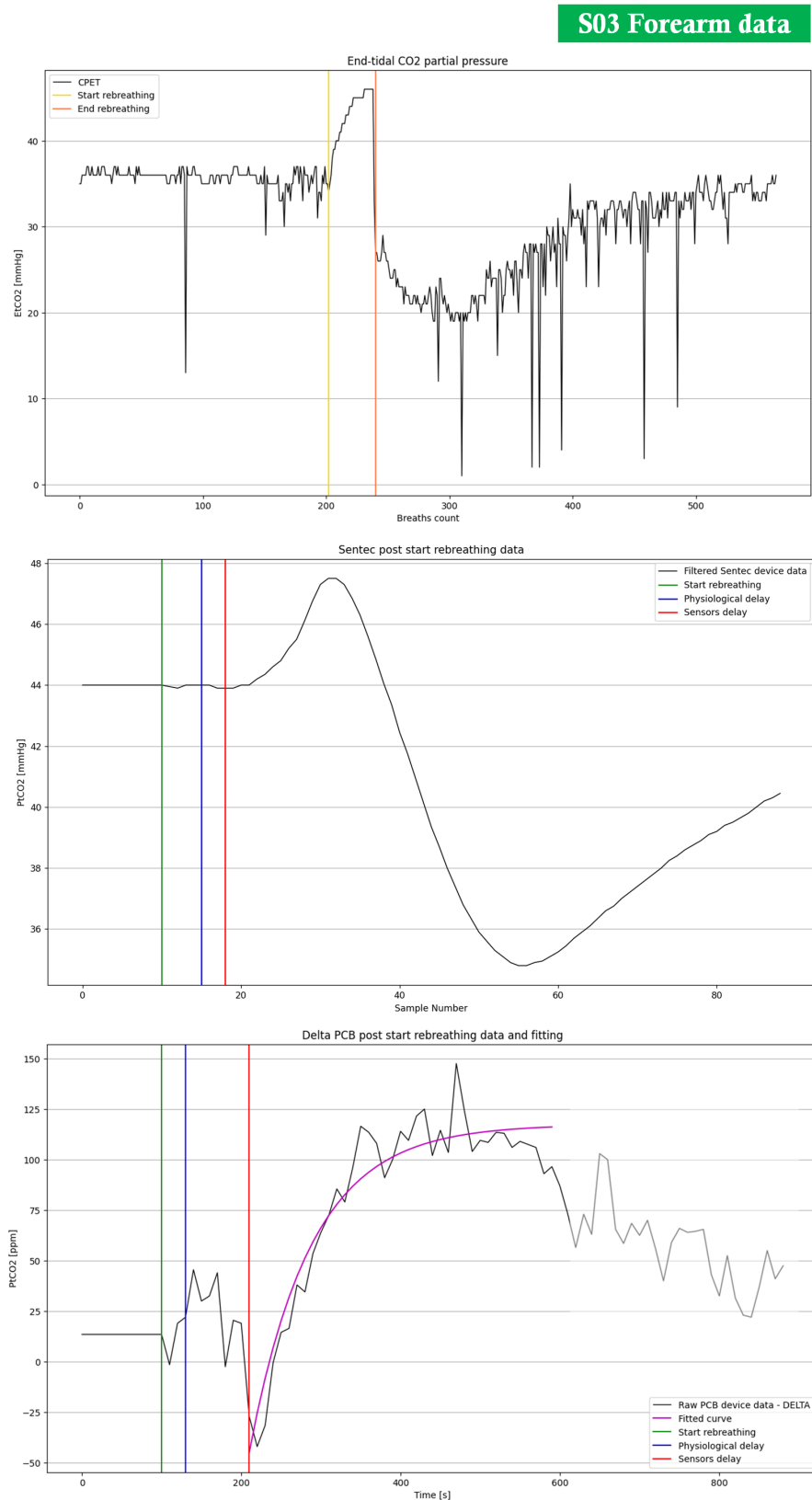


Figure 3.12: The first plot shows breath-by-breath capnometry data of the whole test, the second plot represent the Sentec device data from the beginning of the rebreathing and the third plot the PCB device data from the beginning of the rebreathing.

In both the piled plots for the Sentec device and PCB device, the following time instant are underlined:

- **Start rebreathing:** this time line marks the beginning of the rebreathing maneuver and the time instant where the baseline value is extracted.
- **Physiological delay:** it represents the delay that passes between the increase of carbon dioxide in blood due to respiration and the circulation time that brings the increased in CO₂ blood to the sensor's site. It is an unknown quantity that is displayed in the plots for the sake of representation.
- **Sensor's delay:** it is the time between the administration of the stimulus and the sensed increase in carbon dioxide level from the sensor on the skin. It includes the physiological delay and the sensor's capability of detecting CO₂ variations. It is a known quantity that is computed as the time difference between the beginning of the rebreathing maneuver and the increase in sensed CO₂.

4 | Conclusion

In this chapter faced issues, achieved results and future developments are presented.

4.1. Faced Issues and Achieved Results

The developed device is light, compact and easy to be worn. The hardware, firmware and case design are optimized to prevent excessive skin heating but at the same time creating a chamber where diffused carbon dioxide can easily accumulate. In fact, in designing the case it has been given a particular importance to the chamber dimensions; excessive dimensions lead to an incapability of the CO₂ sensor to detect carbon dioxide variations. Moreover, the firmware is optimized with interrupts so that data are collected within fixed time intervals.

The created smartphone application is capable to register the user, hence providing a user-custom experience. In additions, it can detect any type of BLE device and connect to it. The application also displays real-time analog data from the sensor and eventually real-time plots with the collected data. There is also the possibility to store locally or online the results, to operate deletions of measurements and disconnection directly from the app.

The experimental campaign has reached 2/3 of its progress, testing an almost equal amount of men and women so far. The test procedure consists in 10 minutes of normal breathing in air, followed by 2 minutes of rebreathing in a bag and concluded by 12 minutes of normal breathing in air. From the collected data, the PCB device shows almost always the same behaviour. From a statistical analysis, it can be concluded that the device is capable of repeating its measurement capabilities among different subjects in all the time instants of the test (this follows the Kruskal-Wallis test). Furthermore, the Friedman test followed by Dunnett's multiple comparison method indicates that after 5.3 minutes the beginning of the rebreathing procedure a sensible variation in detected CO₂ levels can be seen for all the next time instants. Having a statistical difference means that the device is capable of measuring diffused CO₂ variation through the skin.

Fitting with an exponential curve the PCB device collected data leads to the conclusion that an average time of $4*(135.8) \pm 119.2$ seconds (i.e. $4*\tau$, where τ is the time constant of the exponential curve) elapses between the start of the rebreathing maneuver and the reaching of a plateau. This is in concordance with the results in output to the Friedman test.

4.2. Future Developments

In the future, this project can benefit from some improvements.

From the hardware point of view, dimensions can be theoretically diminished using only the microcontroller of the Arduino without the whole breakout kit. Moreover, the choice of a more compact CO₂ sensor could further reduce the size of the overall device, still maintaining the same working principle.

With the added component in the second version of the PCB (Section 2.3), also the firmware needs to be updated to host a successful communication with these components. First of all, an analog sampling of the Battery Level monitor circuit needs to be implemented. Then the driving circuit for the fan needs a proper activation depending on the need. Lastly, the firmware needs to implement a Closed Loop controller for the temperature sensor monitoring the PCB temperature in the region where overheating may occur.

Following the previous considerations, also the case needs to be re-designed so that it can properly host the Fan and eventually a smaller carbon dioxide sensor.

As for what concerns the smartphone application, it can include specific binary codifications depending on the BLE device that is connected to it, so that data can be read correctly not only from the PCB device, but also from any BLE device that is connected to the smartphone. Moreover, also better visualization of the data can be achieved with a better-looking plot. In addition, also connection to Google drive can be implemented, so that user data is not stored in the Firebase account but on a Drive folder.

Lastly, with the conclusion of the experimental campaign it is needed a more detailed investigation on the correlation between the Senetec device and the PCB device, so that a conversion factor is found to convert transcutaneous CO₂ partial pressure from ppm to mmHg.

Bibliography

- [1] SciPy documentation. <https://docs.scipy.org/doc/scipy/>.
- [2] A. Aliverti. Wearable technology: role in respiratory health and disease. *Breathe*, 13(2):e27–e36, 2017.
- [3] A. Aliverti. Bioengineering of the respiratory system. 2021.
- [4] C. V. Anikwe, H. F. Nweke, A. C. Ikegwu, C. A. Egwuonwu, F. U. Onu, U. R. Alo, and Y. W. Teh. Mobile and wearable sensors for data-driven health monitoring system: State-of-the-art and future prospect. *Expert Systems with Applications*, page 117362, 2022.
- [5] S. Bernasconi. A wearable device for transcutaneus carbon dioxide measurement: a proof of concept. Master’s thesis, Politecnico di Milano, 2021.
- [6] W. B. Cannon. Organization for physiological homeostasis. *Physiological reviews*, 9(3):399–431, 1929.
- [7] E. Dervieux, M. Théron, and W. Uhring. Carbon dioxide sensing—biomedical applications to human subjects. *Sensors*, 22(1):188, 2021.
- [8] E. R. Dorsey and E. J. Topol. Telemedicine 2020 and the next decade. *The Lancet*, 395(10227):859, 2020.
- [9] S. et al. 10th anniversary of the centre for chemical sensors and chemical information technology (ccs). pages 261–262, 2005.
- [10] FDA. *Cutaneous Carbon Dioxide (PcCO₂) and Oxygen (PcO₂) Monitors—Class II Special Controls Guidance Document for Industry and FDA*. U.S. Department Of Health and Human Services: Washington, DC, USA, 2002.
- [11] J. Finci and D. Salzmann. Noninvasive optical determination of partial pressure of carbon dioxide, Mar. 9 2021. US Patent 10,939,854.
- [12] C. Gomez, J. Oller, and J. Paradells. Overview and evaluation of bluetooth low

- energy: An emerging low-power wireless technology. *Sensors*, 12(9):11734–11753, 2012.
- [13] Google. Firebase. <https://firebase.google.com/>.
- [14] P. Grangeat, S. Gharbi, M. Accensi, and H. Grateau. First evaluation of a transcutaneous carbon dioxide monitoring wristband device during a cardiopulmonary exercise test. In *2019 41st Annual International Conference of the IEEE Engineering in Medicine and Biology Society (EMBC)*, pages 3352–3355. IEEE, 2019.
- [15] P. Grangeat, S. Gharbi, A. Koenig, M.-P. Comşa, M. Accensi, H. Grateau, A. Ghaith, S. Chacaroun, S. Doutreleau, and S. Vergès. Evaluation in healthy subjects of a transcutaneous carbon dioxide monitoring wristband during hypo and hypercapnia conditions. In *2020 42nd Annual International Conference of the IEEE Engineering in Medicine & Biology Society (EMBC)*, pages 4640–4643. IEEE, 2020.
- [16] T. B. Hackett. Pulse oximetry and end tidal carbon dioxide monitoring. *Veterinary Clinics: Small Animal Practice*, 32(5):1021–1029, 2002.
- [17] E. J. Hurst. Evolutions in telemedicine: from smoke signals to mobile health solutions. *Journal of Hospital Librarianship*, 16(2):174–185, 2016.
- [18] S. H. Lee and S. W. Kang. Noninvasive optical transcutaneous pco₂ gas sensor. *Sens. Mater.*, 17:249–257, 2005.
- [19] A. Mari, H. Nougue, J. Mateo, B. Vallet, and F. Vallée. Transcutaneous pco₂ monitoring in critically ill patients: update and perspectives. *Journal of thoracic disease*, 11(Suppl 11):S1558, 2019.
- [20] A. H. Omre and S. Keeping. Bluetooth low energy: wireless connectivity for medical monitoring. *Journal of diabetes science and technology*, 4(2):457–463, 2010.
- [21] J. Portnoy, M. Waller, and T. Elliott. Telemedicine in the era of covid-19. *The Journal of Allergy and Clinical Immunology: In Practice*, 8(5):1489–1491, 2020.
- [22] S. T. Selby, T. Abramo, and N. Hobart-Porter. An update on end-tidal co₂ monitoring. *Pediatric emergency care*, 34(12):888–892, 2018.
- [23] Sentec. *Sentec Digital Monitoring System*, 2020.
- [24] G. S. Solutions. *CozIR®-LP, Low Power CO₂ Sensor*, 2020.
- [25] C. R. Taylor and E. R. Weibel. Design of the mammalian respiratory system. i. problem and strategy. *Respiration physiology*, 44(1):1–10, 1981.

- [26] V. V. Tipparaju, S. J. Mora, J. Yu, F. Tsow, and X. Xian. Wearable transcutaneous co monitor based on miniaturized nondispersive infrared sensor. *IEEE Sensors Journal*, 21(15):17327–17334, 2021.
- [27] W. Van Weteringen, T. G. Goos, T. Van Essen, C. Ellenberger, J. Hayoz, R. C. De Jonge, I. K. Reiss, and P. M. Schumacher. Novel transcutaneous sensor combining optical tcpo₂ and electrochemical tcpc_o2 monitoring with reflectance pulse oximetry. *Medical & Biological Engineering & Computing*, 58(2):239–247, 2020.
- [28] M. Waller and C. Stotler. Telemedicine: a primer. *Current allergy and asthma reports*, 18(10):1–9, 2018.
- [29] P. D. Wimberley, K. Grønlund Pedersen, J. Olsson, and O. Siggaard-Andersen. Transcutaneous carbon dioxide and oxygen tension measured at different temperatures in healthy adults. *Clinical chemistry*, 31(10):1611–1615, 1985.
- [30] M. Woolley. Bluetooth core specification v5. 1. In *Bluetooth*, 2019.
- [31] G. S. Zavorsky, J. Cao, N. E. Mayo, R. Gabbay, and J. M. Murias. Arterial versus capillary blood gases: a meta-analysis. *Respiratory physiology & neurobiology*, 155(3):268–279, 2007.

A | Appendix A: PCB Version 1

In this appendix it is shown the complete device schematic circuit. It is composed by an Arduino nano 33 either IoT or BLE, whose output pins are connected to wire and valve driving circuits, while its inputs are connected to the two temperature sensors and to a button to mediate the user's interactions with the device. The button is in pull-down configuration, with an anti-debouncing RC hardware filter to prevent false triggerings. The TX and RX pins of the Arduino are also connected to the correspondingly RX and TX pins of the CozIR sensor, which is powered between 3.3V and ground. A ground pin is also inserted (Figure A.1).

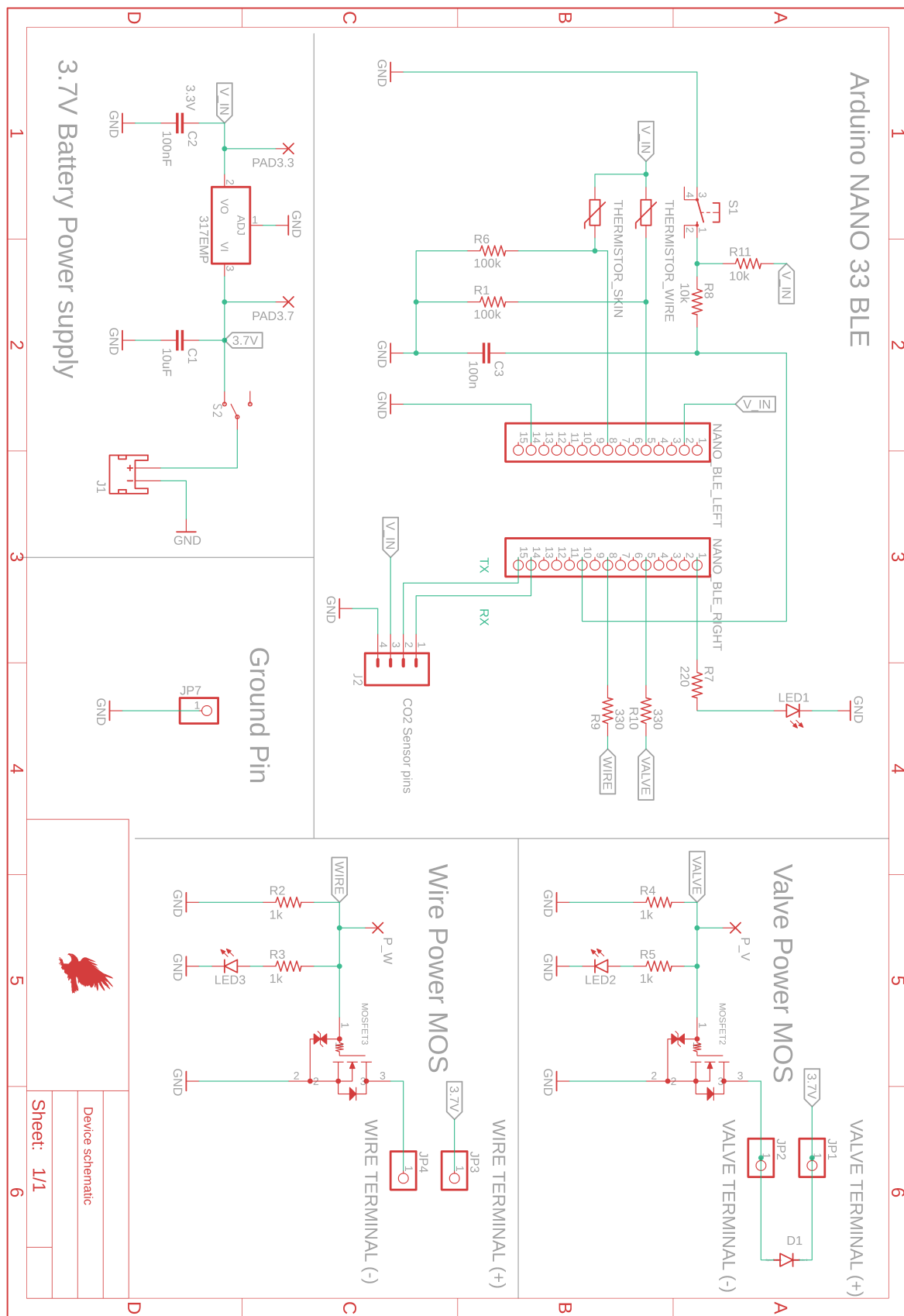


Figure A.1: Complete device schematic with the different parts.

B | Appendix B: PCB Version 2

In this appendix it is shown the complete device schematic circuit for version 2. The backbone of the device and the core features are the same of version 1. To reduce power consumption, LEDs that were connected to MOSFETs' gates are removed. Moreover, two solder bridges are added. One is placed in parallel to a 330 Ohm resistance that links the Arduino Pin controlling the motor fan with the gate of the MOSFET controlling the motor fan. By shortening the bridge the V_{GS} is increased and a higher drain current is permitted to pass through the fan. The second solder bridge is in parallel with the switch that mediates the connection between the battery and the recharge circuit.

The recharge circuit is composed by a Micro-USB port that can be plugged in a socket or to a PC with a proper cable, a recharge module and a switch. Two LEDs are used to indicate when the battery is charging (Red LED) and when the charging is finished (Blue LED).

Furthermore, the Wire MOS temperature sensor is a NTC temperature sensor that is placed close to the MOSFET driving the wire. Since that transistor is prone to self-heating, measuring the temperature of the PCB very close to the MOSFET allows for a control loop where V_{GS} voltage on this transistor can be tuned to prevent MOSFET failure. The resistive temperature sensor is in a simple voltage divider configuration with a 1 kOhm resistance between 3.3V and ground.

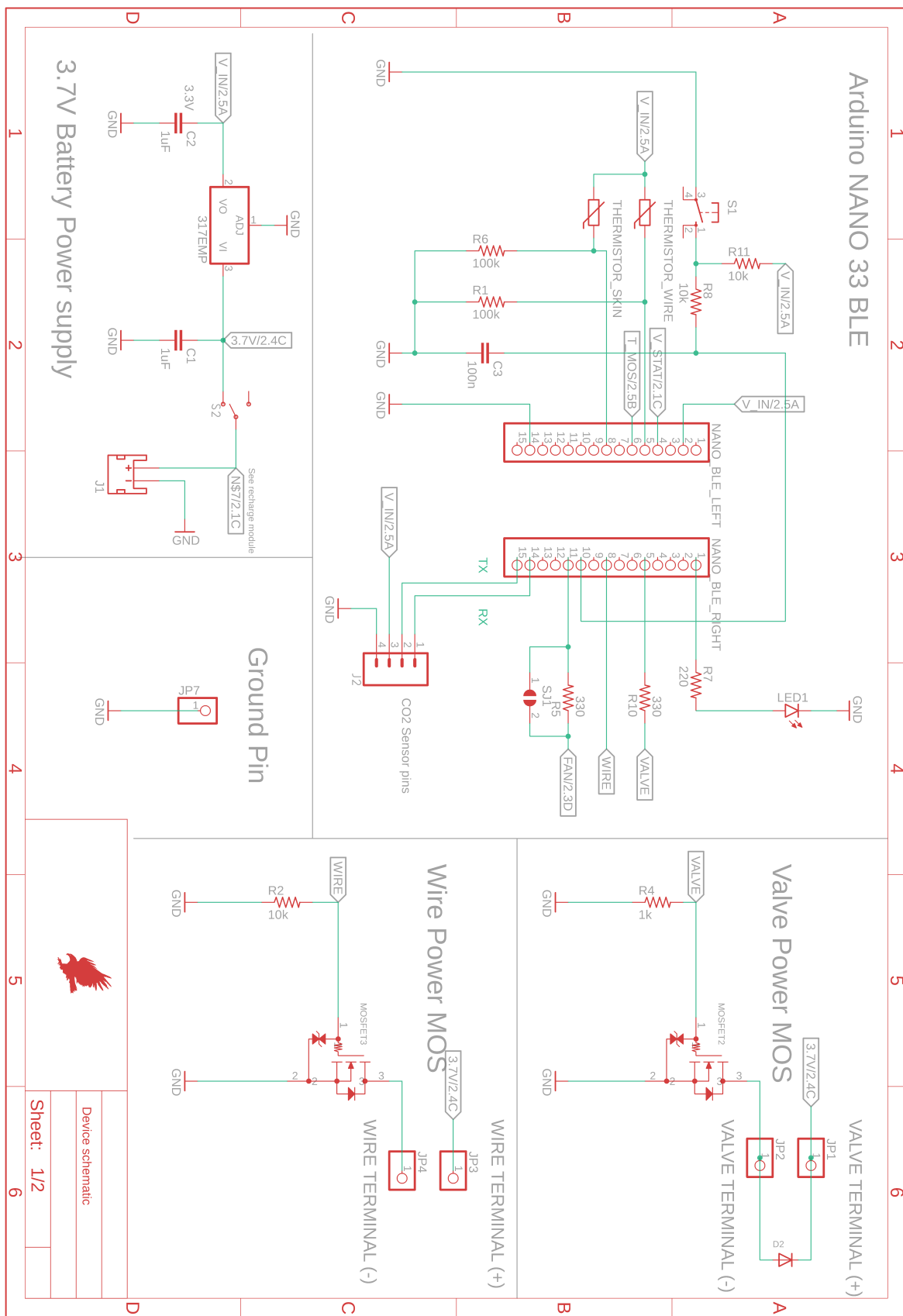


Figure B.1: Complete device schematic with the different parts (Sheet 1).

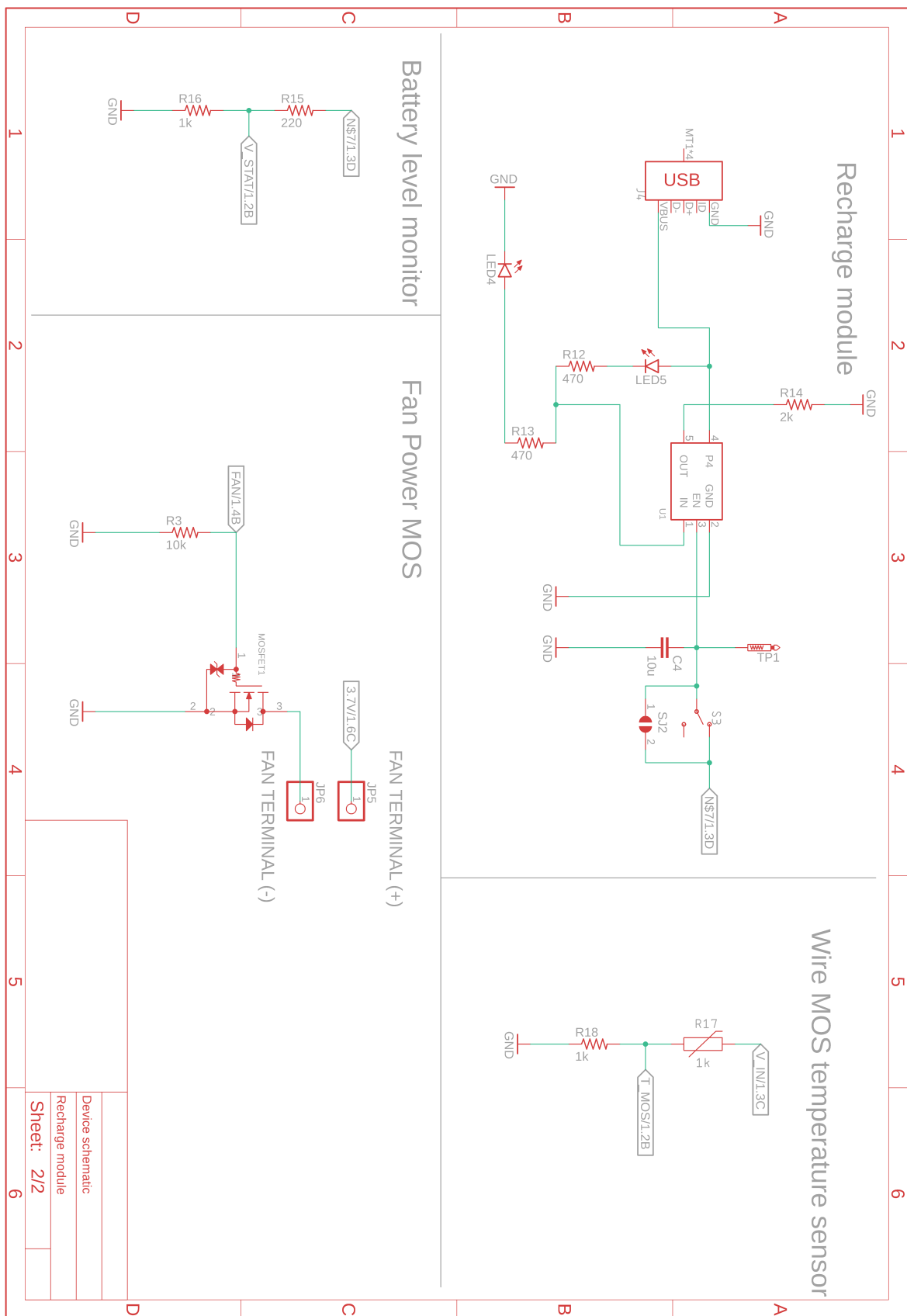


Figure B.2: Complete device schematic with the different parts (Sheet 2).

C | Appendix C: Case 3D rendering and dimensioning

In this appendix technical insights on the case of the device are presented.

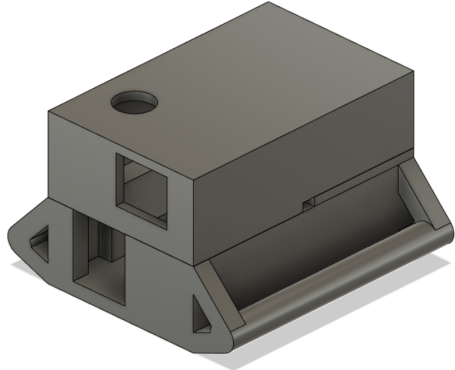
The device has a dimension $57.22 \times 37.00 \times 35.97\text{mm}$, with a chamber for CO₂ accumulation with a diameter of 9.00 mm and a height of 3.00 mm, resulting in an overall area of 763.41 mm^2 . The wire is placed in a housing having a 2 mm height and an outer radius of 11.50 mm (Figure C.1d).

As for the closure, it is divided in two parts. A bigger cap closes the overall device where the PCB with the electronics is placed (Figure C.1a), whereas a smaller closing cap is used to isolate the sensor from the environment (Figure C.1b).

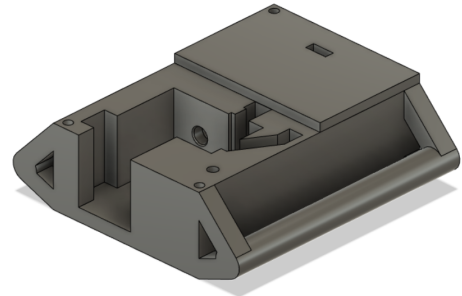
This is needed to prevent CO₂ to dissipate from the chamber to the surrounding environment, hence reducing leakages. The only bigger closure is not sufficient because it has holes where to plug in the PCB and interact with the user-button.

In the horizontal section in Figure C.1e it is noticeable the duct which allows or prevents the passage of ambient air in the chamber depending on the status of the solenoid valve.

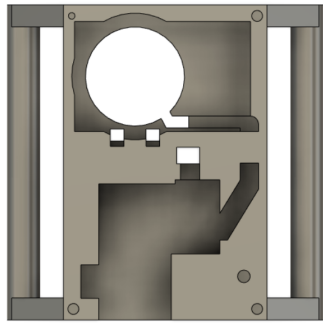
The valve is placed in a concavity having dimensions $24.72 \times 13.20 \text{ mm}$ (Figure C.1c). For other technical details, they can be found in Figure C.2.



(a) Complete device.



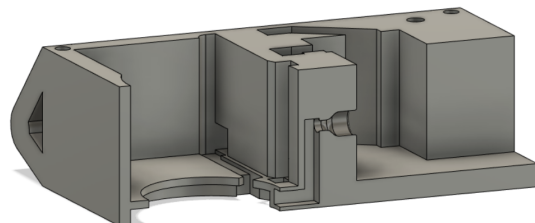
(b) Device without the closing cap.



(c) Top view.



(d) Bottom.



(e) Horizontal section.

Figure C.1: Different views of the case in 3D rendering provided by Fusion 360, Autodesk Inc.

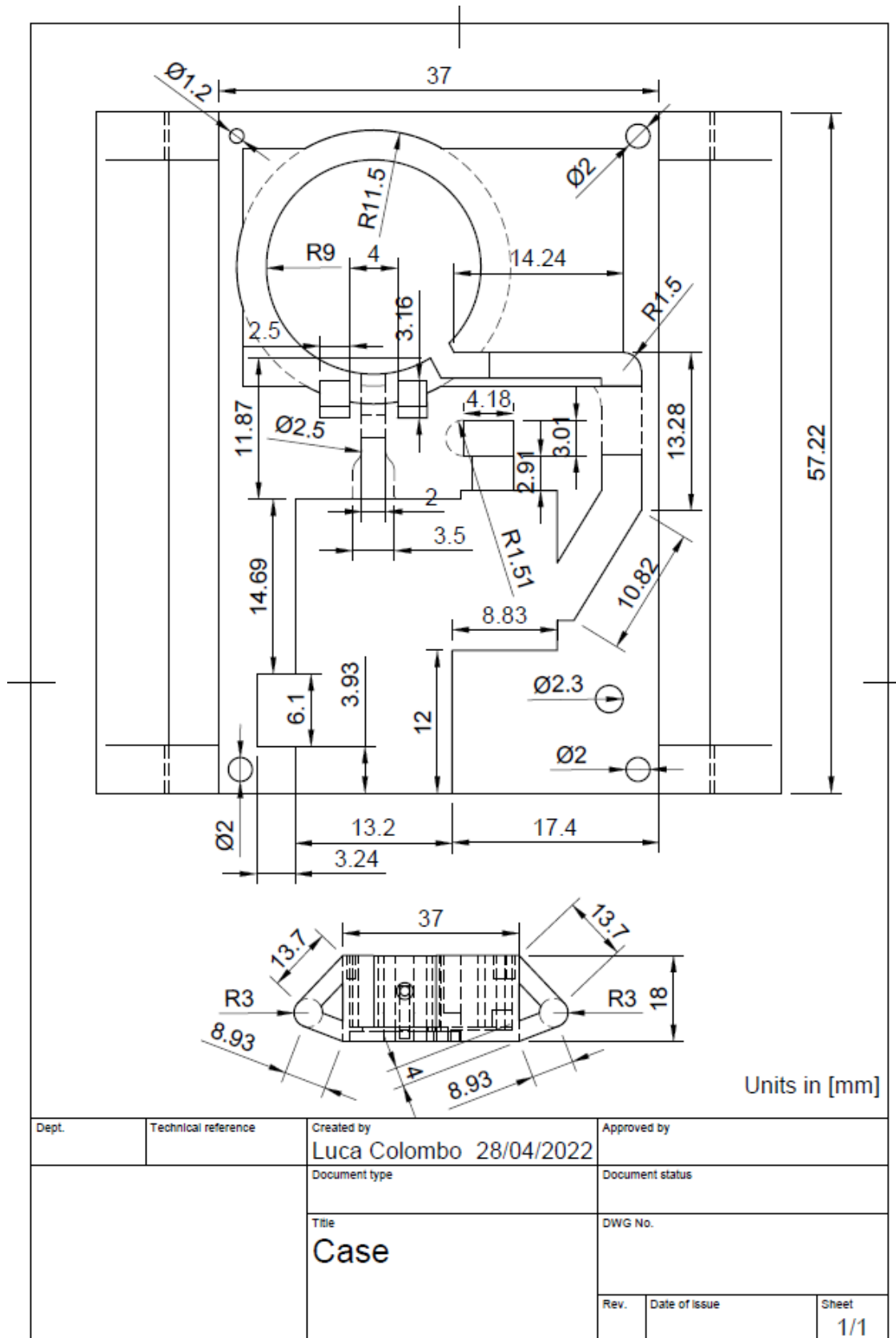


Figure C.2: Dimensioning of the case.

List of Figures

1	BAN architecture with sensors possibilities.	3
1.1	Model of the respiratory system and cascade of pressure gradients from [25].	6
1.2	Schematic description of central chemoreceptors' role and CO ₂ sensing [3]	9
1.3	Illustration of a state-of-the-art Stow-Severinghaus electrodes [7].	13
1.4	Illustration of an ISFET sensor [7].	14
1.5	Schematic representation of combined reference and measured channels in a NDIR sensor [7].	16
1.6	Schematic representation of the working principle of a photoacoustic sensor sensor [7].	16
1.7	Typical expected representation from a Capnogram with the four different phases clearly underlined [22].	19
1.8	Sentec Digital Monitor.	24
1.9	Schematic representation of the sensor created by Salzmann [11].	25
1.10	Schematization of the different chambers and fluid flux in the CAPNO device	27
2.1	Parker® Solenoid Valve.	34
2.2	Solenoid Valve conditioning circuit.	35
2.3	Voltage regulator conditioning circuit.	36
2.4	MOSFETs characteristic curves	37
2.5	Nichrome Wire conditioning circuit.	40
2.6	Board panel	43
2.7	PCB Version 2	46
2.8	Device	49
2.9	Firmware workflow	51
2.10	BLE protocol stack from [12].	57
2.11	Simplified flowchart representing the application functioning described in Section 2.6	62
2.12	Application Icon designed on Adobe Illustrator.	65
2.13	App logo and appearance on the smartphone.	65

2.14 Welcome Screen.	66
2.15 Registration screen.	67
2.16 App log-in screens	68
2.17 Forgot email screen.	69
2.18 Example of the received mail when the user asks for a password reset.	70
2.19 In yellow the user email. In blue the disclaimer.	70
2.20 Scanning Screen	72
2.21 Attention Pop-Up when "Data Visualization" button is pressed before pressing the synchronization button. In the background the complete characteristics of the connected device can be seen.	73
2.22 Data Visualization Screen	74
2.23 Real time data chart representing the CO ₂ values sampled from the sensors.	75
2.24 Apparatus used to perform the rebreathing maneuver. 1 is the three ways valve, 2 the rebreathing bag, 3 the flowmeter, 4 the mouthpiece.	78
2.25 Experimental instrumentation	78
2.26 Schematic representation of the test protocol	79
2.27 Grouping Algorithm	82
3.1 Devices responses	87
3.2 Questionnaire averages	90
3.3 Boxplots for aggregated data	93
3.4 Aggregated median data	94
3.5 Kruskal-Wallis test result	95
3.6 Wilcoxon Matched Pairs Test test result	96
3.7 Friedman test results	99
3.8 Bland-Altman Plots	100
3.9 Correlation result - Lobe	101
3.10 Correlation result - Forearm	102
3.11 Fitting result - Lobe	107
3.12 Fitting result - Forearm	108
A.1 Complete device schematic with the different parts.	118
B.1 Complete device schematic with the different parts (Sheet 1).	120
B.2 Complete device schematic with the different parts (Sheet 2).	121
C.1 Case 3D rendering	124
C.2 Dimensioning of the case.	125

List of Tables

2.1	Tested population	79
3.1	Averages scores for the questionnaire responses, compared with the corresponding ideal values.	90
3.2	Friedman test results after Dunnet's Method for Lobe data. Time stamps refer to the beginning of the rebreathing maneuver	97
3.3	Friedman test results after Dunnet's Method for Forearm data. Time stamps refer to the beginning of the rebreathing maneuver	98
3.4	Exponential fitting curve parameters for each subject Lobe data. * Non-exponential behaviour. ** Linear behaviour	104
3.5	Exponential fitting curve parameters for each subject Forearm data. * Non-exponential behaviour. ** Linear behaviour	105

Nomenclature

CO₂ Carbon Dioxide chemical formula

O₂ Oxygen chemical formula

P_A Partial pressure of oxygen in the alveoli

P_b Capillary partial pressure of oxygen

P_E Partial pressure of oxygen in the expired air

P_I Partial pressure of oxygen in the inspired air

artPCO₂ Arterial CO₂ partial pressure

EtCO₂ End-Tidal CO₂

pCO₂ Partial pressure of CO₂

PaCO₂ Arterial CO₂ partial pressure

petCO₂ End-Tidal CO₂ partial pressure

PtCO₂ Transcutaneous CO₂ partial pressure

BGA Blood Gas Analysis

BLE Bluetooth Low Energy

COPD Chronic Obstructive Pulmonary Disease

CPET Cardio-Pulmonary Exercise Test

DC Duty Cycle, Direct Current

ECG Electrocardiograph

ISFET Ion-Sensitive Field Effect Transistor

LED Light Emitting Diode

MEMS Micro Electro-Mechanical System

MOSFET Metal Oxide Semiconductor Field Effect Transistor

NADH Nicotinamide Adenine Dinucleotide and Hydrogen

NDIR Non-Dispersive Infrared

NTC Negative Temperature Coefficient

PCB Printed Circuit Board

PPM Parts Per Million

RGB Red, Green and Blue

RX Receiver

SDK Software Development Kit

SDMS Sentec Digital Monitoring System

TX Transmitter